MEMS THIN FILM PIEZOELECTRIC ACOUSTIC TRANSDUCER FOR COCHLEAR IMPLANT APPLICATIONS

A THESIS SUBMITTED TO
THE GRADUATE SCHOOL OF NATURAL AND APPLIED SCIENCES
OF
MIDDLE EAST TECHNICAL UNIVERSITY

BY

BEDİRHAN İLİK

IN PARTIAL FULFILLMENT OF THE REQUIREMENTS
FOR
THE DEGREE OF MASTER OF SCIENCE
IN
ELECTRICAL AND ELECTRONICS ENGINEERING

OCTOBER 2018

Approval of the thesis:

MEMS THIN FILM PIEZOELECTRIC ACOUSTIC TRANSDUCER FOR COCHLEAR IMPLANT APPLICATIONS

Submitted by **BEDİRHAN İLİK** in partial fulfillment of the requirements for the degree of **Master of Science in Electrical and Electronics Engineering Department, Middle East Technical University** by,

Prof. Dr. Halil KALIPÇILAR
Dean, Graduate School of **Natural and Applied Sciences** _____

Prof. Dr. Tolga ÇİLOĞLU
Head of Department, **Electrical and Electronics Eng. Dept.** _____

Prof. Dr. Haluk KÜLAH
Supervisor, **Electrical and Electronics Eng. Dept., METU** _____

Examining Committee Members:

Prof. Dr. Tayfun AKIN
Electrical and Electronics Engineering, METU _____

Prof. Dr. Haluk KÜLAH
Electrical and Electronics Engineering, METU _____

Assoc. Prof. Dr. Ender YILDIRIM
Mechanical Engineering, Çankaya University _____

Assist. Prof. Dr. Selçuk YERCİ
Electrical and Electronics Engineering, METU _____

Assist. Prof. Dr. Kıvanç AZGIN
Mechanical Engineering, METU _____

Date: 23.10.2018

I hereby declare that all information in this document has been obtained and presented in accordance with academic rules and ethical conduct. I also declare that, as required by these rules and conduct, I have fully cited and referenced all material and results that are not original to this wok.

Name, Last name : BEDİRHAN İLİK

Signature :

ABSTRACT

MEMS THIN FILM PIEZOELECTRIC ACOUSTIC TRANSDUCER FOR COCHLEAR IMPLANT APPLICATIONS

İlik, Bedirhan

M.Sc., Department of Electrical and Electronics Engineering

Supervisor: Prof. Dr. Haluk Külah

October 2018, 101 pages

In this thesis, a multi-frequency thin film piezoelectric acoustic sensor concept to be placed on the eardrum has been proposed for the development of next generation and fully implantable cochlear implants (FICIs). The design consists of several thin film piezoelectric cantilever beams, each of which resonates at a specific frequency within the daily acoustic band. The device will exploit the functional parts of the natural hearing mechanism and mimic the function of the hair cells in the cochlea, where the signal generated by the piezoelectric transducers will be processed by interface electronics to stimulate the auditory neurons.

The limited volume (<0.1 cm^3) in the middle ear, the mass tolerance (<25 mg) and the size of the eardrum (9 mm × 10 mm) and the requirement for covering the audible frequency band (250-5000 Hz) with enough number of channels are the main limitations/challenges for obtaining an adequate voltage output for neural stimulation. In this direction, design, modeling, fabrication and characterization of a multi-frequency thin film piezoelectric acoustic sensor have been accomplished to overcome the main bottlenecks of CIs. Pulsed Laser Deposited (PLD) Lead Zirconate Titanate (PZT) is preferred among other thin film piezoelectric alternatives due to their superior ferroelectric and piezoelectric properties for acoustic sensing.

To demonstrate the feasibility of the proposed fabrication scheme, a single cantilever thin film PLD-PZT transducer prototype is fabricated. The realized device is assembled onto a flexible parylene carrier and placed on a parylene membrane, mimicking the operation of the eardrum. The mechanical, electrical and acoustical properties are characterized by a shaker table and an acoustic setup. Acceleration characteristic of the sensor attached to the membrane is obtained by using a Laser Doppler Vibrometer (LDV) as the output voltage was measured by an oscilloscope. A maximum voltage output of 114 mV is obtained, when the single channel device was excited at 110 dB Sound Pressure Level (SPL) at 1325 Hz. Experimental results show that the voltage output of the device exceeds the minimum required sensing voltage (100 μV) for the neural stimulation circuitry.

Fabricated single-channel prototype is modeled using finite element modeling (FEM) which are within 92% agreement with the experimental results. Based on this model, a multi-channel thin film piezoelectric acoustic sensor is designed. The total volume, area and mass of the transducer are $5\times5\times0.2$ mm^3, 5×5 mm^2, and 12.2 mg, respectively.

The multi-channel prototype is fabricated and characterized. The electromechanical properties are measured by a shaker table and LCR meter. The test results show that, fabricated device, consists of several piezoelectric cantilever beams, each of which resonates at a specific frequency within the daily acoustic band (500 Hz – 2600 Hz). Consequently, the device provides mechanical filtering and shows a clear frequency selectivity mimicking the operation of the cochlea. Experimental results show that the voltage output of the device exceeds the minimum required sensing voltage for the neural stimulation circuitry and decreases the required power for readout circuitry.

Expected to satisfy all the requirements (volume, mass, area, and stimulation signal at hearing band) of FICI applications for the first time in the literature, the fabricated device has a groundbreaking nature and it can be referred to as the next generation FICIs since it revolutionizes the operational principle of conventional CIs.

Keywords: Cochlear Implants, Multi-channel Sensor, Thin Film Piezoelectric, MEMS, Acoustic Transducer, PLD-PZT

ÖZ

KOKLEAR İMPLANT UYGULAMALARI İÇİN MEMS İNCE FİLM PİEZOELEKTRİK AKUSTİK DÖNÜŞTÜRÜCÜ

İlik, Bedirhan

Yüksek Lisans, Elektrik ve Elektronik Mühendisliği Bölümü

Tez Yöneticisi: Prof. Dr. Haluk Külah

Ekim 2018, 101 sayfa

Bu tezde, yeni nesil tamamen implante edilebilir koklear implantların geliştirilmesi için kulak zarına yerleştirilecek çoklu-frekans yapılı ince film piezoelektrik akustik sensör konsepti önerilmiştir. Tasarım, her biri günlük akustik bandın içindeki belirli frekanslarda rezonansa giren ince film piezoelektrik tramplen yapılardan oluşmaktadır. Cihaz, doğal işitme mekanizmasının işlevsel parçalarını kullanacak ve piezoelektrik dönüştürücüler tarafından üretilen, kokleadaki işitsel nöronları uyaracak olan sinyali ara-yüz elektronikleri aracılığıyla işitme tüylerinin işlevini taklit edecektir.

Sinirlerin uyarılması için yeterli voltajı elde etmekteki temel sınırlamalar: orta kulaktaki sınırlı hacim (<0.1 cm^3), kütle toleransı (<25 mg), kulak zarının alanı (9 mm × 10 mm) ve akustik bandın (250-5000 Hz) yeterli sayıda kanal ile kapsanmasıdır. Bu doğrultuda, koklear implantların temel engellerini aşmak üzere hacim, kütle, alan ve uyarı sinyali kısıtlamaları düşünülerek, çoklu frekans yapılı ince film piezoelektrik akustik sensörün modellemesi, tasarımı ve optimizasyonu ortaya koyulmuştur. Akustik algılamadaki üstün ferroelektrik ve piezoelektrik özelliklerinden ötürü diğer ince filmli piezoelektrik alternatifleri arasından Darbeli Lazer Depozit (PLD) Kurşun Zirkonat Titanat (PZT) tercih edilmiştir.

Önerilen yapının elverişliliğini göstermek amacıyla tek-tramplen yapılı ince film PLD-PZT dönüştürücü üretilmiştir. Üretilen cihaz, esnek bir parilen taşıyıcı üzerine yerleştirilmiş ve kulak zarının çalışmasını taklit eden parilen bir zar üzerine yapıştırılmıştır. Mekanik, elektrik ve akustik özellikler standart bir sarsıntı masası ve daha gelişmiş bir akustik düzenek ile ilk kez karakterize edilmiştir. Çıkış voltajı osiloskop ile ölçülürken ince zar üzerine bağlanan sensörün ivme özelliği, bir Lazer Doppler Titreşimölçer (LDV) kullanılarak elde edilmiştir. Tek kanallı cihaz 110 dB Ses Basıncı Seviyesi (SPL) ile 1325 Hz frekansında uyarıldığında 114 mV büyüklüğünde bir maksimum voltaj çıkışı elde edilmiştir. Analiz sonuçları göstermektedir ki cihazın voltaj çıktısı sinirsel uyarma devresi için gereken minimum duyma voltajını (100 μV) fazlasıyla aşmıştır.

Üretilen tek kanallı prototip analiz sonuçları ile %92 oranında uyum gösteren sonlu elemanlar yöntemi ile modellenmiştir. Bu modele dayanarak bir çoklu-frekans yapılı ince film piezoelektrik akustik sensör tasarlanmıştır. Dönüştürücülerin toplam hacmi, kapladığı alan ve kütlesi sırasıyla $5 \times 5 \times 0.2$ mm^3, 5×5 mm^2 ve 12.2 mg'dır.

Tasarlanan çoklu prototip üretilip karakterize edilmiştir. Elektromekanik özellikler bir bir sarsıntı masası ve LCR metre ile ölçülmüştür. Test sonuçları göstermektedir ki üretilen cihaz her biri günlük akustik bandın (500 Hz – 2600 Hz) içindeki belirli frekanslarda rezonansa giren çoklu film piezoelektrik tramplen yapıdan oluşmaktadır. Sonuç olarak cihaz mekanik filtreleme gerçekleştirmekte ve kokleanın görevini taklit ederek net bir frekans seçilimi göstermektedir. Deneysel sonuçlara göre cihazın voltaj çıkışı, nöral uyarım devresi için gerekli minimum duyma voltajını aşmakta ve okuma devresi için gerekli gücü azaltmaktadır.

Tez kapsamında üretilen cihaz FICI uygulamalarının, hacim, kütle, alan ve işitme bandında uyarım sinyali olarak özetlenebilecek, tüm gereklerini literatürde ilk kez karşılamıştır. Çığır açan doğasıyla geleneksel koklear implantların çalışma prensibine köklü bir değişim getirdiği için yeni nesil FICI olarak anılabilir.

Anahtar Sözcükler: Koklear İmplant, Çok Kanallı Sensör , İnce Film Piezoelektrik, MEMS, PLD-PZT, Akustik Sensör

To My Family

ACKNOWLEDGMENTS

I would like to express my deep thanks to my thesis advisor, Prof. Dr. Haluk Külah, for the support and guidance he gave me during my graduate study and also for giving me the opportunity to work on an exciting project. I would also like to thank Prof. Dr. Tayfun Akın for his contributions and supports during my studies.

I specially thank to my project-partner Aziz Koyuncuoğlu for the valuable times to work with them and for their help in any respect. It was true fun to have enjoyable times in daily life and at work and brainstorming with Aziz.

I am also thankful to my new project partners Berat Yüksel, Salar Chamanian and Hasan Uluşan for their immense contributions to the project and this thesis study. I would like to express my gratitude to Dr. Özlem Sardan Sukas for her patience and helps during my thesis especially in writing phases. I would like to also thank to all members of BioMEMS research group for their collaborations and supports, but most importantly for their sincere friendship. In no specific order, I am thankful, Berkay Çiftci, Akın Mert Yılmaz, Furkan Gökçe, Mahmut Kamil Aslan, Eren Aydın, Mustafa Kangül, Begüm Şen Doğan, Parinaz Ahsrafi, Gürhan Özkayar, Zeynep Çağlayan, Yağmur Demircan, Kaan Sel, Didem Çetin, Andaç Yiğit, Alper Kaan Soydan, Meltem Aydın, Yasemin Engür, Ceren Özcan, Dilek Işık, Metin Dündar Özkan, Oğuz Yaşar and Kaveh Gharehbaghi. My special thanks go to Taylan Berkin Töral and METU-MEMS Center staff for their kind helps in the cleanroom. Many thanks particularly to Orhan Akar for sharing his deep knowledge on microfabrication and for his helps in the cleanroom.

I am deeply thankful to Cem Şahiner, Deniz Şengül and Bahaattin Taşkın for their endless supports. I am deeply thankful to (IQ's) Pınar Akıncı, Ergün Kar, Ceyda Taşçıoğlu, Lütfi Boyacı, Merve Seren, Damla Özel and Can Carlak, for such a great friendship more than eight years in ODTÜ.

Kaan Hakan, İrem Aksoy, Onur Koyuncu, Arda Deveci, Gökhan Gültepe, Ozan Ağma, and Okan Altıngövde also deserve thanks for their priceless friendships. I would also

like to (L1's) Utku Civelek, Sezil Solta, Berat Can Cengiz, Cemre Cingöz and Anıl Öztürk for their endless motivation.

My special thanks go to Özge Güven not only for her support in the duration of this thesis but also for her love, motivation, faith and advices. She believed in me in every respect and I was not be able to do this without her supports.

Finally, I would like to express my deepest gratitude to my parents Hüseyin and Sakine İlik and my sisters Nazlıcan and Berivan for their never-ending support, encouragement and unconditional love through all my life.

This work has received funding from the European Research Council (ERC) under the European Union's Horizon 2020 research and innovation programme (grant no:682756

TABLE OF CONTENTS

LIST OF TABLES

TABLES

LIST OF FIGURES

FIGURES

LIST OF ABBREVIATIONS

CI	Cochlear Implant
DRIE	Deep Reactive Ion Etching
FEA	Finite Element Analysis
FICI	Fully Implantable Cochlear Implants
IPA	Isopropyl Alcohol
MEMS	Microelectromechanical Systems
PDE	Partial Differential Equation
PDMS	Polydimethylsiloxane
PLD	Pulsed Laser Deposited
PZT	Lead Zirconate Titanate
SEM	Scanning Electron Microscope
SPL	Sound Pressure Level

CHAPTER 1

INTRODUCTION

The loss of hearing and its impairment have been believed to be one of the biggest mystery in human history for centuries. It was not until 200 years ago that Ludwig van Beethoven had written in a letter to his friends “For two years I have avoided almost all social gatherings because it is impossible for me to say to people 'I am deaf'. If I belonged to any other profession it would be easier, but in my profession, it is a frightful state." Beyond composing without hearing a note, Beethoven grappled with living in the 1800s when few understood deafness, hindering his ability to communicate, to work as a musician and even to find a place to live. Once Donato Cabrera, the music director of California Symphony, described the Beethoven situation as “How he dealt with this deafness is one of the great stories of humanity, not just of music”. His deafness forced him to become a very special and exclusive person throughout his life.

It is obvious that hearing loss has a significant impact on people’s social, emotional, and economic well-being. The tragedy of the situation was described as “…inhuman silence which separates and estranges…” by the famous blind-deaf writer, lecturer, and social advocate, Helen Keller (1880-1968).

In those times when Beethoven and Keller suffered from hearing loss, most probably they would not believe that it was a solvable problem. In fact, it was believed that only a miracle could cure deafness and the stories which told defeating the “inhuman silence” were the unreal stories. However, do not forget that there are two kinds of stories: the real stories and the stories which are supposed to come true.

First giant strides of this miraculous story have been started in Como, Italy 200 years ago by the inventor of battery, Alessandro Volta. Volta had a crazy idea in which he first attempted to use of this newfound source of electricity to stimulate hearing. During an experiment he placed one of the two ends of a 50-volt battery in each ear and described his observation with a "…crackling and boiling sensation…" He wrote the following sentences:

"At the moment when the circuit was completed, I received a shock in the head, and some moments after I began to hear a sound, or rather noise in the ears, which I cannot well define: it was kind of crackling with shocks, as if some paste or tenacious matter had been boiling. The disagreeable sensation, which I believe might be dangerous because of the shock in the brain, prevented me from repeating this experiment." [1]

Volta's experiment sparked crude applications of electric stimulation all over Europe. For more than 150 years, scientists continued to investigate the subject, seeking ways to improve the hearing of both old and young. Many scientists studied the problem and conducted experiments. However, their work achieved varying degrees of success, and the results were inconclusive.

This chapter presents the details of the centuries-long challenge for finding a solution to hearing loss. It starts with the basics of ear anatomy, hearing mechanism, and deafness. Then, the main drawbacks of conventional cochlear implants are pointed out. Later, a literature survey on implantable sensors is presented. Finally, the motivation, the research objectives, and the organization of the thesis are given.

1.1. Ear Anatomy and Hearing Mechanism

Cochlea, ossicles, and eardrum together form one of the most elaborated structures in mammalians. It provides a very large frequency selectivity (20 Hz – 20 kHz) and sound perception (0-140 dB SPL), which makes the ear the best acoustic sensor in nature.

This delicate structure converts acoustic sound waves into electrical signals that are transferred through the auditory system. The auditory system is mainly composed of two sections. The first section is called the peripheral auditory system which is composed of the outer ear, middle ear, and inner ear (Figure 1.1).

Hearing mechanism starts at the outer ear, which is the only visible part of the auditory system, and responsible from directing sound waves into the eardrum through the ear canal. The pinna (auricle) is the first part of the outer ear and helps sensing of the pressure differences between inside and outside the eardrum. The pinna transmits these sensed sound waves to the eardrum (tympanic membrane) through the ear canal (auditory canal). Sound waves travel a distance of 2.5 cm through the length of ear canal, during which the sound signals are amplified up to 12 dB Sound Pressure Level (SPL) depending on the oscillation frequency of sound.

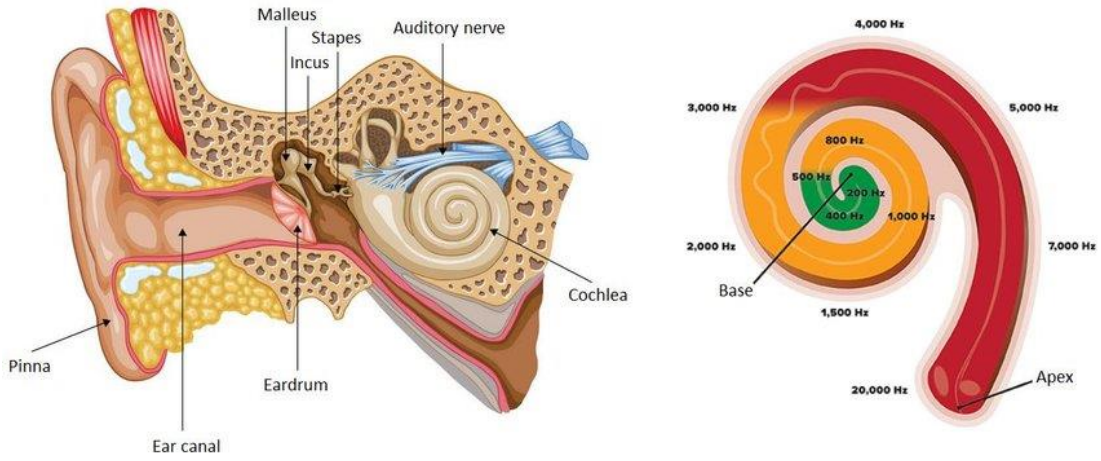

Figure 1.1 The auditory system (left) and the cochlea frequency distribution within the cochlea (right) [2].

Hearing mechanism continues at middle ear with the eardrum, which is the end section of the ear canal. The eardrum basically converts amplified acoustic sound waves into mechanical vibrations depending on the frequency of the incoming sound.

Then, the generated mechanical vibrations are transferred to the cochlea by a series of ossicles, which are the smallest bones in the human body. The ossicles help amplification of the sound waves by nearly two times. The first bone, malleus, is attached to the mobile portion of the tympanic membrane (eardrum) and transmits the mechanical vibrations of the membrane produced by sound waves. The incus connects the malleus and stapes, and work as a bridge between them.

The three bones are arranged so that they work as a lever mechanism and amplify the mechanical vibration during their motion caused by the movement of the tympanic membrane. The end section of the stapes is termed as footplate and, it causes movement of the fluid within the cochlea when it pushes on the oval window. Oval window has 17 times smaller area than the ear drum which enables the transfer of acoustic vibration from air to liquid medium of the cochlea. The main amplification is due to the 30 fold area reduction from tympanic membrane (55 mm^2) to the oval window (3.2 mm^2) [3].

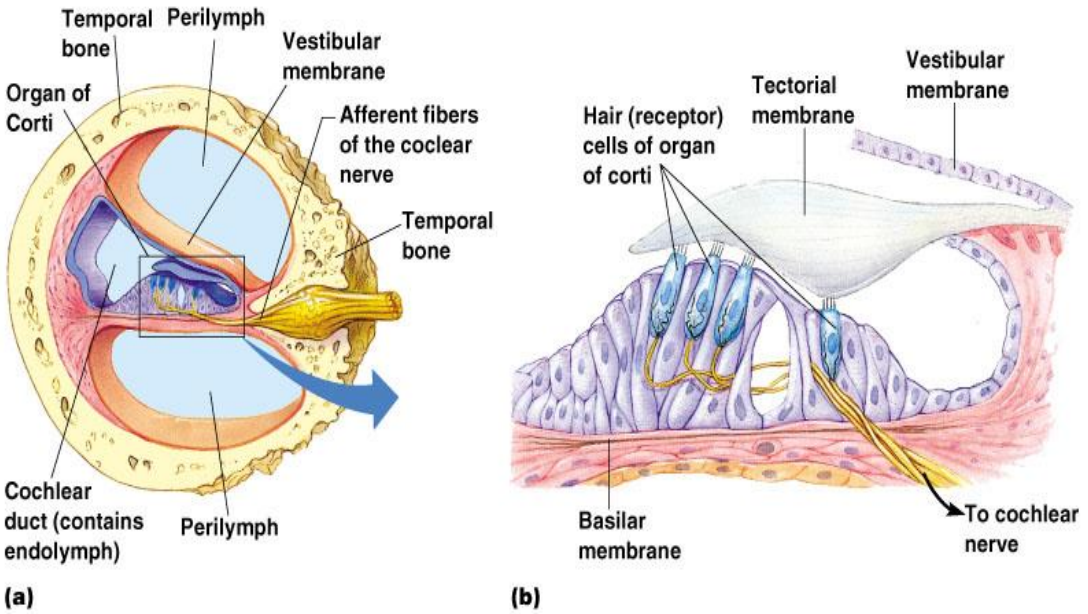

Figure 1.2 A detailed image of the cochlea (a), the organ of corti and the hair cells (b) [4].

Figure 1.2 (a) shows the cross-sectional view of the cochlea, a snail-shaped cavity filled with fluid, which transfers the mechanical vibrations into the cochlear fluids. The cochlea is a 2.5-turn spiral shaped and responsible from the frequency discrimination of the incoming sound. Pressure variations within the cochlear fluids leads to oscillations of a basilar membrane. These oscillations contain information about the acoustic sensing frequencies ranging from 20 Hz to 20 kHz. Depending on the frequency of the sound, specific portions of the basilar membrane resonate, and the resonating portion causes movement of the hair cells at that section.

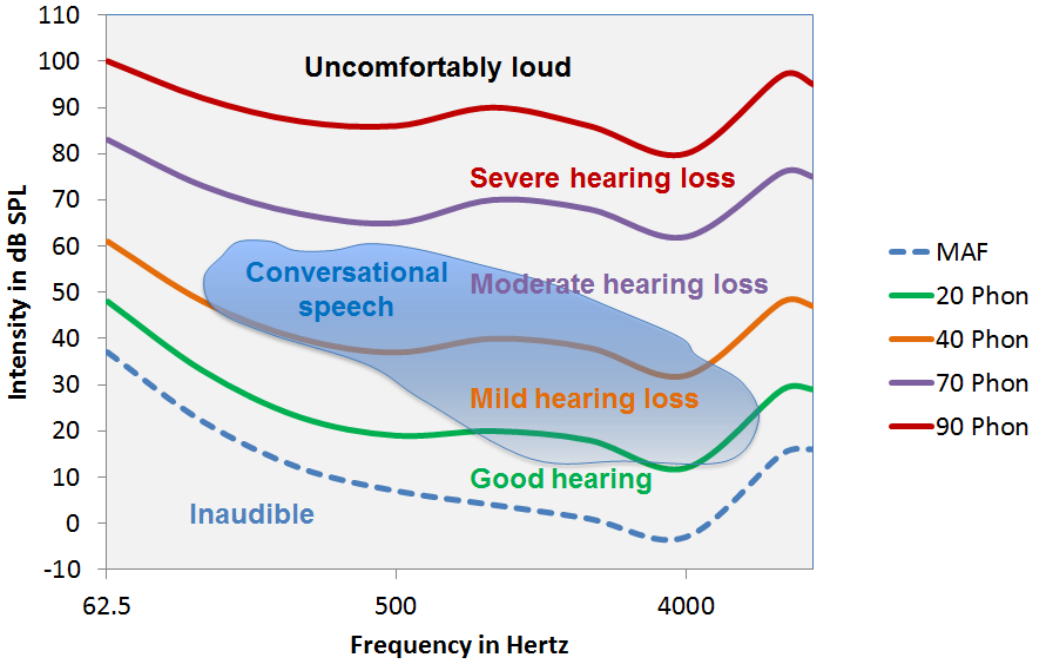

Figure 1.3 Frequency distribution of speech perception in different sound pressure levels and hearing thresholds of ear [5], where Phon is unit of loudness level (dB SPL).

The organ of corti which has sensory cells called hair cells, is placed on the basilar membrane (Figure 1.2 (b)). The function of the hair cells is to generate electrical potential when a sound wave is received. Deflection of the hair cells causes positively charged ions to enter the cell. Outer hair cells provide positive mechanical feedback amplification, named as cochlear amplification. On the other hand, inner hair cells generate an electrical stimuli from fluid pressure. Voltage is generated resulting in the

stimulation of the auditory nerve. Stimulation signals are transferred to the central auditory system, and finally, incoming sound is heard by brain.

Therefore, the cochlea acts like a spectrum analyzer and decomposes the complex sound into its frequency components. Figure 1.3 shows the frequency distribution of speech perception, and hearing thresholds of the human ear at different sound pressure levels (SPLs).

To summarize, in a healthy ear, the eardrum (tympanic membrane) vibrates with the sound waves coming through the ear channel (auditory canal). External ear (pinna and auditory canal) amplifies the incoming sound waves according to the incoming wave frequency, where the maximum amplification is around 12 dB. Eardrum is connected to the ossicles in the middle ear, which add further amplification to the sound vibration using a lever-like mechanism. This amplification by the ossicles is required to compensate the energy loss due to the interface between the media of air in the middle ear and the liquid media in the cochlea (inner ear). This loss amounts to a decrease in sound energy of approximately 30 dB. If the middle ear did not exist and the membranous entrance of the fluid-filled inner ear (oval window) replaced the eardrum, sound waves carried in the air would impinge directly on the fluid-filled inner ear.

1.2. Deafness and Hearing Impairments

This delicate structure of the cochlea makes it prone to degradation without recovery. Approximately 15% of the world's adult population has some degree of hearing loss according to the World Health Organization (WHO). In total, there are 360 million people living with a hearing loss to SPLs higher than 40 dB as of 2015, where 32 million of these patients are children [6]. Deafness is a partial or total inability to hear, and the level of hearing loss can be classified as mild, moderate, severe or profound as shown in Figure 1.3. For mild-to-moderate hear loss, the sound waves do not reach the cochlea due to ear canal malfunction in ossicles or eardrum. For mild-to-moderate damage, a hearing aid can be used to restore the hearing loss with sound amplification

[7]. On the other hand, sensorineural impairment, which represents the majority of the profound deafness, cannot be restored using hearing aids.

Sensorineural deafness is caused by an irreversible damage to the hair cells, thus a hearing impairment. Figure 1.4 shows the anatomical differences between a healthy and a deafened ear. In the healthy ear (Figure 1.4 (a)), hair cells are connected to the central nervous system with spiral ganglion cells. On the other hand, there is no connection between hair cells and central auditory system for a deafened person.

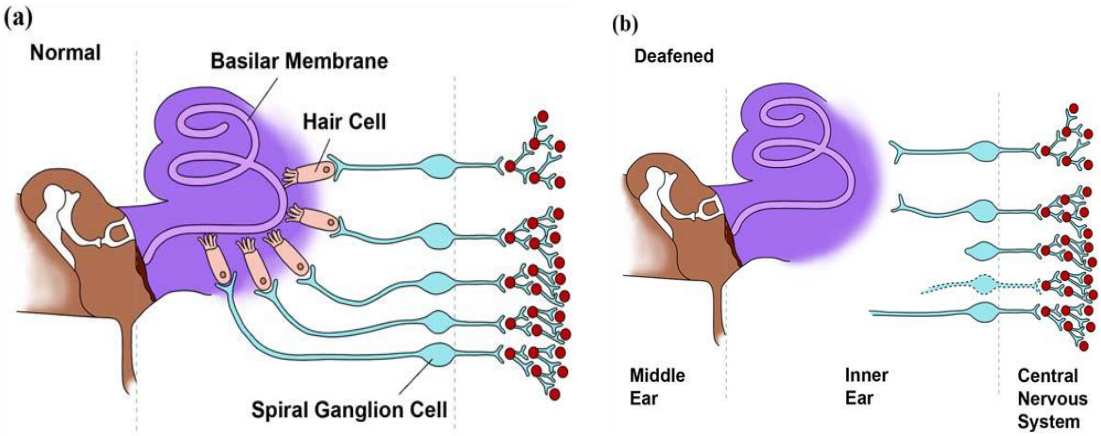

Figure 1.4 Hair cell connections in normal (a) and deafened ear (b) [8].

A schematic of a modern CI is presented, and its operation principle is described in Figure 1.6. The overall system is mainly composed of two units: external and internal. The external unit includes a microphone that picks up the sound and converts to a digital signal. The digital signal is then processed by a speech processor and encoded into an RF signal. The RF signal is sent to the transmitter coil through a power amplifier.

Cochlear Implants (CIs) can be utilized for the treatment of severe-to-profound hearing loss (>90 dB sound pressure level (SPL) in both ears) caused by irreversible damage of the hair cells [9]. Figure 1.5 shows an illustration of cochlear implants (CIs), which electrically stimulate the auditory nerve to repair hearing in people with severe-to-profound hearing. By this means, the cochlear implant is one of the most successful

neural prosthesis, which uses electrical stimulation to provide a functional hearing at the degradation or absence of sensory hair cells in the inner ear. CIs operate by directly stimulating the auditory nerve, bypassing the damaged hair cells, ossicles, and eardrum. CIs are used for more than 40 years and today implanted in around 220.000 individuals worldwide.

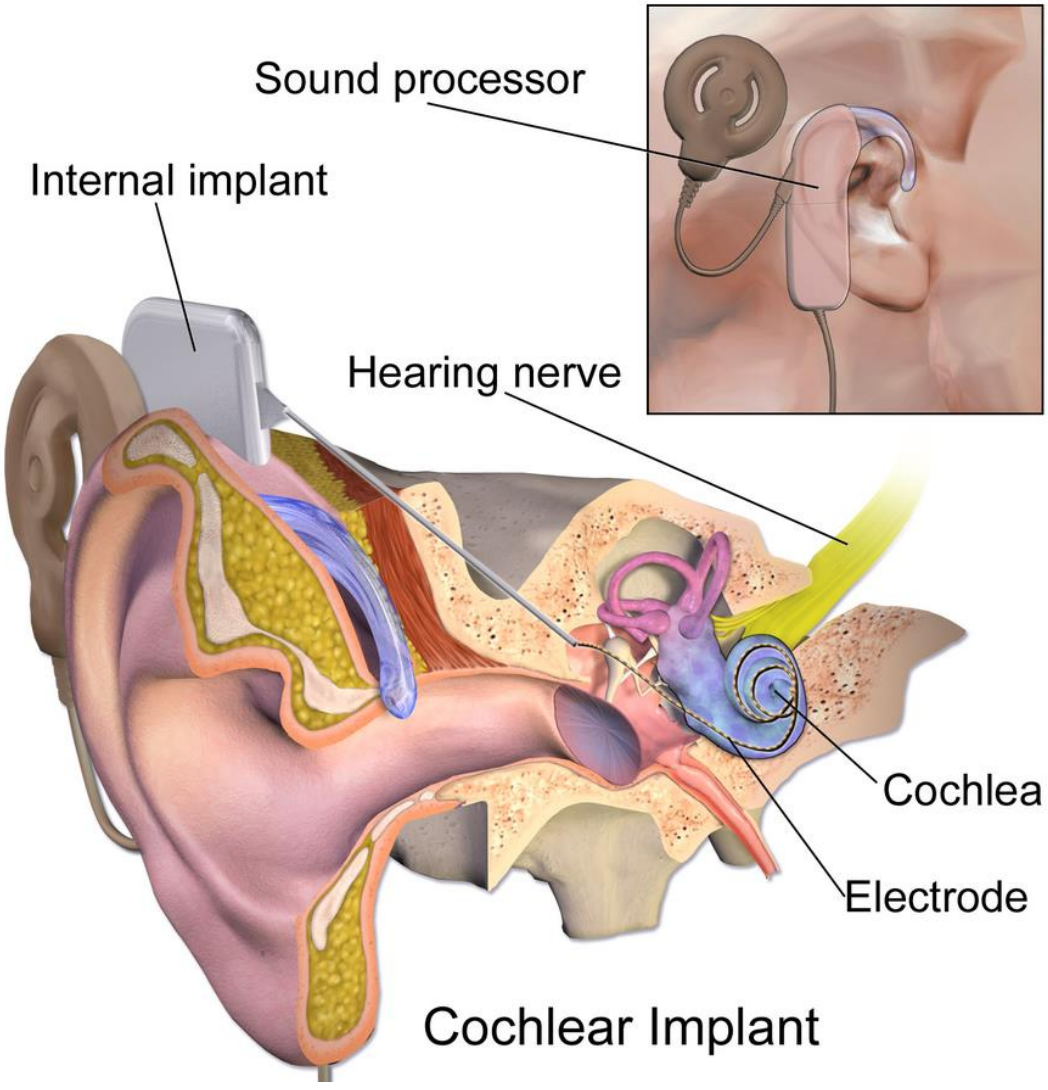

Figure 1.5 An illustration of conventional cochlear implants showing the external and internal components [10].

The transmitted RF signal is received by a receiver coil at the internal unit. The information at the signal is then decoded and used for generating an electric current at the stimulator. The generated electrical signals are sent to the appropriate electrodes, which are wires threaded along the cochlea and used for stimulating the auditory nerves within the inner ear. The power required by the decoder and the stimulator blocks is provided by a power unit, which uses the received RF signal to generate the required energy.

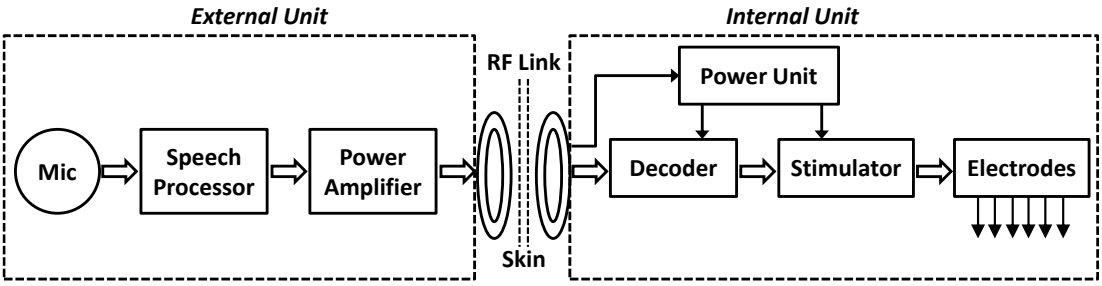

Figure 1.6 Block diagram of a modern cochlear implant system.

Modern cochlear implant systems also include a patient fitting option to adjust the stimulation current level according to the needs of the patient. The speech processor holds the patient-specific information that can be modified using a by a PC through a user interface [11], [12].

However, conventional CIs have major drawbacks such as replacement of the entire natural hearing mechanism with electronic hearing, even though most parts of the hearing system (such as the eardrum and ossicles) are operational. Moreover, daily battery recharge/replacement requirement, damage risk of the external components especially if exposed to water (e.g. shower, rain, swimming, etc.), and aesthetic concerns, particularly for children and young adults, are other critical drawbacks. Therefore, researchers in this field try to eliminate these problems via fully implantable, self-powered, and stand-alone cochlear implants.

1.3. A General Review on Implantable Sensors

Recent advancements in the field point out that the solution of the above-mentioned issues lies in the fully implantable sensors for next-generation cochlear implant systems. Implantable sensors in the literature show a great variety in terms of placement of sensors, used transduction mechanism, and sensor type. Each of these sensors responds to critical requirements and challenges of conventional cochlear implants. Figure 1.7 shows the different types of implantable sensors available in the literature in terms of transduction mechanism and sensor type.

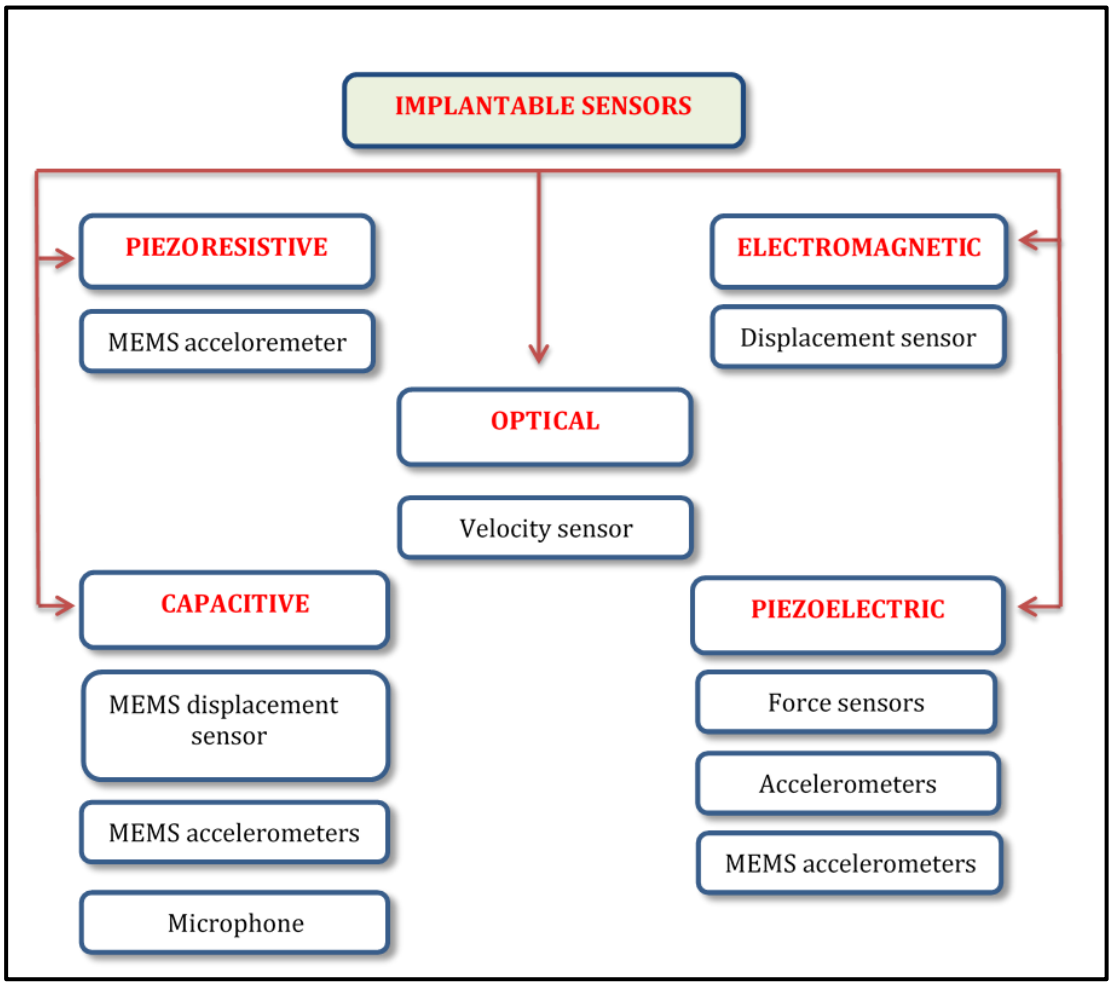

Figure 1.7 Classification of available implantable sensors in terms of transduction mechanism and sensor type.

The first classification of implantable sensors is based on the transduction mechanism, which could be piezoresistive [13], optical [14], [15], electromagnetic [16], capacitive [17]–[21] and piezoelectric [22]–[25]. Next classification is based on the implanted sensor type that can be used as an accelerometer, displacement sensor, force sensor, and microphone.

Piezoresistive MEMS-based accelerometers are the first alternative for implantable sensors. Earlier studies mainly focused on MEMS-based piezoresistive accelerometer based acoustic sensors [13] in 2007. Figure 1.8 shows the detailed description of the measurement setup, where the accelerometer utilizes the natural mechanical conduction mechanism in the middle ear as it is attached to the ossicles in the middle ear. The fabricated piezoresistive sensor has been placed to the incus, presenting the first prototype for a totally implantable hearing device in the literature.

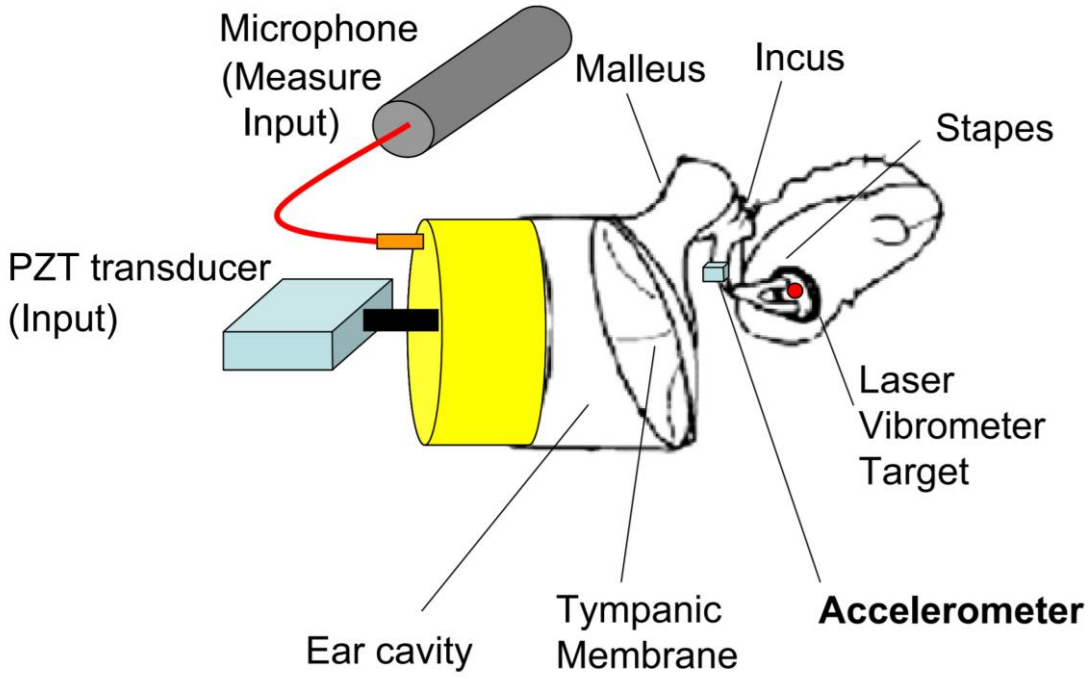

Figure 1.8 A schematic view of the piezoresistive measurement setup using a human cadaveric temporal bone [13].

Optical velocity sensors were also used as alternative approaches for implantable sensors. Recently, Vujacic et al. improved an optical sensor prototype to use an optical fiber providing laser beam radiation for measuring the vibration level of the tympanic membrane [14]. Contactless measurements without any mechanical interaction with the sensors is the main advantage of the proposed device. However, the optical sensor suffers from high power consumption. In another study, Djinovi et al. proposed a similar application of implantable optical sensor that measures the vibration level of the ossicles using a contactless fiber-optic interferometry [15]. Figure 1.9 shows the schematic of the fiber optic interferometry system. By performing in vitro and in vivo animal experiments, they demonstrated that the proposed system can accurately measure the vibration level inside the middle ear.

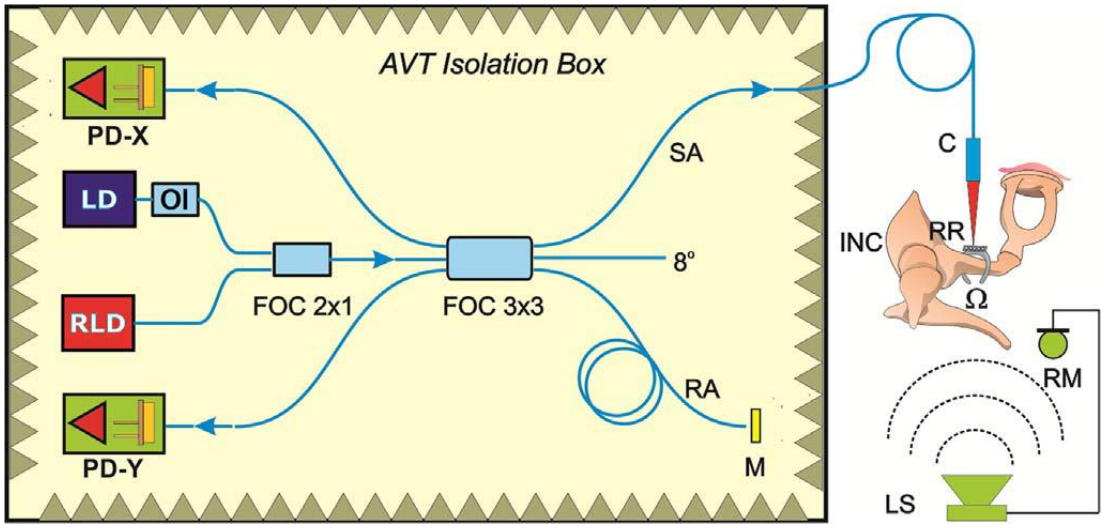

Figure 1.9 Schematic of the fiber optic sensing configuration [15].

Electromagnetic displacement sensors are another promising alternatives for implantable sensor applications. In 2001, Maniglia et al proposed a 29 mg electromagnetic displacement sensor for a totally implantable cochlear implant application [16]. The device is encapsulated with titanium and placed at 1 mm distance from the magnet of the system. Although the system provides an efficient implantable

sensor, they have a limited output voltage and an undesirably high system noise. Such systems also require external control and RF battery charging units [26].

Capacitive transduction mechanism is another application of implantable sensors and widely used in recent studies [16]–[20]. In a recent study, Ko et al proposed an accelerometer-based capacitive implantable middle ear microphones for next-generation CIs that is attached on umbo [27]. The structure is shown in Figure 1.10 and they manage to measure the displacement at umbo using a Laser Doppler Vibrometer (LDV) system [17]. MEMS capacitive accelerometers can also be used as implantable sensors [28] as shown in Figure 1.11, but they lack sensitivity and suffer from high power consumption.

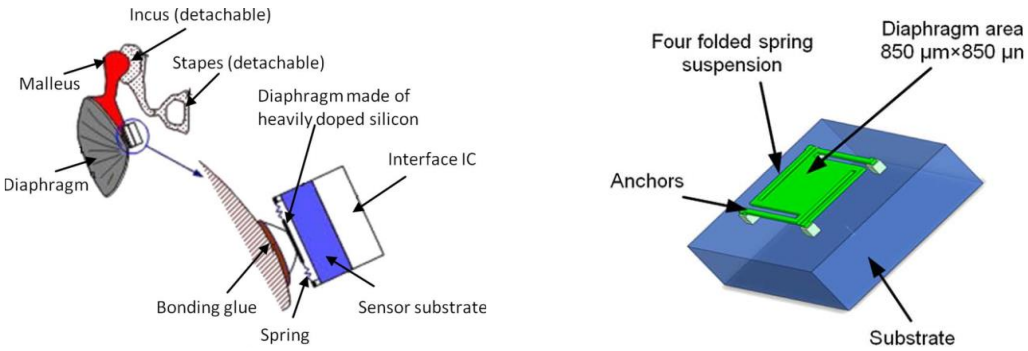

Figure 1.10 Concept of a capacitive displacement sensor structure and its assembly on the umbo [17].

Among other transduction mechanisms, piezoelectric transducers are widely used to convert mechanical vibrations directly into electricity without the need for an external source [29]. Compared to conventional cochlear implants, the stimulation electrodes of the piezoelectric transducers are inserted into the liquid medium within the cochlea and the hair cells are directly stimulated with an electrical charge.

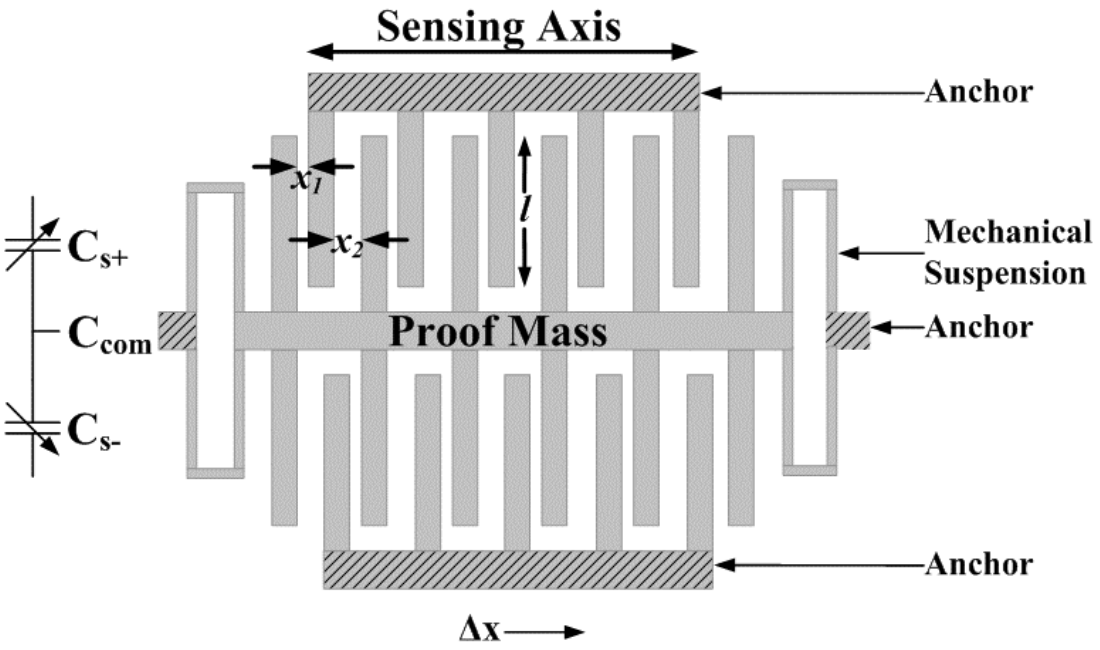

Figure 1.11 MEMS capacitive accelerometer prototype architecture [28].

The acoustic sound can be collected and converted to electrical energy with the vibration of the tympanic membrane by a piezoelectric sensor. Since the wave propagation at the cochlea is not utilized in this setup, the mechanical amplification of the ossicles can be disregarded.

Figure 1.12 shows an accelerometer type piezoelectric sensor to be used for an implantable sensor. However, the device has an enormous mass (67 mg) that is not feasible for implantation [22].

Although piezoceramic devices have been proposed as promising alternatives for CI applications [23], [24] there are still major scientific and technical challenges. Recently, Jang et al. reported successful use of a piezoelectric cantilever array for stimulation of the auditory neurons in deafened guinea pigs [25]. Yet, the maximum output voltage obtained (<50 μV) is well below the lower limit that could be detected by an interface circuit without external amplification. Furthermore, the working

frequency of the implemented sensor does not cover the audible frequency range for humans.

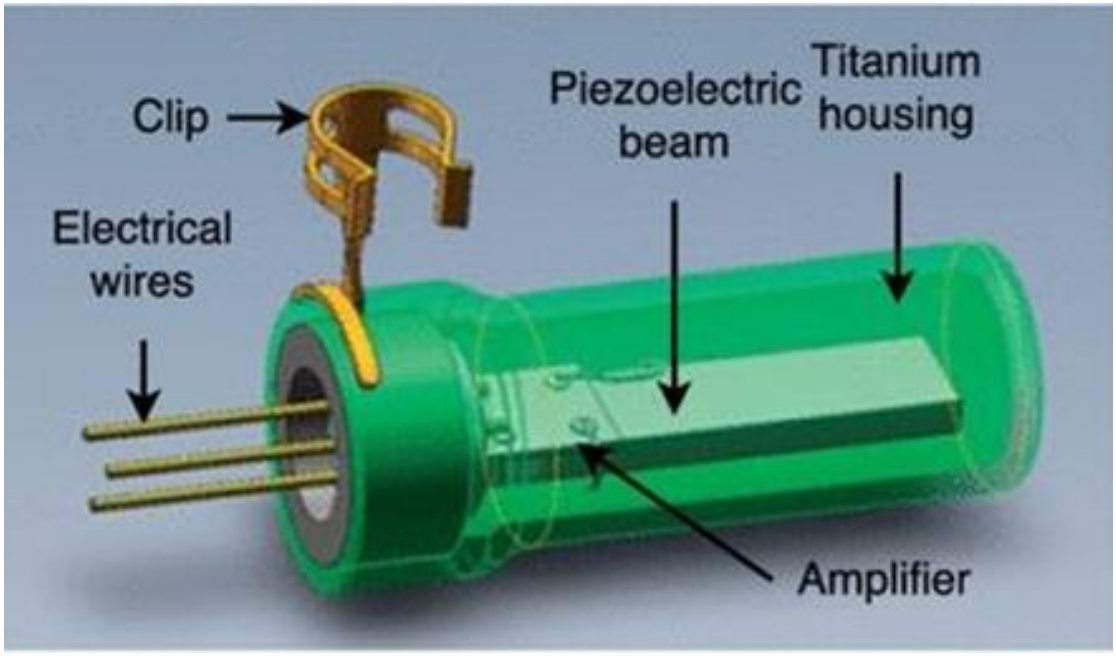

Figure 1.12 Schematic of the piezoelectric accelerometer [22].

1.4. Research Objectives and Thesis Organization

The feasibility of piezoelectric transduction due to the eardrum vibrations has already been demonstrated in the literature [25]. However, implementation of the method to next-generation CIs still has significant challenges and requires an advanced design procedure.

In this thesis, a multi-frequency thin film piezoelectric acoustic sensor transducer concept has been proposed to overcome the main bottlenecks of conventional cochlear implants considering the limitations regarding volume, mass and stimulation signal. The sensor is to be placed on the eardrum for fully-implantable cochlear implant (FICI) applications. The design consists of several thin film piezoelectric cantilever beams, each of which resonates at a specific frequency within the daily acoustic band. The

device will exploit the functional parts of the natural hearing mechanism and mimic the function of hair cells in the cochlea, where the signal generated by the piezoelectric transducers will be processed by interface electronics to stimulate the auditory neurons. Expected to satisfy all the requirements (volume, mass, and stimulation signal at hearing band) of FICI applications for the first time in the literature, the proposed concept has a groundbreaking nature. Also, it can be referred to as the next generation of FICIs since it revolutionizes the operational principle of conventional cochlear implants.

The overall objectives of this thesis are summarized as follows:

a. Proposing a multi-frequency thin film piezoelectric acoustic transducer system that demonstrates the feasibility of the next generation cochlear implants. The proposed sensor:
    - is to be placed on the eardrum.
    - consists of several cantilever beams, each of which resonates at a specific frequency within the daily acoustic band.
    - exploits the functional parts of the natural hearing mechanism.
    - mimics the function of hair cells.
    - generates AC signals that will be processed by interface electronics to stimulate the auditory neurons in the cochlea.

b. Design, modeling, and optimization of a thin film Pulsed Laser Deposited (PLD) piezoelectric acoustic transducer. Design should satisfy:
    - enough number of channels to cover daily acoustic band.
    - the footprint of the eardrum and limited volume of the middle ear.
    - limited mass of the transducer.

- to generate the maximum stimulation signal for neurons.

c. When modeling of the thin film Pulsed Laser Deposited (PLD) piezoelectric acoustic transducer:

    - material parameters of the thin film PLD-PZT and silicon should be included in the simulations.

    - anisotropic properties of piezoelectric and silicon material, and boundary conditions in between should be modeled carefully.

    - a parametric model should be considered to optimize the design parameters that satisfy the requirements.

d. When fabricating the thin film Pulsed Laser Deposited (PLD) piezoelectric acoustic transducer:

    - Pulsed Laser Deposited lead zirconium titanate (PLD-PZT) has been considered to be able to satisfy system limitations and maximize the generated output voltage.

    - an optimized fabrication flow replacing bulk PZT with PLD-PZT should be developed.

    - PLD-PZT wet etch and platinum wet etch techniques should be optimized.

e. During the characterization of thin film Pulsed Laser Deposited (PLD) piezoelectric acoustic transducer:

    - a single channel thin film piezoelectric acoustic sensor (PLD-PZT) prototype should be characterized in the acoustical, mechanical and electrical domain.

    - experimental analysis of multi-channel thin film piezoelectric acoustic sensor should be completed.

- a comparison between experimental and simulation results should be to verify the feasibility of the proposed structure.

The thesis is organized as follows:

Chapter 2 explains the design, modeling, and parametric optimization of proposed multi-frequency thin film piezoelectric acoustic sensor. The chapter starts with the details of the proposed application and elaborates on the main limitations and requirements of the system. Next, preferred piezoelectric thin film material, pulsed laser deposited (PLD) PZT, and its properties are presented as an alternative satisfying all the requirements. The chapter continues with the details an optimization of the design parameters using finite element modeling. Finally, the chapter ends with the explanation of the relation between acoustic sound and acceleration level.

Chapter 3 explains the fabrication procedure of the single and multi-channel thin film piezoelectric acoustic sensor. The chapter starts with the fabrication flow of single-channel thin film sensor using pulsed laser deposited (PLD) as a piezoelectric layer. The chapter continues with the fabrication of a flexible parylene carrier to be used in acoustic experiments. Next, fabrication of the 1st generation multi-channel thin film transducer is elaborated in detail, which is continued with the 2nd generation multi-channel thin film transducer. The chapter conclude with the identification of the problems of the fabrication and achieved solutions to the problems.

Chapter 4 presents the experimental results of the fabricated single and multi-channel thin film piezoelectric acoustic sensor. First, various experimental setups are introduced for characterization and verification of the thin film piezoelectric sensors. Then, mechanical and acoustical experimental results of fabricated single channel piezoelectric devices are presented and discussed. The chapter continues with the verification of the developed device comparing the experimental results with the simulation results. Finally, mechanical and electrical experimental results of 1st and 2nd generation multi-channel thin film piezoelectric sensors are presented in detail.

The last chapter, Chapter 5, summarizes the overall work and highlights the key points of the thesis. The chapter is concluded with the governing idea, future works, and suggestions on the related to the research topic.

Moreover, Appendix summarizes the mask layout of the designed multi-channel thin film piezoelectric acoustic transducer structure in wafer level.

CHAPTER 2

DESIGN AND MODELING OF THIN FILM PIEZOELECTRIC ACOUSTIC TRANSDUCER

This chapter explains the design, modeling, and parametric optimization of proposed multi-frequency thin film piezoelectric acoustic sensor. The chapter starts with the proposed application in detail and then elaborates on the main limitations and requirements of the system. Next, the piezoelectric thin film material chosen for the application, pulsed laser deposited (PLD) PZT, and its properties are presented as a solution to next-generation cochlear implants. The chapter continues with the details of the finite element modeling and the specifications of the optimized design. The chapter concludes with the explanation of the relation between acoustic sound and acceleration vibration.

2.1. Proposed Application: Multi-Frequency Thin Film Piezoelectric Sensor

The feasibility of piezoelectric transduction due to the eardrum vibrations has already been demonstrated in the literature [25]. However, implementation of the method to next-generation CIs has significant challenges and requires an advanced design procedure to be followed considering several limitations.

In the proposed system, an array of the piezoelectric cantilevers will be mounted on the eardrum or ossicles for fully-implantable cochlear implant (FICI) application to provide the necessary signal for neural stimulation. Proposed multi-frequency thin film piezoelectric acoustic sensor concept to overcome the main bottlenecks of CIs, considering the limitations regarding footprint, volume, mass and stimulation signal.

The design consists of several thin film piezoelectric cantilever beams, each of which vibrates at a resonance frequency to cover the daily acoustic band.

The piezoelectric device, placed on the eardrum or ossicles, generates electricity with the vibration of hearing elements when an incoming sound impinges. The device will exploit the functional parts of the natural hearing mechanism and mimic the function of the hair cells in the cochlea. Each cantilever resonates at a different frequency. By this means, the transducers provide mechanical filtering. The piezoelectric output is then to be processed by an interface circuit and converted into stimulation pulses which are fed to the cochlear electrode. Finally, the auditory nerves in the cochlea are stimulated, and hearing is realized. The conditioning electronics is relatively simple and dissipates much less power since active microphone and front-end filtering are not required.

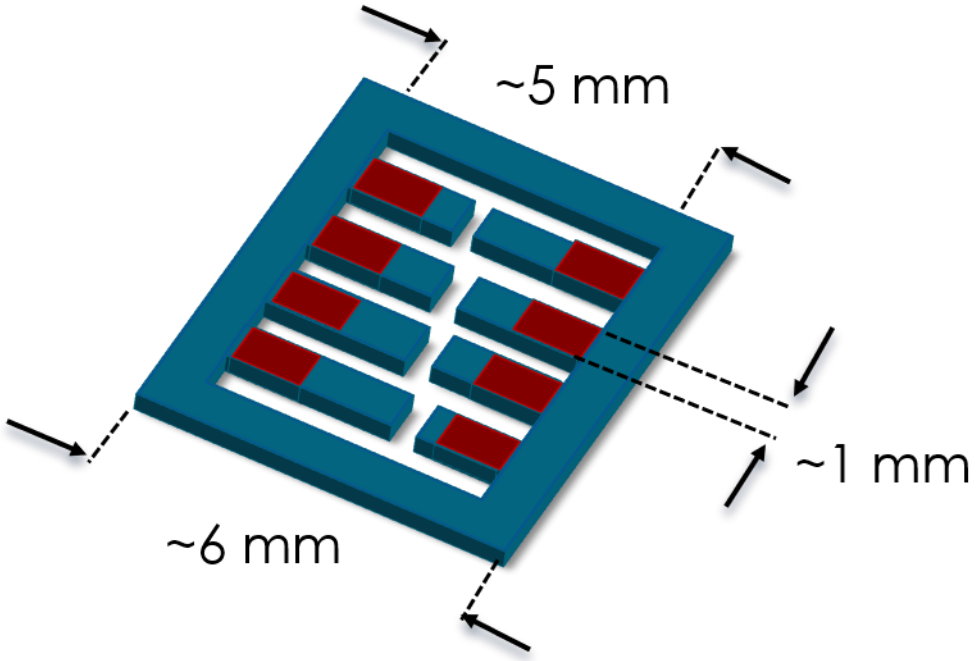

Figure 2.1 Structure of the proposed 8 channel thin film piezoelectric transducer.

2.2. Design Limitations and Requirements for Thin Film Piezoelectric Sensors

There are major challenges and limitations in the design of the piezoelectric cantilevers. These include minimum number of channels required, limited volume and footprint of middle ear and eardrum, level of the produced stimulation signal, and the total mass of the implanted device. Each of these will be analyzed and possible solutions will be discussed in detail as follows:

i. **Number of Channels:** The major challenge for designing a multi-channel piezoelectric transducer is covering the daily acoustic band with an adequate number of channels within the small volume of the middle ear. While the size of the device should be minimized, there should be enough number of transducers covering a meaningful range of acoustic frequencies.

   The quality of sound perception will typically be improved as the number of the channel increases, due to the increased resolution of stimulation frequencies. However, this also increases the hardware complexity and the power consumption. Therefore, a balance should be sought between the sound perception level and the power consumption.

   It has been reported that the average hearing performance increases up to 8 channels, and no further improvement is observed with higher numbers of electrodes (10- 20) [30], [31]. Furthermore, a recent study demonstrates that 8-channel FICI systems can operate with sub-mW power dissipation [20]. Considering these, an 8-channel transducer is considered to be good enough for the proposed design to cover the daily acoustic band (250 to 5000 Hz) and to provide adequate spectral resolution [32]–[34]. The optimization between the bandwidth and the quality factor should also be studied separately for each transducer. Besides, the operation band and other harmonics of each piezoelectric transducer should be well separated to avoid crosstalk.

ii. **Limited Volume and Footprint:** The limited footprint of the eardrum (9 mm × 10 mm) [35] and volume of the middle ear (<0.1 cm^3) [36] is one of the main challenges of the implantable sensors for obtaining an adequate voltage output for neural stimulation. Since the quality of the sound perception requires an 8-channel structure, there will be 8 piezoelectric transducers placed eardrum.

Beker et al. reported that use of bulk piezo-ceramics can generate a significant amount of energy [37], where a single-channel device occupies a minimum of 5×5 mm^2 footprint due to the impact of the relatively thick bulk piezoelectric layer on the design parameters. It is obvious that such a device in a multi-channel configuration cannot satisfy the eardrum footprint limitation. The footprint may be reduced by stacking the single-channel bulk transducers on top of each other. However, this stacked structure cannot fit into the designated volume and increases the mass of the transducer. Also, there will be coupling issue in this multi-stacked configuration.

iii. **The Total mass of the Transducer:** The mass tolerance (<25 mg) [17] of the eardrum is the most critical limitation for obtaining an adequate voltage output for neural stimulation. Moller [38] reported vibration characteristics of middle ear components under 124 dB SPL excitation. It was shown that the highest displacement occurs at umbo (connection point of malleus and tympanic membrane). Figure 2.2 shows the given displacement data for umbo along with the calculated acceleration values. Acceleration values for higher frequencies may have a higher error margin as the tympanic membrane vibrations deviate from pure harmonic motion.

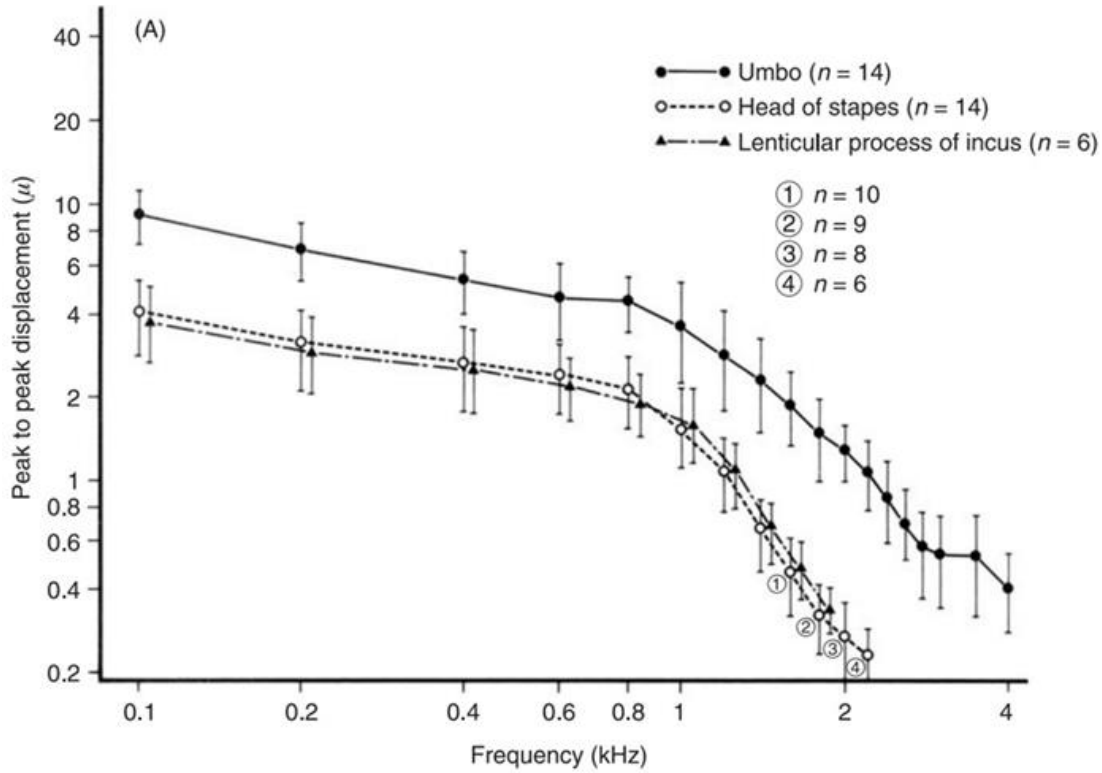

Figure 2.2 Average displacements of the umbo, the head of the stapes and the lenticular process of the incus [38].

The footprint may be reduced by stacking the single-channel bulk transducers on top of each other, which results in an increased mass. This results in an increase in the level of the challenge due to the coupled motion with the eardrum and leads to a lower vibration amplitude at the same acoustic input level [39].

The vibration characteristics of the tympanic membrane are also studied by Young et al [40], [28]. In that study, a MEMS accelerometer microphone is placed on the umbo (Figure 2.3). The vibration of umbo is measured by a Laser Doppler Vibrometer (LDV) at different sound pressures and frequencies.

Figure 2.3 Location of umbo and LDV measurement axes [41].

Figure 2.4 shows the acceleration results for 80 and 100 dB SPL from four cadaveric ears with and without incus (the second ossicles bone).

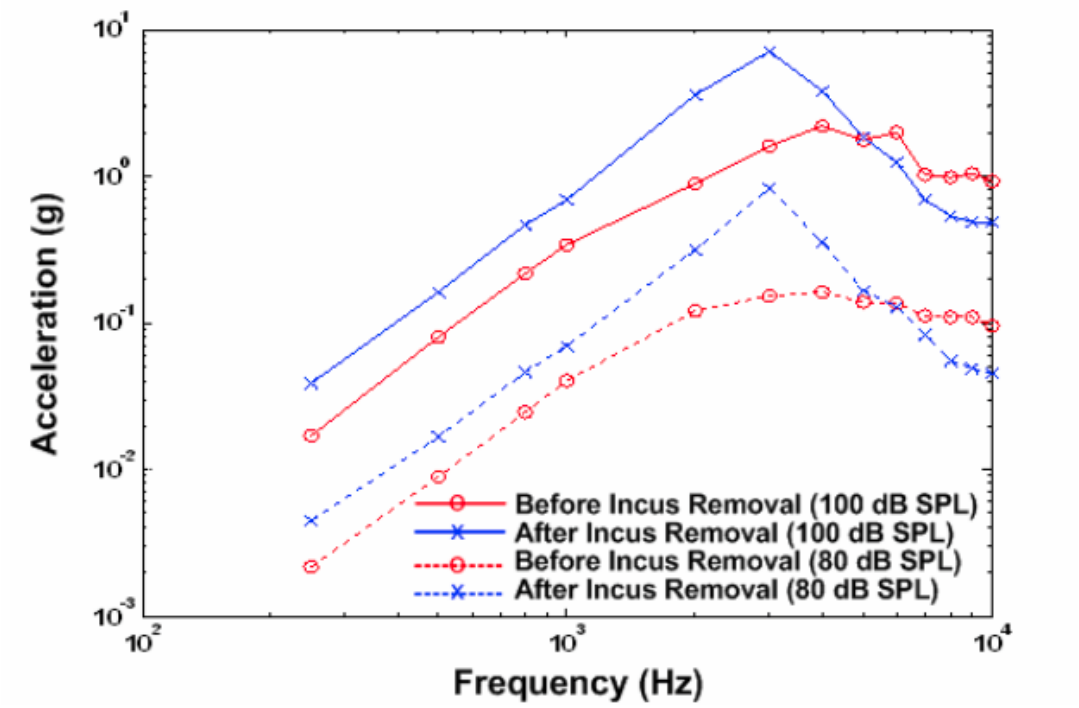

Figure 2.4 Effect of incus change on acceleration characteristics of umbo at various sound pressure levels (SPL) [40].

In many cochlear implant operations, incus is removed to enlarge the available space in the middle ear cavity. Removal of the incus increased the tympanic membrane acceleration up to three times, depending on the vibration frequency.

The same group made several tests and placed the sensor on the umbo and observed that acceleration level is decreased due to the additional mass. It was shown that the sensor mass larger than 25 mg significantly decreases the vibration amplitude [39].

Therefore, the usage of bulk piezoelectric transducers as multi-channel acoustic sensors is not convenient for FICI applications. Sol-gels and most of the thin film piezoelectric materials can be integrated into MEMS. Usage of these materials may result in a decrease in the device volume, however, their piezoelectric properties are not adequate for nerve stimulation.

iv. **Stimulation Signal:** The most significant issue is to be able to generate sufficient sensing voltage for auditory nerve stimulation. The proposed device will stimulate the auditory nerves by generating the required minimum voltage using a set of frequency-selective piezoelectric cantilevers coupled to the eardrum.

Among other transduction mechanisms, piezoelectric transducers are widely used to convert mechanical vibrations directly into electricity without a need for an external source [29].

Mukherjee et al [24] investigated the possible use of piezoelectric materials in the cochlea as the charge generating device. They have conducted preliminary *in vivo* tests on guinea pigs with limited success. Guo et al [42] made similar experiments with four different piezoelectric materials implanted between oval and round windows of cats. They observed a maximum of 12 dB recovery in hearing loss of the cats. Inaoka et al [43] experimented with the small

piezoelectric device placed on the basilar membrane in the cochlea. Tests with guinea pigs showed that the output voltage was not sufficiently high for direct stimulation of the auditory nerves and required amplification in the order of thousands.

There are also other studies utilizing methods other than piezoelectric transducers to stimulate the nerves. For example, one recent study by Mercier et al [44] suggested using intracochlear potential for energy extraction to be used in biological sensors. Minimum output power measured from a guinea pig using this method was 1.12 nW during a 5-hour experiment.

At another study, Accoto et al [45] stated that the acoustic energy from normal speaking is not enough to stimulate the nerves directly; therefore they tried to use head movement as a source for powering the implants. No experimental measurements or vibration analysis in the middle ear were provided.

Placing the piezoelectric materials inside the cochlea to generate voltage from the traveling wave inside the cochlear fluid has not been very successful for stimulating the auditory nerves.

In a previous study by Beker et al., an alternative method was suggested [26] using a unimorph cantilever piezoelectric energy harvesters placed on eardrum. A prototype was fabricated and tested on a shaker table. However, the requirement of such a system in multi-channel configuration cannot be satisfied due to mass tolerance, volume, and footprint of the middle ear.

Therefore, a novel design and an alternative material should be considered and investigated as a solution for a fully implantable cochlear implant application to meet all the requirements and limitations of the system.

2.3. Solution: Usage of PLD-PZT Materials as Multi-Frequency Sensor

The proposed system introduces a fully implantable cochlear implant to stimulate the auditory nerves mimicking the hair cell with a multi-frequency thin film piezoelectric acoustic sensor. The proposed concept should overcome the main bottlenecks of CIs, considering the limitations regarding volume, footprint, mass and stimulation signal.

Thin film piezoelectric materials can be integrated with MEMS in the desired volume [46], which makes them a promising alternative for the application. Pulsed Laser Deposited (PLD) material is preferred among other thin film piezoelectric alternatives due to their superior ferroelectric and piezoelectric properties for acoustic sensing [47]. Using PLD-PZT, a more compact multi-channel piezoelectric acoustic sensor can be designed, where all cantilevers can be placed on a single layer. This is possible since the thin film fabrication procedure allows for reduction of both the cantilever size and the distance between individual cantilevers. Consequently, mechanical filtering for an adequate number of channels to cover the daily acoustic band within the 25 mg maximum loading requirement will be facilitated, ensuring that there is no significant effect on the eardrum acceleration.

Performance of sensors utilizing different piezoelectric layers is compared in [48]. Here the coupling coefficient (Equation 2.1) and the maximum output (Equation 2.2) are defined, respectively, as follows:

$$K^2 = \frac{2{e_{31,f}}^2}{\varepsilon_0 \varepsilon_{33,f}} \left(\frac{1-\nu}{Y}\right)_{Si} \tag{2.1}$$

$$P_{max} = \frac{K^2 m (QA)^2}{4\omega} \tag{2.2}$$

where, $e_{31,f}$ is the transverse piezoelectric coefficient, ε_0 is the permittivity of free space, $\varepsilon_{33,f}$ is the dielectric permittivity, ν and E are the Poisson's ratio and Young's modulus of the cantilever material, m, Q, A and ω are the mass, the quality factor, the

input acceleration and the natural frequency of the cantilever, respectively. Please note that a figure of merit (F.O.M.) can be defined in Equation 2.3 being proportional to the square of the coupling coefficient.

$$F.O.M. = \frac{{e_{31,f}}^2}{\varepsilon_0 \varepsilon_{33,f}} \tag{2.3}$$

PLD PZT (1 μm-thick deposited at Solmates BV) properties are given in Table 2.1 and performance of PLD PZT sensors with different dimensions is evaluated in Table 2.2.

Table 2.1 Material properties of thin film pulsed laser deposited (PLD) PZT [48].

ε_{33} (@1 kHz, 0 V)	$\tan\delta$ (@1 kHz, 0 V)	Remnant Polarization, P_r [μC/cm^2]	$-e_{31,f}$ [C/m^2]	F.O.M. [GPa]
2000	0.01-0.02	20	7.7	3.5

Table 2.2 Performance of PLD PZT thin film sensors at different dimensions [48].

Size [mm] L_b x W_b x L_m	Frequency [Hz]	Sensitivity [μW/g^2]	Q_{total}	A_{max} [g]	P_{max} [μW]
1.3 x 7.0 x 7.0	355	21	239-230	0.7	10
1.1 x 5.0 x 5.0	615	63.6	650-598	0.9	51
1.7 x 3.0 x 3.0	860	23.4	905-796	1.4	41.3
1.4x 3.0 x 3.0	1012	20.4	963-558	2.1	53.5

Therefore, it is beneficial to use PLD PZT materials for sensing purposes in a multi-channel thin film piezoelectric configuration. Advantages can be listed as follows:

i. The final chip will be more compact since all sensing devices can be gathered on a single layer. This is possible since cantilever size can be reduced and the distance between individual cantilevers can be smaller, restrained by the fabrication procedure involving flip-chip bonding. With flip-chip bonding, it is not possible to bond chips smaller than 2x4 mm^2 area. It is possible to bond a larger chip and then etch smaller structures on it. However, this still requires bonding and thinning processes which are followed by additional lithography and PZT etching processes.

ii. By using thin film PLD-PZT, it would be much easier to stay within the 20 mg maximum loading requirement on the eardrum. The eardrum acceleration will not be decreased dramatically due to extra mass, while we can still provide mechanical filtering for as many channels as required.

iii. The voltage output from the PLD PZT cantilevers was on the order of mV range, which is sufficiently high for the sensing circuit of the cochlear implant [48]. A similar structure was used for mechanical filtering with cantilevers with a piezoelectric (AlN) output less than 10 mV [25]. Compared with AlN, PLD PZT has a FOM three times higher.

2.4. Finite Element Modeling of Thin Film Piezoelectric Transducer

In the proposed system which is shown in Figure 2.5, the main aim is to build a thin film piezoelectric multi-frequency cantilever structure. The cantilevers will sense the incoming sound and vibrate according to their resonance frequency. The resonance frequencies of the 8-channel filter are distributed between 300 and 4800 Hz, where each cantilever will resonate within the hearing band. The resonance frequencies of the cantilevers are arranged such that they will increase linearly up to 1200 Hz, and after that logarithmically up to 4800 Hz considering the working frequencies of conventional cochlear implants [49], [50].

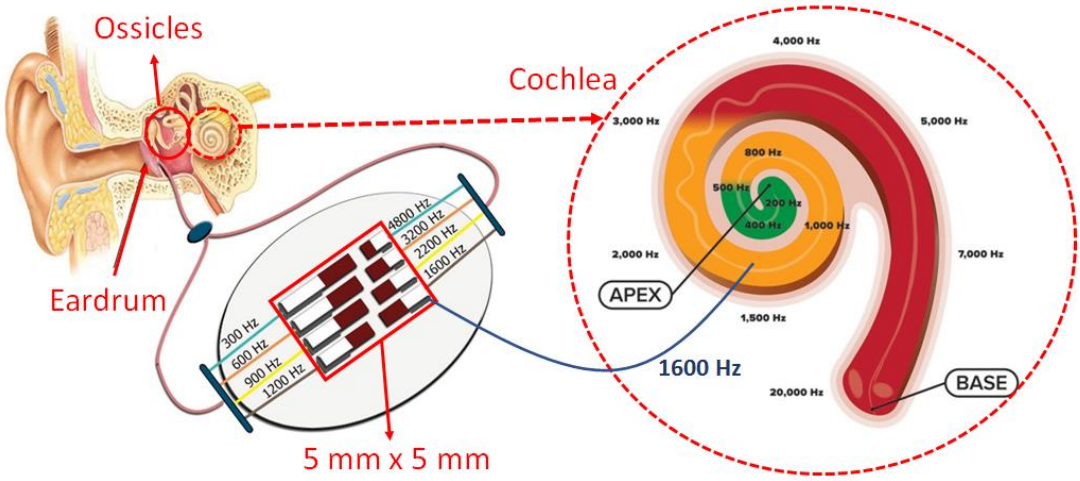

Figure 2.5 The proposed system for sensing the sound with close-up views of the cochlea and the cantilever array.

As discussed in section 1.3, one of the most widely used vibration sensing technique is piezoelectric transduction. Piezoelectric materials are preferred for sensing applications due to their high energy density and higher voltage output capacity.

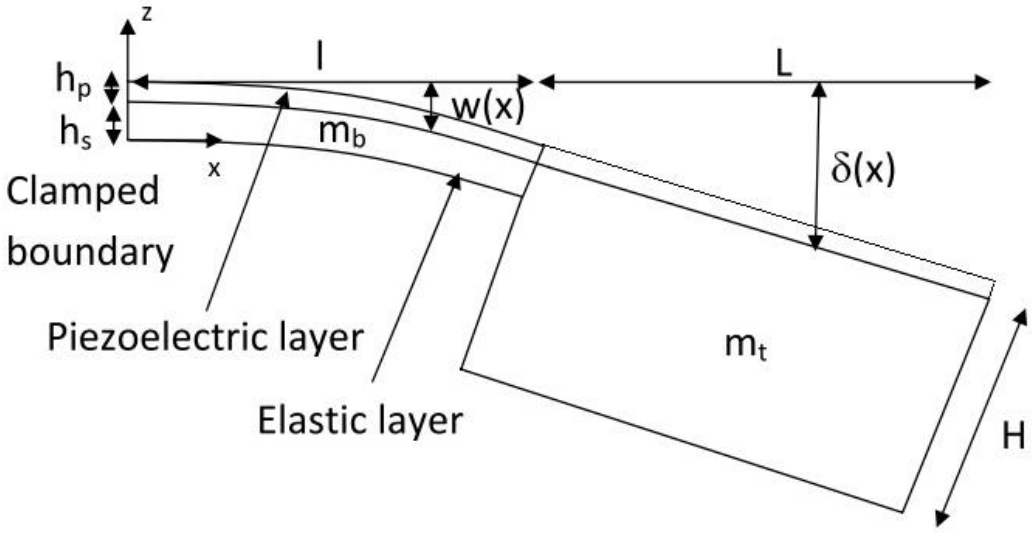

Figure 2.6 Schematic view of the piezoelectric cantilever beam with tip mass structure used in modeling [51].

The most common structure used in sensing systems is a vibrating cantilever with piezoelectric material placed on the base of the cantilever as shown in Figure 2.6. Generally, a tip mass, m_t, is attached to the moving end of the cantilever to adjust the resonance frequency of the structure, where ω and δ shows the deflection along the top surface of the beam and of the mass.

There are mainly three methods modeling and analysis of piezoelectric cantilever structures: lumped parameter analysis, distributed parameter modeling, and finite element analysis (FEA).

The equivalent model of the piezoelectric bending beam is represented in the form of two ports electrical network as shown in Figure 2.7 [51]. The left side of the circuit corresponds to the mechanical domain and the right to the electrical properties of piezoelectric material. In the mechanical domain, a capacitor in Equation 2.4 shows the reciprocal mechanical stiffness (i.e. compliance) and the effective beam mass is represented by an inductance in Equation 2.5.

$$C_m = {}^{1}/_{k_c} \tag{2.4}$$

where C_m is the equivalent mechanical capacitor, k_c is the mechanical stiffness. The electromechanical conversion is virtualized by a perfect transformer Γ_c related with piezoelectric coupling factor. In this particular application, the piezoelectric sensors are subjected to steady state vibrations. Therefore, the ac voltage source is connected to the mechanical parts of the network as a source of mechanical energy.

$$L_m = m_{eff} \tag{2.5}$$

where L_m is the inductance and m_{eff} is the effective beam mass. Force expression is assumed as in Equation 2.6

$$F = m_{eff} a_0 \sin(2\pi f t) \tag{2.6}$$

where a_0 and f stand for the excitation acceleration amplitude and excitation frequency, respectively. On the other side, the electrical ports are connected to an electrical load in which energy is stored or dissipated in parallel with piezoelectric capacitance C_p in Equation 2.7.

$$C_p = \varepsilon_{33} \frac{W l_p}{h_p} \tag{2.7}$$

where C_p is the piezoelectric capacitance, ε_{33} is the dielectric permittivity, $W l_p$ and h_p are the area and thickness of the piezoelectric layer, respectively.

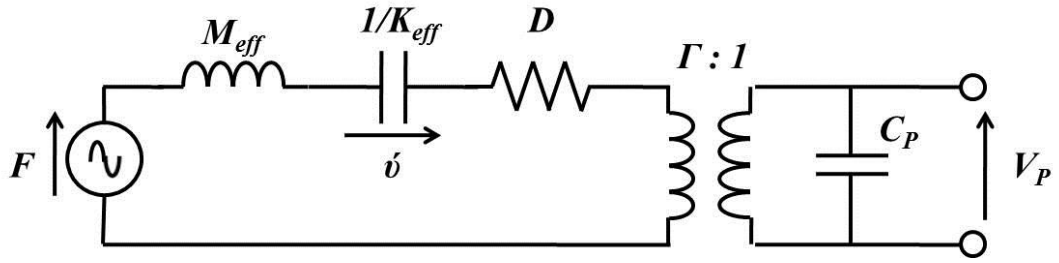

Figure 2.7 Equivalent network model for piezoelectric transduction mechanism.

The total stiffness of a composite beam by contributing each individual layer can be obtained in equation 2.8 as follows:

$$k_{c,eff} = \frac{3}{l_b^3}\left[\sum_1^2 Y_i \left(\frac{w_i h_i}{12} + l h_i \left(\sum_j^i h_j - \frac{h_i}{2} - Z\right)^2\right)\right] \tag{2.8}$$

According to [32], the expression of the effective mass is given in equation 2.9:

$$m_{eff} = \frac{33}{140} m_b cof_b + \rho W l h_m cof_m \tag{2.9}$$

Finally, the open circuit resonance frequency of harvester modeled as the spring-mass system is expressed in equation 2.10 as follows:

$$f_r = \frac{1}{2\pi}\sqrt{\frac{k_{p,eff}}{m_{eff}}}\left(\sqrt{1 + K^2}\right) \tag{2.10}$$

where K is generalized electromechanical coupling, which represents the performance of the piezoelectric sensor and joint with extracted output power. K can be expressed in term of equivalent circuit parameters as in equation 2.11:

$$K^2 = \frac{\Gamma^2}{kC_p} \tag{2.11}$$

In the proposed structure, required frequencies are distributed up to 4800 Hz and tip mass usage is inevitable in order to tune the resonance frequency of the transducers and the induced stress level, which increases the vibration level and voltage output. In these frequencies, the length to width ratio of the cantilevers will be relatively low compared to macroscale cantilevers. Also, tip mass part of the cantilever beams should be modeled as a solid structure instead of a single concentrated mass. Moreover, piezoelectric layer lengths will be different for each cantilever and will not be covering the silicon layer completely. Therefore, distributed and lumped parameter modeling cannot be applied to multi-frequency thin film piezoelectric cantilevers due to the structure complexity, nonlinearity, and boundary conditions.

The detailed analysis of piezoelectric cantilever beams with tip mass structure showed that it cannot be modeled using distributed and lumped parameter modeling due to the structure complexity, nonlinearity, and boundary conditions. In this study, a finite element modeling (FEM) method is used to model the multi-channel thin film piezoelectric cantilever structure. COMSOL Multiphysics is preferred among various available FEM programs due to user-friendly interface and advanced optimization tool properties, where the design is established using the parametric sweep property of the COMSOL Multiphysics. Another advantage of the COMSOL Multiphysics is that every boundary condition, the effect of tip mass layer, and length to width ratios can be modeled without making any assumptions. Besides, COMSOL Multiphysics is widely used in modeling of MEMS and piezoelectric transducers.

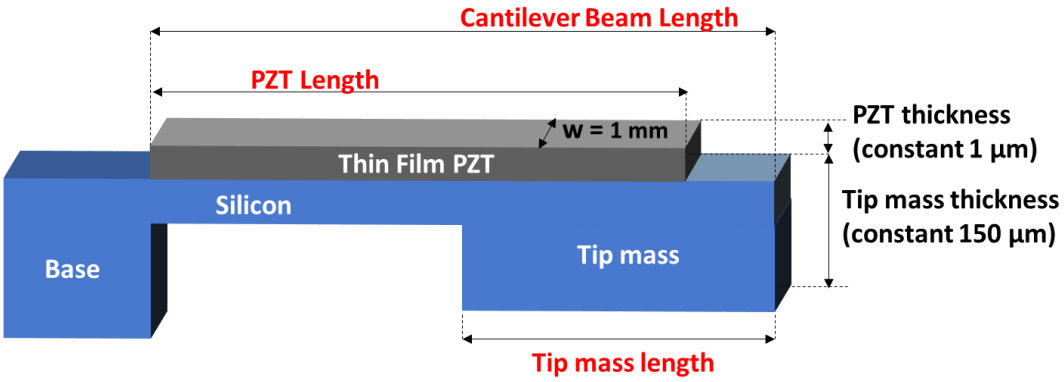

Figure 2.8 Schematic view of the transducer showing all the dimensions.

Figure 2.8 illustrates a single cantilever beam structure. There are three essential parameters to be determined in order to satisfy design requirements that are: length of the cantilever beam, length of thin film PZT layer and length of tip mass. The placement of the cantilevers is arranged such that the longest cantilever is inserted facing the shortest length cantilever to reduce the footprint of the device.

Tip mass usage is inevitable to tune the resonance frequency of the transducers since the proposed system provides mechanical filtering and shows a frequency selectivity mimicking the natural operation of the cochlea. Also, a constant tip mass thickness should be selected for all cantilevers that resonates at the desired center frequencies considering the fabrication limitations of the devices into account. After sweeping the tip mass thicknesses, a 150-µm thick tip mass is selected and fixed which provides the highest and the lowest resonant frequency cantilever that are 4800 Hz and 300 Hz, respectively in the restricted area limitation of the design.

Usage of tip mass enhances the induced stress level at the fixed point, which increases the vibration level of cantilevers and provides more voltage output on the piezoelectric layer. PZT length is another critical design parameter to maximize the voltage output. Results show that maximum voltage output occurs when % 44 of the cantilever length is covered with the active piezoelectric layer [52]. For this reason, this constant value is also used in designing silicon and piezoelectric layer lengths. Beam length is varied

for obtaining the desired center frequencies and the cantilever beams arranged to face each other in such a way that the array fits into the 5×5 mm^2 footprint. These design parameters are critical to obtain a sufficiently high signal within the volume and weight limitations.

A finite element model is established using the COMSOL Multiphysics to design the 8-channel transducer within weight (<25 mg) and volume (<0.1 cm^3) constraints. The total volume and mass of the device were 5×5×0.2 mm^3 and 12.2 mg, respectively, which are much lower than the limitations of the system. In order to characterize the device properties accurately, mechanical, electrical and squeeze film damping parameters are inserted into the COMSOL finite element simulations [53]. Damping ratio of 0.098 is obtained by observing experimental results of the PLD-PZT material, and inserted into the simulations.

After modeling the silicon and the piezoelectric layers, and inserting material properties into simulations, the next steps is meshing. One of the key concepts is the mesh convergence: as the mesh is refined, the solution will become more accurate. If the number of mesh is increased enormously, this time an error accumulation will be observed. In the simulations, a fine mesh element structures are selected after reaching the independent number of element. In this study, a free tetrahedral mesh is selected for this structure due to its compatibility without considering shape or topology and providing accurate results in structural mechanics problems, where stress value on piezoelectric layer converges within 2%. Figure 2.9 shows the meshed piezoelectric thin film sensor in detail. In the mesh structure, thickness of the piezoelectric and cantilever beam are divided into five region to catch the any generated stress change on the piezoelectric layer [54].

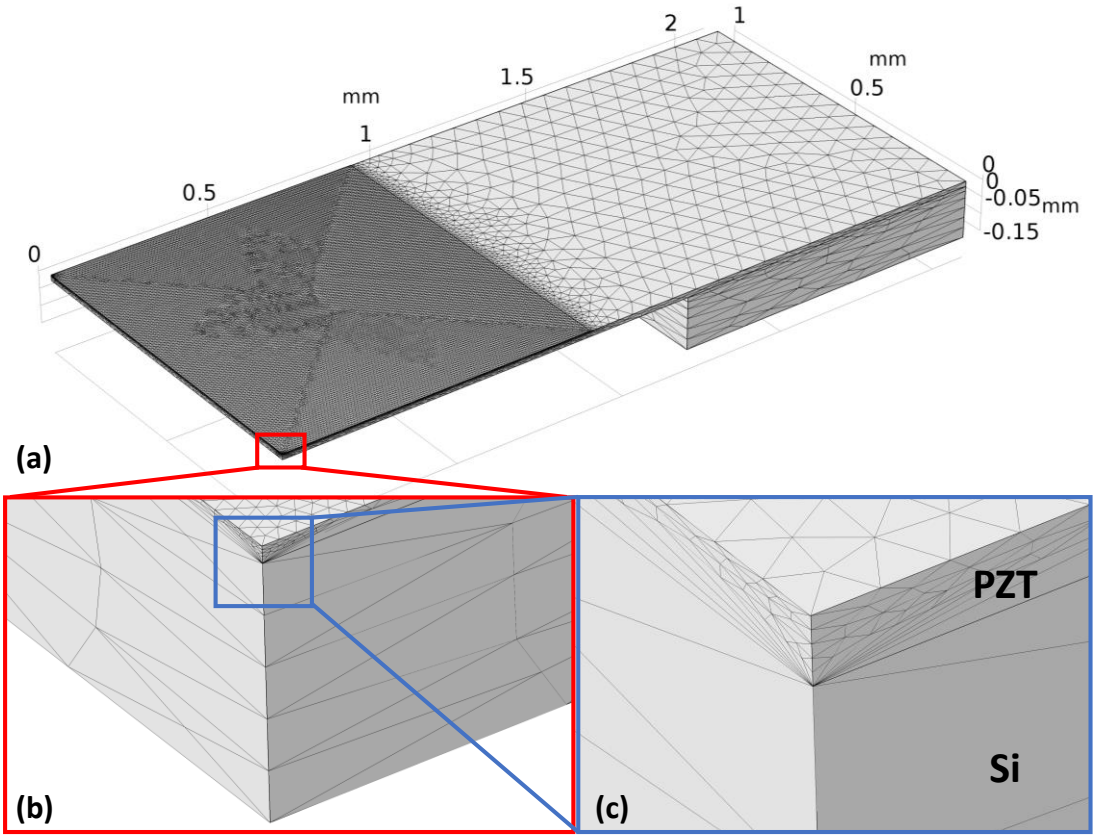

Figure 2.9 Finite element model of the free tetrahedral meshed structure with a close-up view of the PZT and silicon layers.

A silicon wafer is to be used for fabricating the piezoelectric transducers, and the (100) crystal orientation of the wafer is considered in the simulations. Therefore, both silicon and PZT layers are modeled considering their anisotropic properties.

Figure 2.10 demonstrates the Eigenfrequencies of the designed piezoelectric thin film cantilever structure (5^{th} channel), where the modal analysis is used to determine the frequencies. The structure is fixed-free type of cantilever with a fixed boundary condition is defined at the anchor. Figure 2.11 shows the proposed 8-channel multi-frequency structure, where each sensor resonates at a selected frequency within the spectrum. Table 2.3 lists the obtained piezoelectric output voltage, sensitivity to sound and quality factor for each frequency.

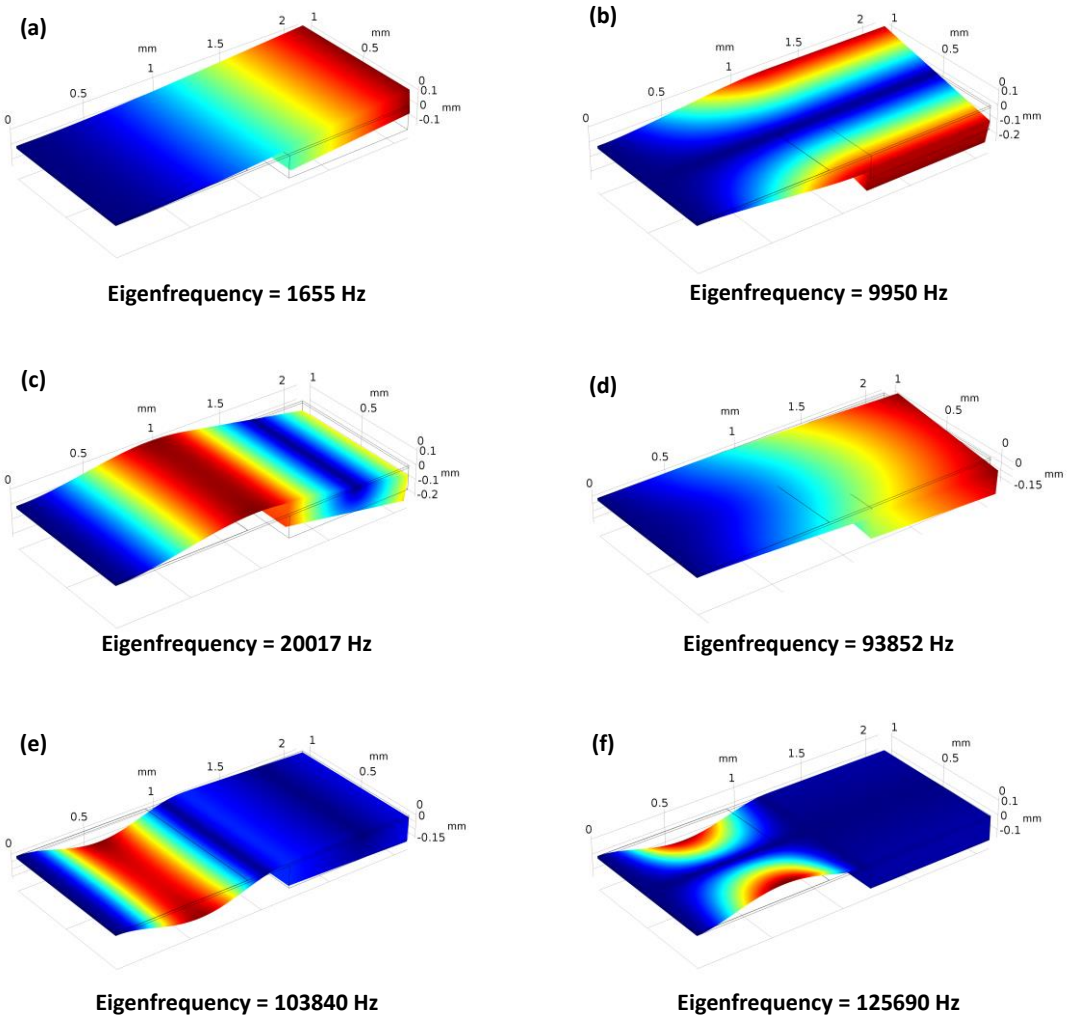

Figure 2.10 Eigenfrequencies of the designed piezoelectric cantilever showing the 5th channel.

Results demonstrate that the proposed design has a clear frequency selectivity with a minimum quality factor of 1285 and mimics the natural operation of the cochlea. Both the sensitivity and the quality factor of the proposed system are higher than the state-of-the-art piezoelectric transducers [25]. Results show that the device generates sufficient output voltage considering the reported sensing voltage requirement of a neural stimulation circuitry for auditory neurons [50]. The proposed system replaces the electrical filters with mechanical ones, which results in a decreased power

dissipation by the circuit, by at least 40 µW [55]. The power dissipation further decreases due to the higher signal-to-noise ratio of the thin film PZT transducers, which result in a lower power requirement by the interface circuitry for detecting the signal. Therefore, it can be anticipated that the battery lifetime of an implantable system increases and the frequency of battery charging decreases.

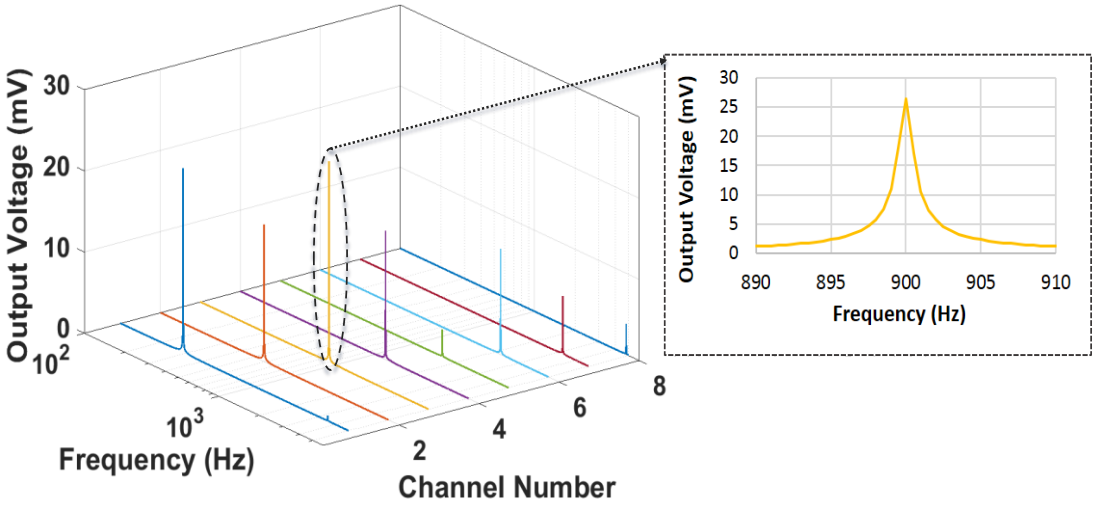

Figure 2.11 Simulation results showing the frequency response of all channels with a close-up view of channel 3 (operating at 900 Hz).

Table 2.3 Specifications of 8-channel structure obtained through simulations.

Frequency (Hz)	Beam length (mm)	Output Voltage (mV)	Sensitivity (mV/Pa)	Quality Factor
300	3.4	22.98	363.34	984
600	2.4	16.87	265.4	1012
900	1.9	24.79	391.9	1285
1200	1.7	15.88	251.2	1196
1600	1.4	22.71	358.94	976
2200	1.2	13.12	204.6	1043
3200	1	7.21	114.1	996
4800	0.8	3.75	59.3	1121

2.5. Relation of Acoustic Sound with Mechanical Acceleration

Human ear is a very complex structure, which converts acoustic pressure waves from the air; first mechanical vibrations on eardrum and ossicles, then electrical potential in hair cells in the cochlea to stimulate auditory nerves. In order to improve a fully implantable cochlear implant system, those mechanical vibrations in the middle ear can be utilized using a piezoelectric acoustic sensor system.

Table 2.4 Umbo vibration levels at different frequencies and sound pressure levels. Umbo vibration data extracted from [50].

Sound Pressure Level (dB)	**g @ 500 Hz ($g \times 10^{-4}$)**	**g @ 1000 Hz ($g \times 10^{-4}$)**	**g @ 2000 Hz ($g \times 10^{-4}$)**	**g @ 4700 Hz ($g \times 10^{-4}$)**
40	1.5	3.3	7.1	3.8
50	4.4	10.7	26.6	12.5
60	13.3	33.7	72.8	29.2
70	44.4	97.7	213.1	104.2
80	155.1	337.2	711.2	334.4
90	444.3	977.1	2130.4	751.2

The relation between acceleration and acoustic sound should also be understood since human ear can detect sound frequencies between 20 to 20000 Hz. A minimum threshold of excellent youthful hearing is taken as 0 dB SPL, which corresponds to 20 μPa sound pressure. Sound pressure level (SPL) or acoustic pressure level is a logarithmic measure of the effective sound pressure of a sound relative to a reference value. Sound pressure level (SPL), denoted L_p and measured in dB, above a standard reference level, is given in equation 2.12.

$$L_p = 10\ log_{10}\left(p_{rms}^2 / p_0^2\right) = 20\ log_{10}\left(p_{rms} / p_0\right) \quad (2.12)$$

where P_{rms} is the root mean square sound pressure P_0 is the reference sound pressure, both measured in Pascal.

Table 2.5 Specifications of the channel at 40 dB SPL in terms of acceleration and output voltage.

Channel Number	**Frequency (Hz)**	**Acceleration (g× 10^{-4})**	**Piezoelectric Voltage (µV)**
1	300	1	960
2	600	2	950
3	900	3	880
4	1200	4	490
5	1600	6.2	770
6	2200	7	420
7	3200	6	240
8	4800	3.5	110

The output of thin film will feed the sensing circuitry and one of the main limitations is the turn-on voltage of transistors. The minimum required voltage level is 100 µV at 40 dB, and at 40 dB the pressure is around 0.002 Pa. Umbo Vibration Levels are summarized in table 2.4, which is derived from literature [50] and COMSOL Simulations summarized in Table 2.5.

2.6. Summary of the Chapter

In this chapter, the design, modeling, and optimization of the proposed multi-frequency thin film piezoelectric acoustic sensor is presented. Then, details of the proposed application are elaborated considering the main limitations and requirements of the design. Next, the selected piezoelectric thin film material and its properties are discussed. Afterwards, the proposed design is modeled and optimized using the optimization module of COMSOL Multiphysics. The chapter also explains the relation between the acoustic sound pressure level (SPL) and the acceleration level.

CHAPTER 3

FABRICATION OF MEMS THIN FILM PIEZOELECTRIC ACOUSTIC TRANSDUCER

This chapter explains the fabrication procedure of the thin film piezoelectric acoustic sensor. The chapter summarizes the fabrication flow of single-channel thin film PLD PZT sensor and the flexible parylene carrier. Moreover, the fabrication of the 1st and 2nd generation multi-channel thin film piezoelectric transducer is elaborated in detail.

3.1. Fabrication of Single Channel Thin Film Transducer

To show the applicability of PLD-PZT fabrication in our facility, a trial fabrication using a previous piezoelectric energy harvester design [37] was done on Si test wafers provided by Solmates BV. The 6-mask process was used for the fabrication of the thin film PLD-PZT transducer. Figure 3.1 shows the detailed flow diagram of the fabrication process. The fabrication starts with deposition of a 500 nm-thick PECVD SiO_2 layer on the front side of a 4-inch (100) silicon wafer. The main aim is to provide isolation of the transducer electrodes from conducting silicon wafer.

3.1.1. Piezoelectric Layer Deposition and Patterning

Bottom electrode was formed with a (10/100 nm) Titanium/ Platinum (Ti/Pt) layer sputtered as the seed layer for the PLD-PZT deposition. The insulation layer, bottom electrode and PLD-PZT (1 μm) layers were deposited at Solmates BV (SMP-700 PLD) and later, patterned using the PZT etchant provided by the same company.

For patterning, SPR 220-3 was used as a photoresist material. It is coated at 3000 rpm and soft baked 4 minutes @ 115 C and then exposed 6 seconds. Developed 57 sec,

which is ideal for this photoresist type and then hard baked @ 120°C. Patterned image of the coated PLD-PZT layer is shown in Figure 3.2. The thickness of the deposited PZT layer was measured as 1024 nm which is very close to the expected value (1 µm). The undercutting is around 1.5 µm after wet etch.

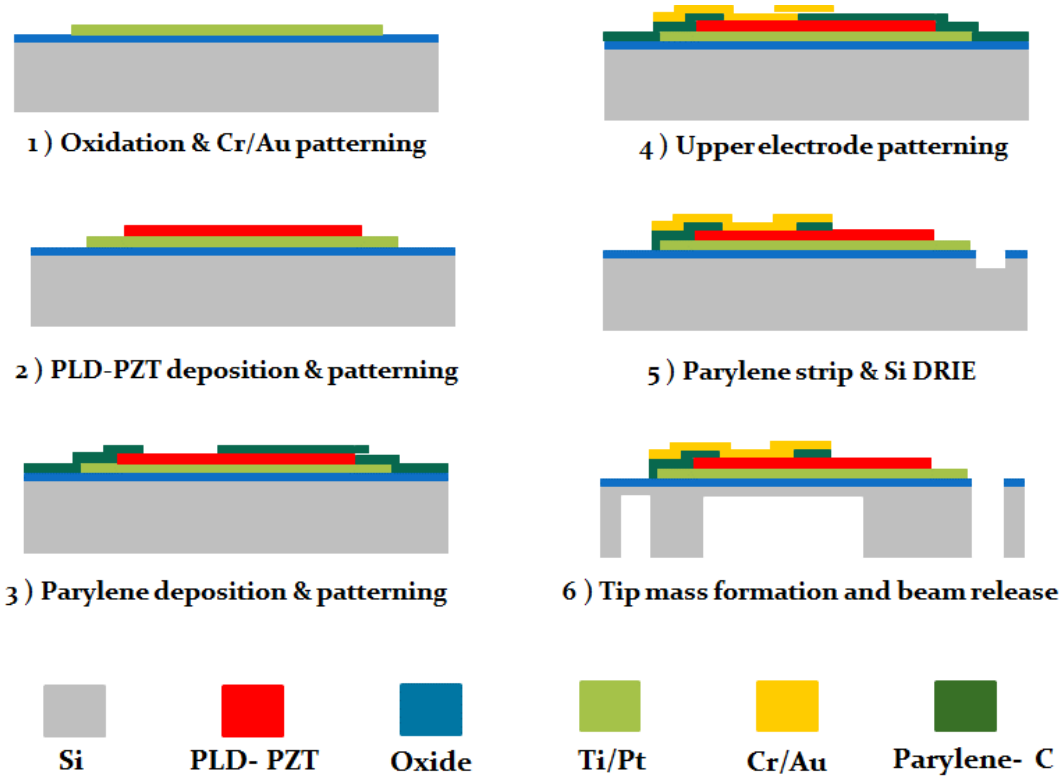

Figure 3.1 Fabrication flow of the thin film piezoelectric acoustic sensor.

3.1.2. Bottom Electrode Patterning

The Ti/Pt layer was utilized as the bottom electrode of the transducer and patterned in a hot aqua-regia solution [56]. The reason of using Ti is selected as adhesion layer and Platinum is being a suitable material fit for high-temperature processes owing to its high melting point (1768 ˚C). Also, Platinum has an inert nature that can prevent oxidation and diffusion-related issues when employed as an electrode material. It is

used in thin film as the base layer for growing Lead Zirconate Titanate (PZT) films with good crystal orientation.

100 nm Pt layer was patterned in hot Aqua Regia solution (60 °C). Thick photoresist masking was used for the metal patterning. Oxygen plasma cleaning was reported to produce a passivation layer on Pt thin film that has adverse effects during wet chemical etching (i.e. longer etching time) [56], therefore, it was not used after the lithography process. Pt etching was completed after 16 minutes per wafer on average.

3.1.3. Isolation and Top Electrode Layers Formation

Following the formation of the bottom electrode, a 5 μm Parylene-C layer (10 g weight) was deposited (SCS PDS2010) for insulation between the bottom and the top electrodes. After the parylene lithography stage, parylene should be etched. This process is handled at the STS RIE system. If the STS RIE device is set to 6" processes, 4" wafers are attached to 6" wafers using crystal bond.

Chromium/Gold (Cr/Au) (30/400 nm) was used as the top electrode and patterned using a wet etch process. After parylene etching, the top electrode deposition step starts with a 30 nm Chromium at AJA sputtering system and continues with a 400 nm gold layer at the same system.

Following metal deposition, SPR 220-3 type of resist is coated at 3000 rpm in the spin coating system to etch the top electrode layers. After the development process, Branson O_2 plasma system is used to ensure the resist-free surface of the exposed area. Then, prior to the metal etch process, hard bake is done to make the resist stiffer and prevent delamination of the resist during etching. To pattern the sputtered metals, commercial Au etchant together with custom-made Cr etchant was used. Figure 3.4 illustrates the front-side view of the transducers at the wafer level.

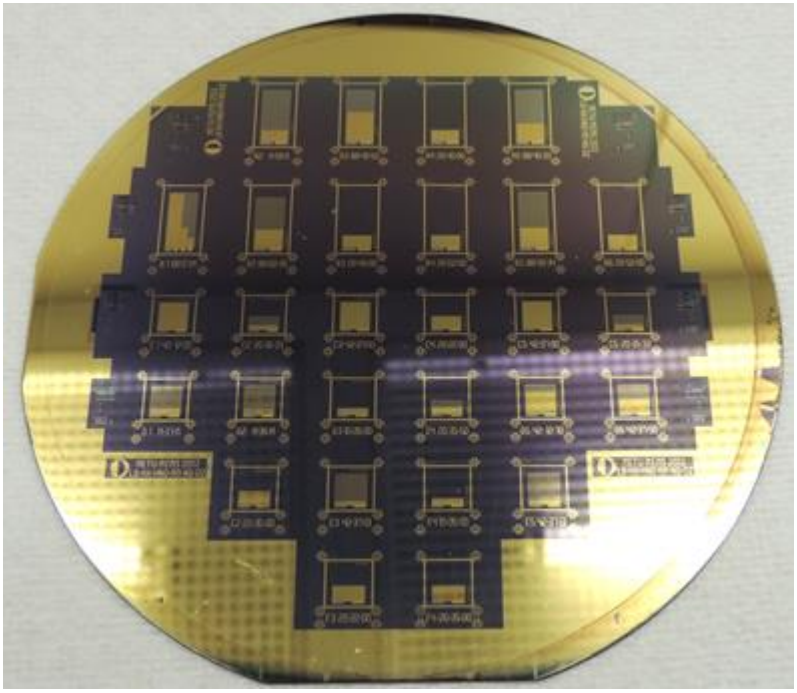

Figure 3.2 Final front side view of the fabricated transducers.

3.1.4. Formation of Cantilever Structures with Front and Backside DRIE

The remaining Parylene-C layer around the top electrode pattern was stripped using RIE. Finally, the cantilever beam and the tip mass structure were formed with front and back-side DRIE processes. Tip mass thickness defines the resonance frequency of the transducer. For the backside DRIE step, spray coating was used for patterning to provide a conformal coating. During this step, a frame was also patterned around the chips to allow the release of individual devices without dicing. Figure 3.5 shows the final back-side image of the fabricated wafer. It is essential to indicate that all processes were realized at low temperatures (<120 °C), which are well below the poling temperature (~200 °C) of PLD PZT [57].

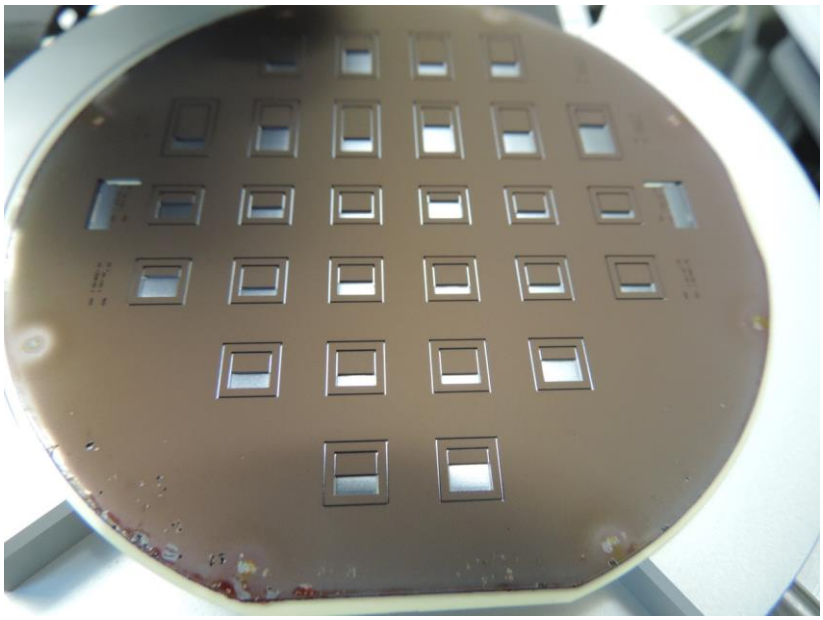

Figure 3.3 Final backside view of the fabricated wafer.

3.2. Fabrication of Multi-Channel Thin Film Transducer

3.2.1. 1st Generation Multi-Channel Thin Film Transducer Fabrication

A 7-mask process was developed for the microfabrication of the multi-channel thin film PLD-PZT transducer. Fabrication procedure is similar to the fabrication of single-channel thin film. Figure 3.8 shows the detailed flow diagram of the fabrication process.

Fabrication started with a piranha solution to clean any organic residue off the SOI substrates before thermal oxidation. A 500 nm-thick thermal oxide (SiO_2) layer was deposited at 1000 °C on both sides of the 4-inch (100) silicon wafers in a 3 hour-process. Patterned image of the coated PLD-PZT layer is shown in Figure 3.9.

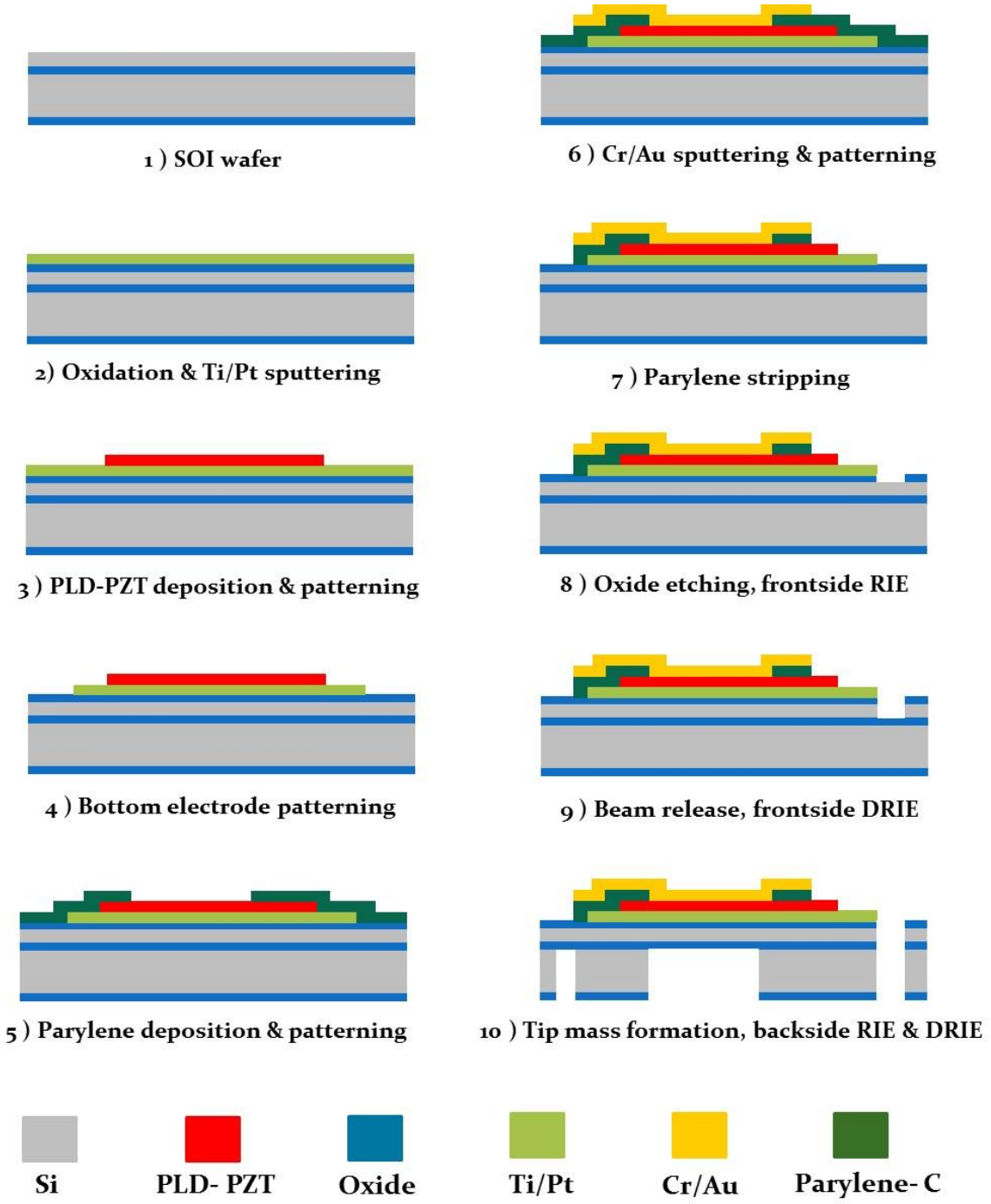

Figure 3.4 Fabrication flow of the multi-channel thin film pulsed laser deposited (PLD) PZT sensor.

The thickness of the deposited PZT layer was measured as 1024 nm after patterning the PZT layer with custom etchant and cleaning solution provided by Solmates BV.

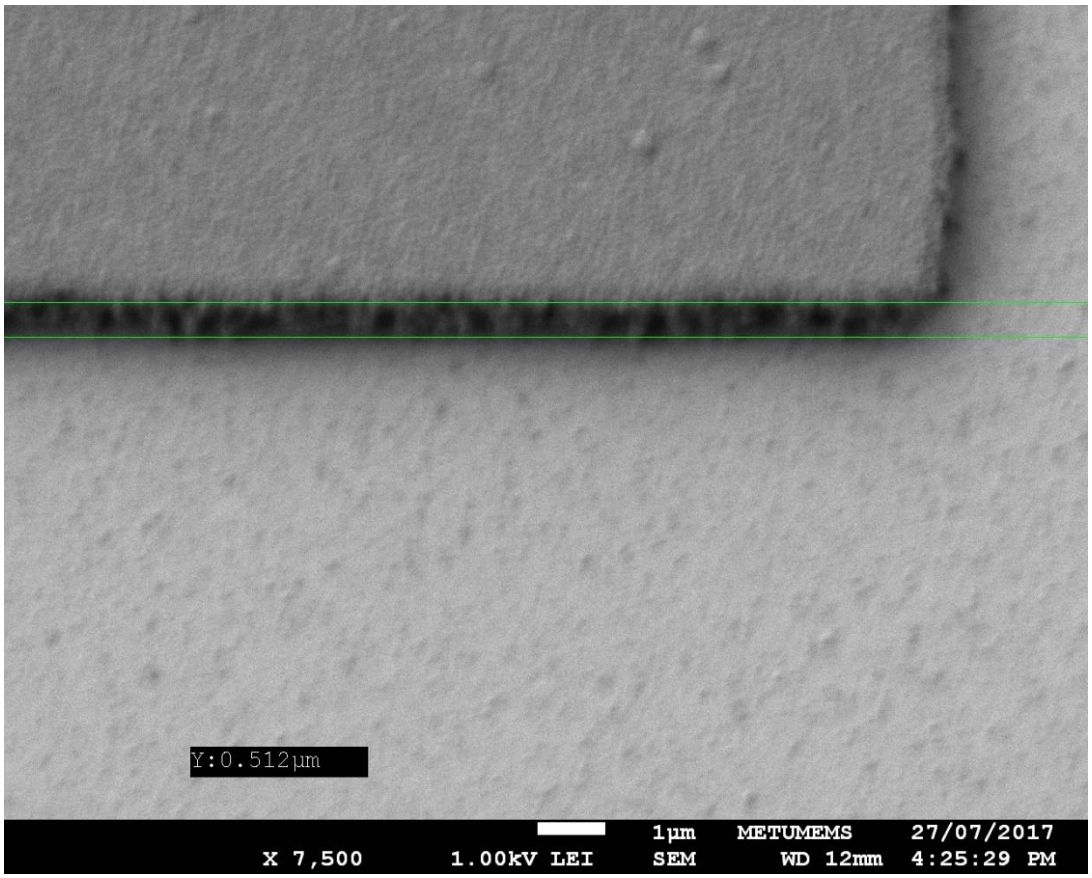

Figure 3.5 SEM image of the PLD PZT layer (thickness is measured around 1 µm).

After deposition and patterning of the piezoelectric layer, the next step is the formation of the bottom electrode. In this step, we have used SPR 220-7 photoresist to be able to protect the piezoelectric material since hot aqua regia is a very aggressive etchant, which also attacks the piezoelectric layer. Through experimental optimization, it was observed that 45 minutes hard baked (110 °C) SPR 220-7 in hot etchant gives the best performance. Formation of PZT and bottom electrode layers are shown in Figure 3.10. SEM image of Pt and PZT layers on silicon wafer after bottom electrode etch is shown in Figure 3.11.

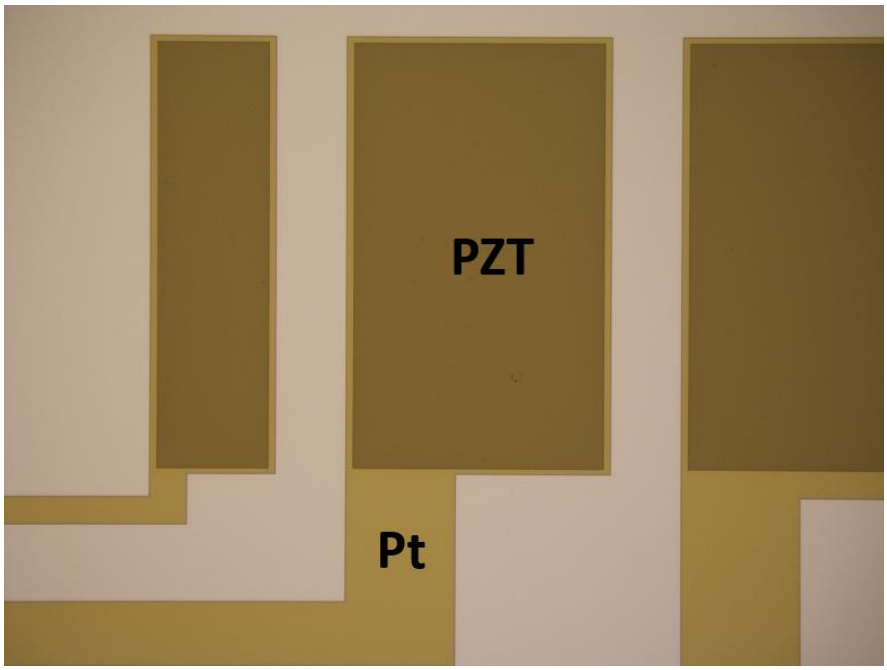

Figure 3.6 Microscope image of piezoelectric cantilevers with layers of PZT and Pt (bottom electrode).

After deposition and patterning of the bottom electrode, the next step is forming the top electrode. Prior to that, a thick parylene layer should be deposited to prevent the possibility of any short circuit between the top and bottom electrodes. A 2.5 μm (5 g) parylene is coated as an insulation layer and patterned using AZ-9260 photoresist. Edge bead removal procedure was carried out using a syringe to prevent mask stiction during exposure. Parylene was etched successfully using standard RIE parylene etching recipe after a 10 minute process. Following the patterning of the parylene layer, Cr/Au (30nm/400nm) top electrode layer was deposited at the BESTEC sputtering system. Deposited top electrode layers were patterned with SPR 220-3 and then etched using Transene metal etchants. Figure 3.12 shows the formation of the bottom and top electrodes, where the piezoelectric layer is sandwiched between these two layers.

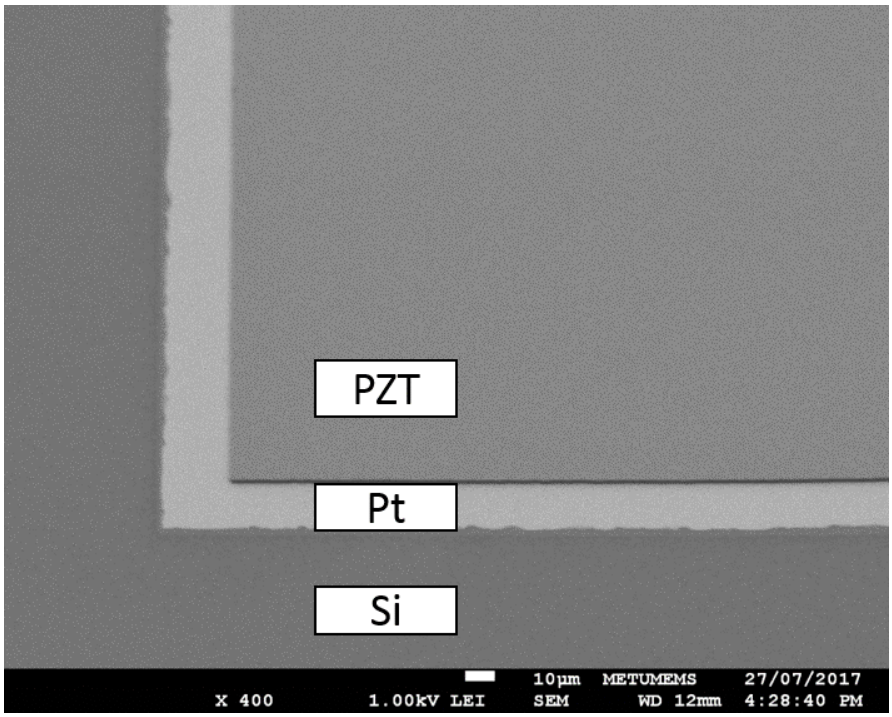

Figure 3.7 SEM image of PZT and Pt layers on silicon wafer after PZT and bottom electrode wet etch.

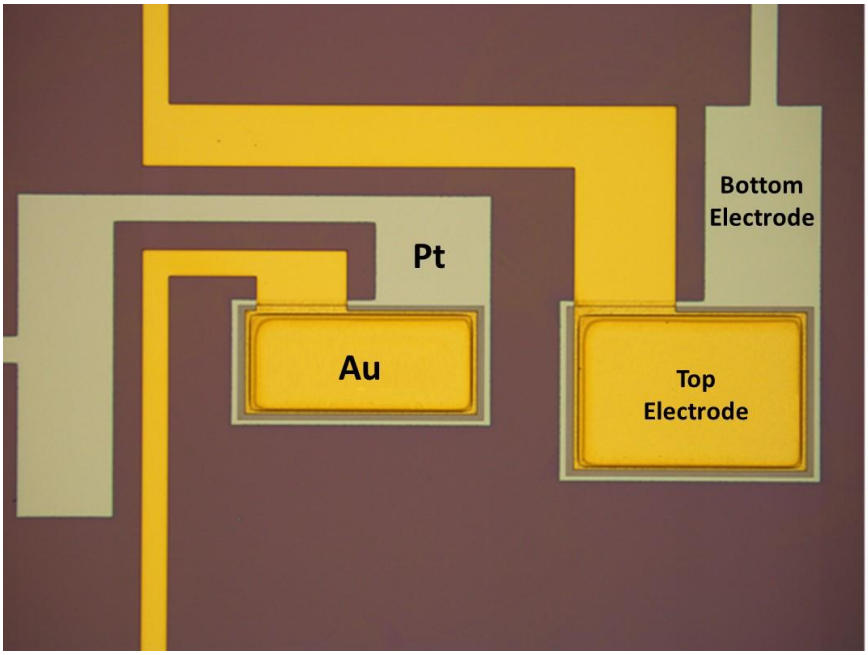

Figure 3.8 Cantilevers with layers of top and bottom electrode.

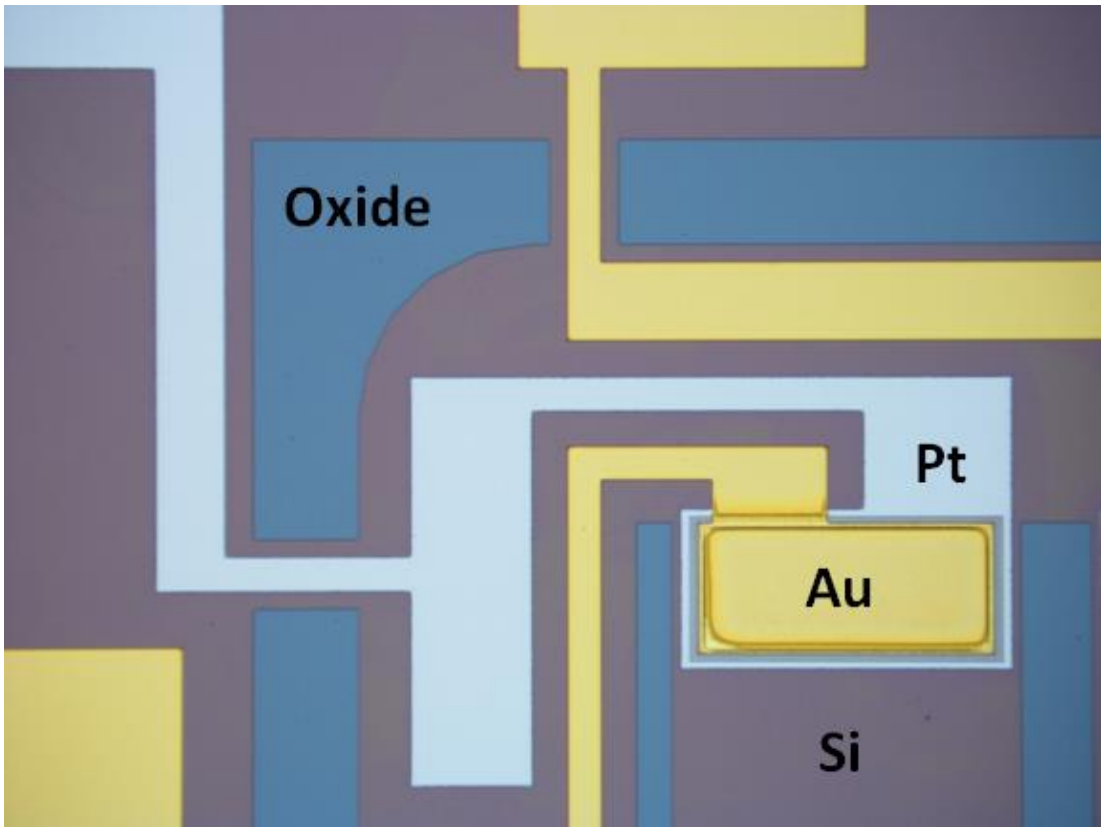

Figure 3.9 Cantilever and bridge structures formation after front DRIE process.

The remaining parylene outside of the top electrode layer was completely removed with the parylene etching recipe at RIE. In order to form the cantilever structures, the oxide and then silicon layers were patterned applying RIE and DRIE processes, respectively. Figure 3.13 illustrates the details of the cantilever and the bridge structures.

Finally, backside cantilever and tip mass structures were tried to form using the DRIE processes after patterning using spray coated photoresists. However, spray coated photoresist could not protect the tip mass structure and hence the final device has no tip mass which requires a solution to this problem. Figure 3.14 shows the front-side view of a finished wafer, which consists of 34 thin film transducers that have no tip mass. Figure 3.14 inset shows one of the fabricated devices with 8 different cantilevers and contact pads for pogo pins.

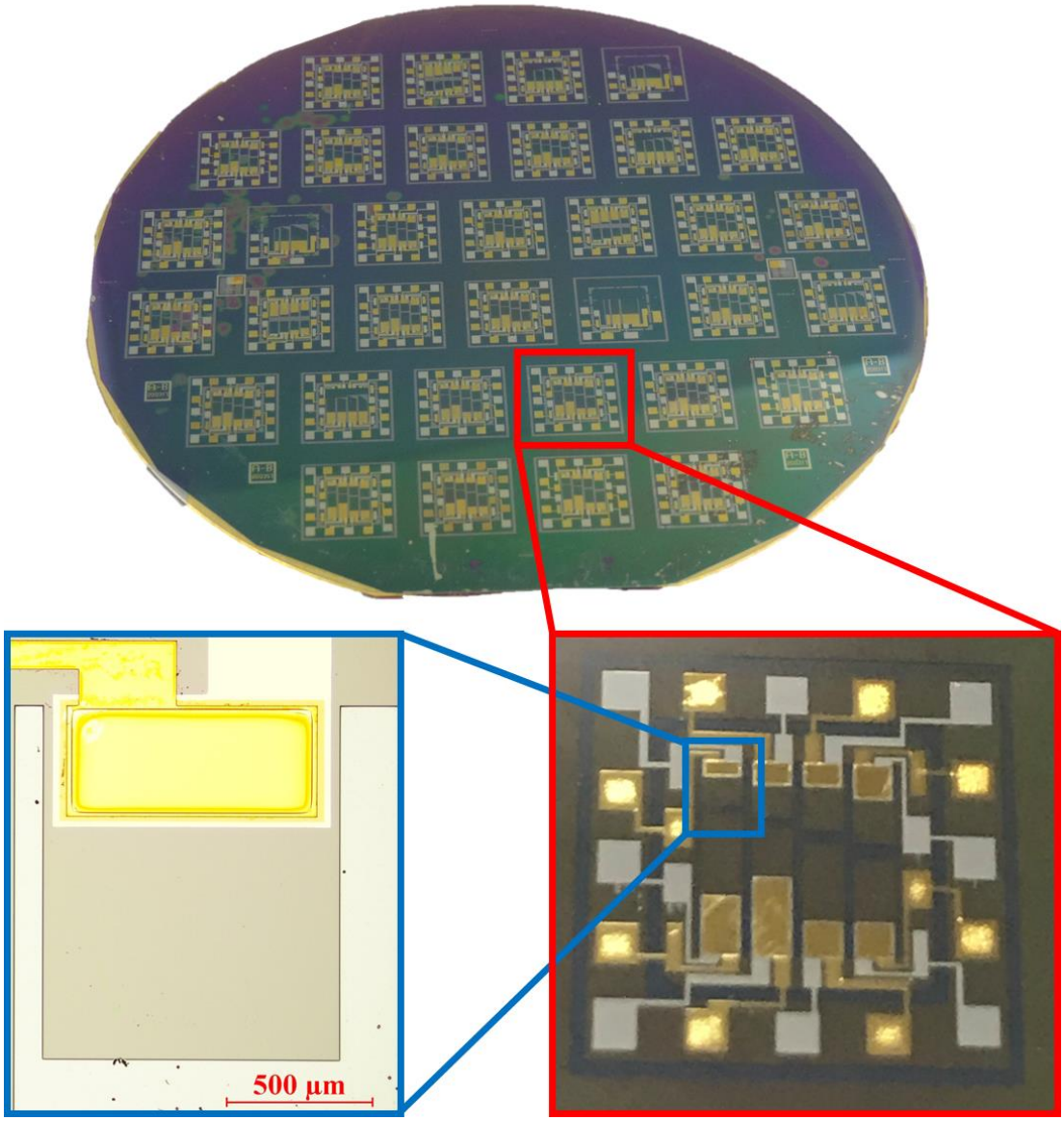

Figure 3.10 Final view of the fabricated wafer with a close-up views of device and cantilever structure with no tip mass.

3.2.2. 2nd Generation Multi-Channel Thin Film Transducer Fabrication

A 6-mask process was developed for the microfabrication of the multi-channel thin film PLD-PZT transducer. Fabrication procedure is quite similar to the fabrication of 1st generation multi-channel thin film transducer, where Figure 3.8 shows the detailed flow diagram of the fabrication process. The main idea of this last (3rd) fabrication run is to address the issues encountered during the final masking step of the previous fabrication run. Details of the above mentioned issues as well as proposed solutions explained below.

i. Forming the tip mass structure with a DRIE processes:

Problem 1: The main difficulty encountered during the fabrication was the formation of the cantilever structure with a tip mass at the free end. A spray coated photoresist was used as a mask during the backside DRIE process. However, this spray coated photoresist layer was insufficient for protecting the device and hence tip mass structure could not be formed. All of the resulting devices were lacking a tip mass, which resulted in a different resonance frequency than expected.

Problem 2: Protection of the front-side of the wafer is also of critical importance during the backside DRIE process. For this purpose, the front-side of the wafer was bonded to a dummy wafer via crystal bond. However, the dummy wafer prevents the cooling of the process wafer, which results in destruction of the crystal bonds and many burned device due to the lack of a protection layer.

Solution: The thickness of the spray coated photoresist was measured to be around 4 μm, which is the main problem during the DRIE processes since this thickness was not sufficient to protect the cantilever structures. In order to solve this problem, a relatively thick photoresist (AZ9260) was coated, which provides a 20 μm-thick layer. This should protect the devices during the DRIE processes, which solves Problem 1. As a solution to Problem 2, a thin photoresist layer should be used to protect the front side of the wafer from crystal bond material during DRIE processes. Table 3.2 shows

the details of the AZ9260 photoresist used and its specifications for front and backside of the wafer.

Table 3.1 Fabrication flow of the used photoresist for front and back side of the wafer.

Process	**Device**	**Detail**
Front side protection		
Spray coating	Spray Coater	
Hard Bake	Oven	40 min @95°C
Backside Lithography		
Dehydration	Oven	10 min @90°C
Primer Spin	Spinner	Primer @ 900 rpm, 30 s
PR spin	Spinner	AZ9260 @ 900 rpm, 30 s
Edge bead removal	Spinner	Using acetone with syringe
Horizontal wait		15 min approx.
Prebake	Hotplate	3 min @ 90°C
Soft Bake	Oven	RT to 90°C, @ 90°C 40 min
Rehydration		Closed wafer box with water at bottom
Expose	Aligner	22 sec, soft contact
Develop	Beakers	AZ826MIF, ~7 min
DI water rinse	Beakers	
Inspection	Microscope	
Descum	Nanoplus	5 min O_2 plasma

Figure 3.15 shows the final view of the front side and backside of the fabricated multi-channel device. In the backside image, Figure 3.15 (b) a 600 μm tip mass structure has been formed at backside DRIE stage successfully.

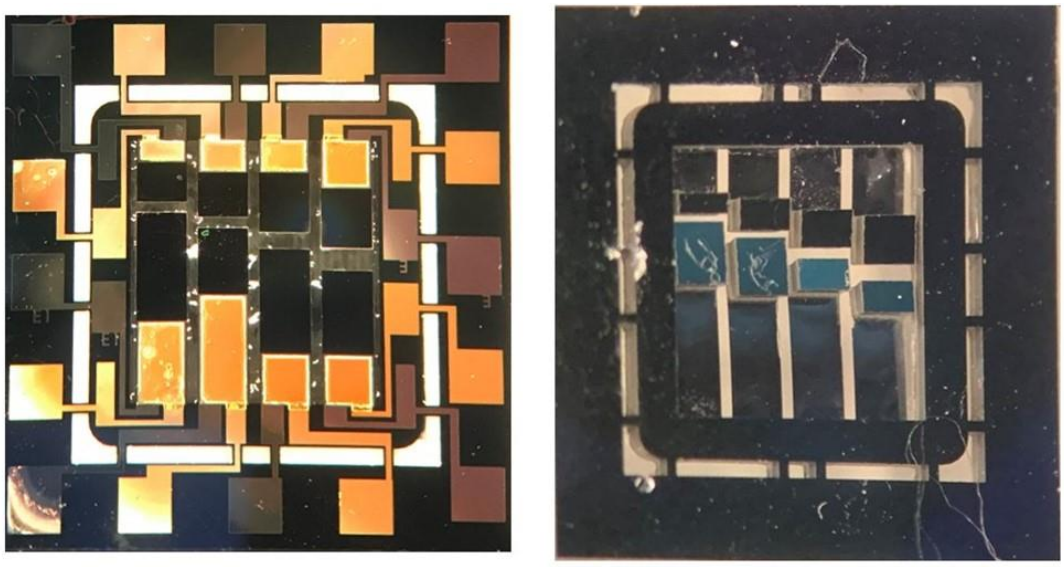

Figure 3.11 (a) front side and (b) backside view of the fabricated multi-channel thin film piezoelectric acoustic transducer with a tip mass structure.

ii. 1st and 2nd channel contact problem for 2nd generation multi-channel sensor:

Problem: During the previous fabrication run, it was observed that, 1st and 2nd channels of the device has no electrical contact. Instead, an approximately 100 Ω resistance has been measured between the two contact pads of the piezoelectric layer, which is actually the contact resistance of the platinum and gold layers. One possible reason of this problem may be the usage of buffered HF (BHF) wet etch, instead of an RIE step, for etching the oxide layer on the front side and possible damage on the contact of the piezoelectric layers.

Solution: In general, BHF is not used in oxide etch stages. However, during the previous fabrication run, the cooling system of the RIE device was not working and the only solution to etch the oxide layer was to use a BHF solution. 1st and 2nd channels are affected since they have a longer piezoelectric length. In next fabrication, RIE usage is recommended.

3.3. Summary of the Chapter

In this chapter, the fabrication procedure of the thin film piezoelectric acoustic sensor is explained. First, fabrication flow of single-channel thin film sensor using pulsed laser deposited (PLD) PZT is introduced, which includes optimization of PZT and Pt etch in detail. The cantilever and tip mass structures are formed with front and back-side deep reactive ion etching (DRIE) processes. The fabrication of flexible parylene carrier using glass wafer also provided that will be used in acoustic experiments. Finally, fabrication of the 1st and 2nd generation multi-channel thin film transducer, and overall fabrication problems and achieved solutions were elaborated in detail.

CHAPTER 4

EXPERIMENTATION OF MEMS THIN FILM PIEZOELECTRIC ACOUSTIC TRANSDUCER

This chapter is devoted to the experimentation of the microfabricated thin film piezoelectric acoustic sensors. Initially, the experimental setup used for characterization and verification of the thin film piezoelectric sensors are introduced. Then, results of mechanical and acoustic experiments on the single channel piezoelectric devices are presented and discussed. The chapter continues with verification of the proposed design by comparing experimental results with simulation results (from Chapter 2). Later, 1st and 2nd generation multi-channel thin film piezoelectric sensors are presented in detail. Finally, electrical and mechanical characterization of the multi-channel structure are presented together with the verification of simulation results.

4.1. Test Setup

Different experimental setups are constructed in order to obtain resonance and output characteristics of the fabricated chips. The characterization procedure for the thin film piezoelectric acoustic transducer is given below:

1. Capacitance/Short Test
2. LCR Circuit Test (Probe Station)
3. Shaker Test,
4. Acoustic and LDV Tests

The existing test equipment is not suitable for measuring device characteristics in a multi-channel configuration due to the insufficient number of output pins. To be able to handle LCR circuit and shaker tests, 16 wire bond connections should be established from the device to the PCB, which is rather time-consuming. Besides, the parylene layer on the top electrode (gold) prevents wire bond connections. For increasing the practicability of tests for the multi-channel device, an 8-channel chip holder and PCB were designed. The designed 8-channel chip holder can be seen in Figure 4.1. There is a specific yard on the base module that prevents dislocation of the chip. Also, the top module includes 16 holes for pogo pins, 2 holes for assembly (of the base module, top module, and PCB) and 4 holes for shaker table connection.

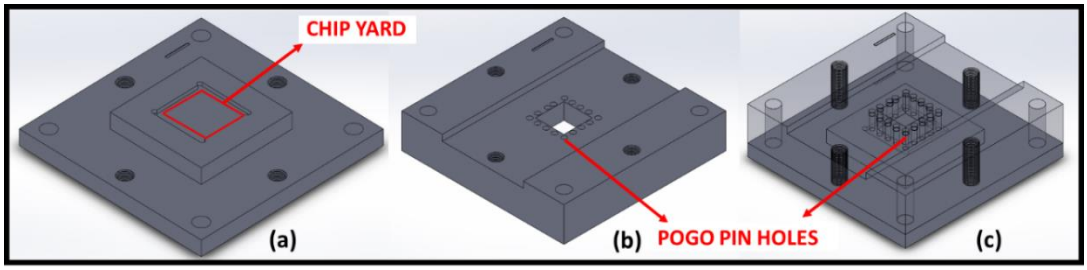

Figure 4.1 Illustration showing (a) the base module, (b) the top module and (c) the assembly of the 8-channel chip holder.

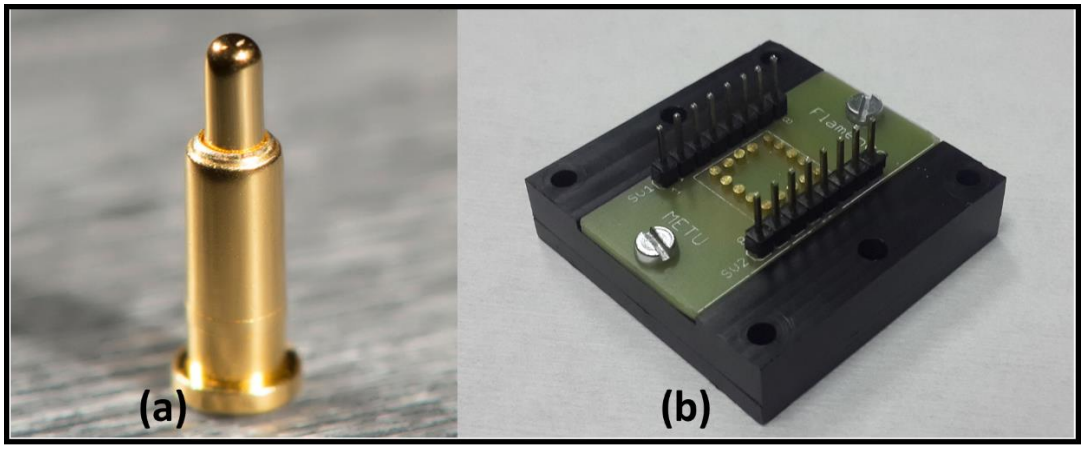

Figure 4.2 Close-up views of a pogo pin (a) and the assembled 8-channel holder (b).

The holder can be modified for different configurations of the chip while keeping the same outer frame. This functionality is provided by a spring inside the pogo pin. Images of the assembled holder and the pogo pins can be seen in Figure 4.2.

4.1.1. Capacitance/Short Test Setup

The first characterization experiment is performed following microfabrication, where each channel of the device is checked for a short circuit.

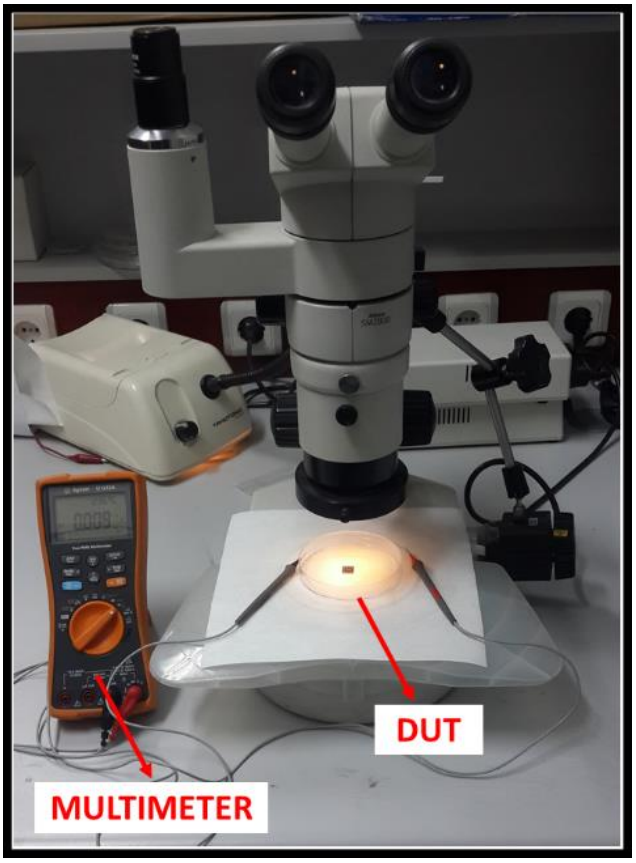

Figure 4.3 Device under test (DUT) for capacitance/short channel measurement.

The experimental setup for these tests can be seen in Figure 4.3, including a multimeter with thin probes and a microscope. This test enables determination of the working channels and the fabrication yield. Results of the test can be interpreted to understand

the short circuits between the top and bottom electrodes of the channel because of the fault occurred during the fabrication process.

4.1.2. Electrical Characterization Test Setup

The devices, which pass the capacitance/short test successfully, are tested using an LCR meter test setup for electrical characterization. This test is performed to obtain resonance characteristics of the channels. The setup is composed of an LCR Meter (Agilent E4980), a probe station and a computer with Keysight IO Suits where the configuration can be seen in Figure 4.4.

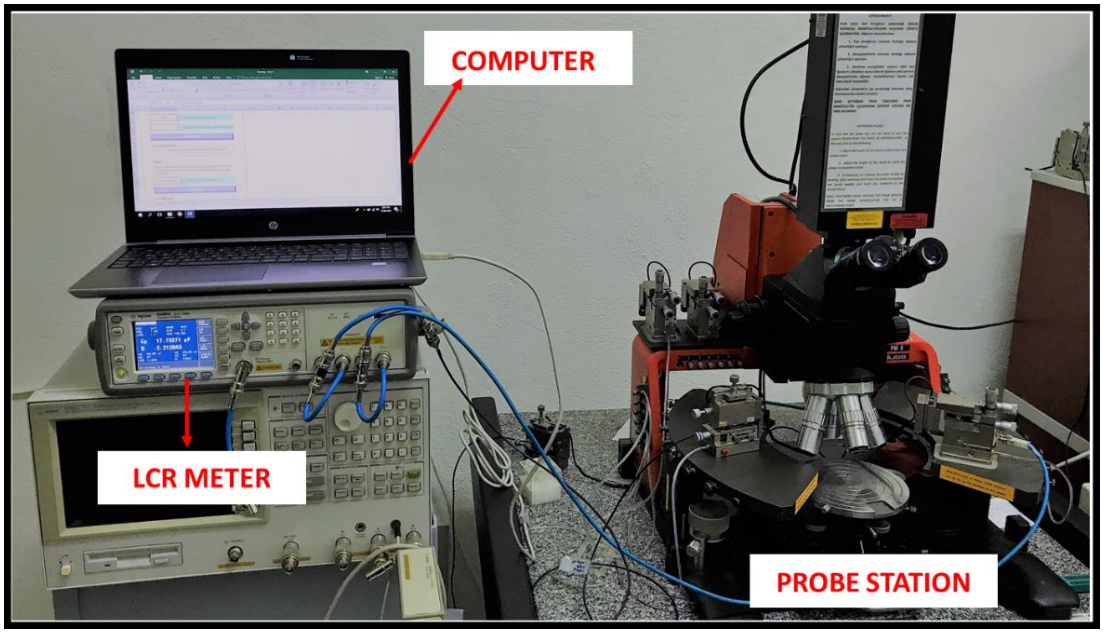

Figure 4.4 Configuration of LCR test setup with probe station.

Electrical connections are established using the probe station. Alternatively, the 8-channel chip holder can be used for the same purpose. Then, the LCR meter is arranged to measure resistance/capacitance vs frequency and obtain the expected resonance frequency. One should notice that triggering mode of the device is important. The internal triggering mode is used for checking the probe connections and the manual triggering mode is used during the frequency sweep. Finally, an Excel file with a VB

macro provided by the LCR manufacturer records the measurements on a spreadsheet. By plotting capacitance/resistance vs frequency, the resonance characteristic can be visualized. Obtained results are used for determining the resonance frequency for the shaker table tests.

4.1.3. Shaker Table Test Setup

Output voltage and bandwidth of the thin film piezoelectric acoustic transducer can be obtained at different acceleration levels through shaker table tests.

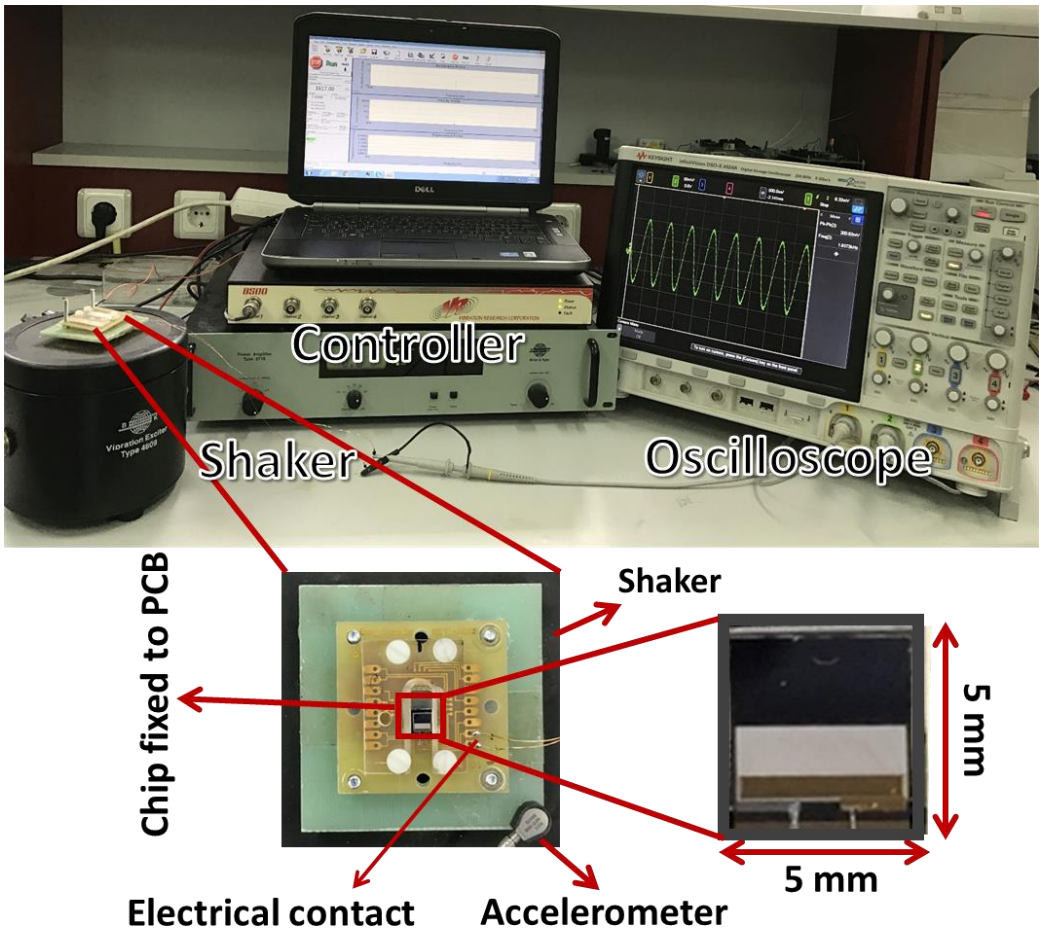

Figure 4.5 The fabricated device with a close-up view of the transducer (bottom) and the experimental setup used for performance evaluation (top).

Main components of the test setup are the shaker table, a controller, an oscilloscope, and a computer, where the configuration can be seen in Figure 4.5.

The single-channel PLD-PZT transducer was assembled onto a custom-made PCB, where the electrical connections between the contact lines on the PCB and the device electrodes were established using wire bonding. For the multi-channel device test, a holder is designed and used. The PCB assembly or holder were mounted on a shaker table, which can be vibrated at various acceleration and frequency levels set via a controller system. The generated electricity by thin film PLD-PZT transducer due to the vibration of the shaker table was monitored through an oscilloscope.

During shaker table tests, the current and the amplification level of the controller should be checked. These two variables limit the movement of the shaker table and an error message appears in the software if the defined acceleration level cannot be reached. Also, the controller does not work properly if the frequency sweep rate is too high.

4.1.4. Acoustic Test Setup

Figure 4.6 (a) shows the acoustic setup used for characterization of the PLD-PZT transducer prototype on a vibrating membrane. In order to attach the transducer to the vibrating membrane a carrier layer is to be used. The carrier should allow for easy placement of the device on the membrane while providing electrical connections. A flexible 20 µm thick Parylene-C with Cr/Au electrodes is used to form the carrier system [58]. The device was glued onto the flexible parylene carrier via epoxy bumps. Electrical connections between the device electrodes and the contact pads on the flexible carrier were established through wire bonding and conductive (silver) epoxy. Electrical connections between the carrier and the equipment were realized using a zero-insertion-force (ZIF) connector. The assembly was placed on a 40 µm thick

Parylene membrane, which mimics the eardrum characteristics. The membrane was fixed at the end of a flexible hollow tube using double-sided tape. The inner diameter and the length of the tube are defined as 9 mm and 3.5 mm, respectively, to match the dimensions of the eardrum and ear canal. The stress level of the membrane was adjusted by stretching and loosening it on the hollow tube.

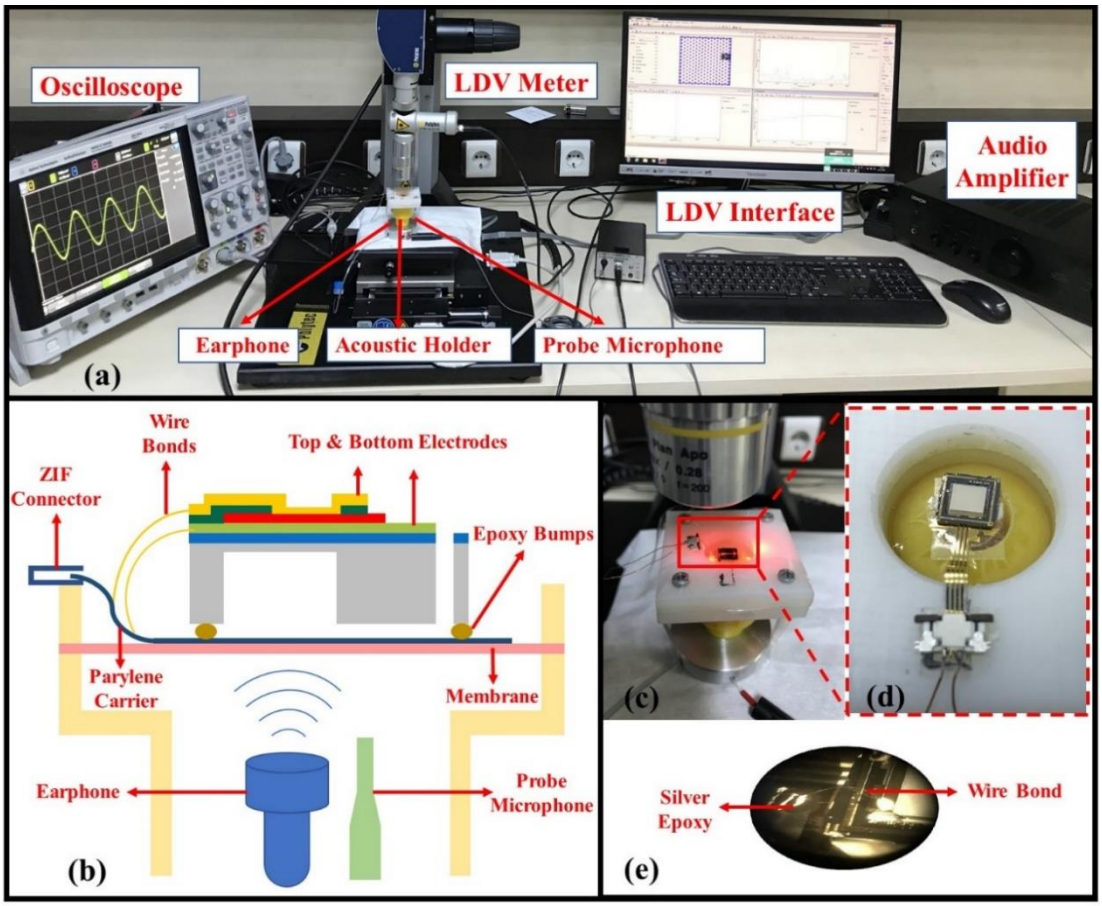

Figure 4.6 (a) The acoustic characterization setup with (b) a schematic view showing the details. (c) Flexible hollow tube and the sensor under LDV measurement. (d) The sensor and carrier attached to the membrane. (e) Tilted view of the glued chip showing the wire bonds and the silver epoxy.

Sound signals were applied to the presented ear canal model through an insert earphone, ER-2, system. The ER-2 provides a flat response for the desired

measurement interval. It is driven by an audio amplifier that produces pure voices. The sound is transmitted through the ear canal model to vibrate the flexible membrane. A probe microphone is positioned approximately 4 mm from the membrane for calibration of the incoming sound.

The displacement output was measured and recorded with a Laser Doppler Vibrometer (LDV) system. The frequency response of the eardrum-cantilever system was obtained under different SPLs above 60 dB. While the piezoelectric transducer vibrates with the incoming sound, the generated voltage is monitored, simultaneously via an oscilloscope.

4.2. Single Channel Thin Film PLD PZT Experimental Results

4.2.1. Shaker Table Test

For demonstrating the feasibility of the proposed structure, a single cantilever thin film PLD-PZT prototype was designed and fabricated. The realized device and the experimental setup for performance analysis can be seen in Figure 4.5. The footprint of the microchip is within 5×5 mm^2 by considering the eardrum dimensions [59].

The frequency response of the PLD-PZT transducer was obtained using the shaker table setup. Figure 4.7 shows the generated voltage waveform from the device around its first resonance (1620 Hz) at 0.018g acceleration. A decrease in the resonance frequency is observed with increased acceleration levels due to the ferroelectric properties of piezoelectric materials [60]. The frequency response of the device was acquired for acceleration levels from 0.006g to 0.6g, each of which corresponds to the vibration of the umbo at specific sound levels from 60 dB to 100 dB, respectively [50]. The output of the acoustic sensor is going to be processed through an interface within the dynamic hearing range in the final device. A current generator circuit will convert the sensed signals to current pulses, which will be sent to the corresponding electrodes to stimulate the auditory neurons according to the incoming sound level [59]. The

critical point is to generate the high output voltages in order to obtain a higher signal to noise ratio (SNR). Interface circuitry will consume less power for detecting the piezoelectric output signal at higher SNR levels. In a relevant study, average noise level over the sound processor is reported as 1.93 µV [50]. Experimental results show that the prototype device generates 2.6 mV at 60 dB Sound Pressure Level (SPL), which provides high enough SNR when compared with the reported sensing voltage of state-of-the-art neural stimulation circuitry for auditory neurons [25]. High output voltages at higher sound levels facilitate implementation of FICI systems and decrease the power requirement of the system, which is highly critical for FICI applications.

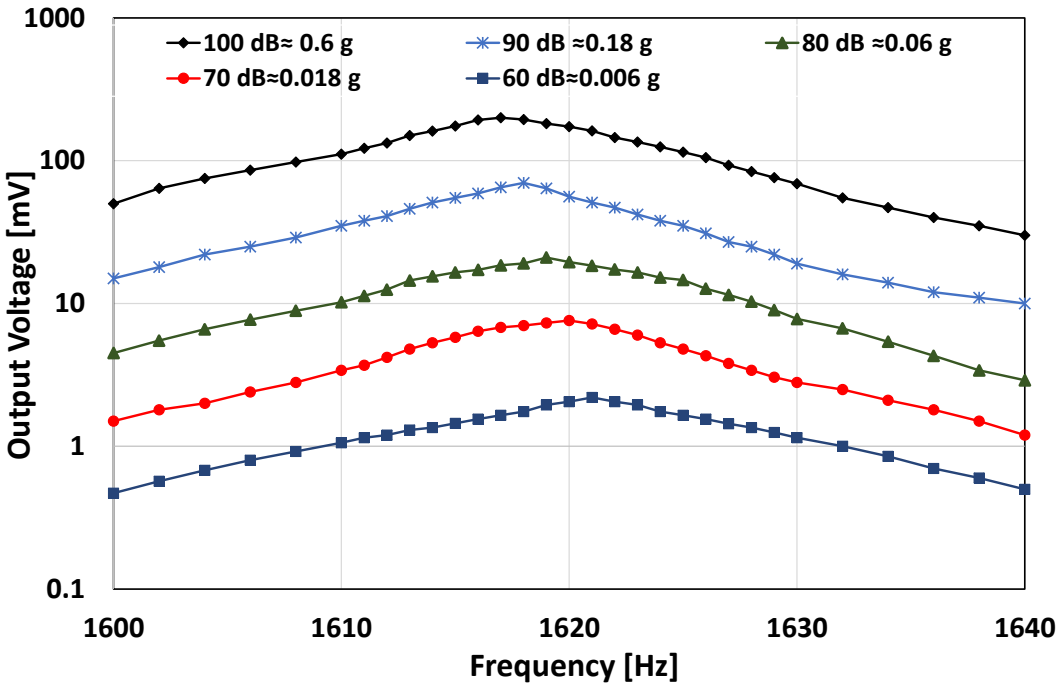

Figure 4.7 Frequency response of single cantilever PLD-PZT on the shaker table at different vibration levels of the umbo and their corresponding input sound levels.

4.2.2. Verification of Test Results Through Finite Element Simulation

Figure 4.8 shows the results of the finite element analysis carried out using COMSOL Multiphysics. Quality factors of experimental and simulation results at 100 dB are

162 and, 154 respectively, while these numbers are found as 135 and 129 at 80 dB. Output voltages of the simulation and experimental results at 100 dB are 225 mV and, 207 mV respectively, while these numbers are found as 20.9 mV and 19.1 mV at 80 dB. The simulation results are within 92% agreement with the experimental results at 100 dB and 80 dB in terms of output voltage [61]. Output voltages of the experimental results are slightly lower than simulation results due to the non-uniformity of the beam thickness, which can be reduced by optimizing the process parameters at DRIE stage of the fabrication or using a silicon-on-insulator (SOI) wafer for the fabrication.

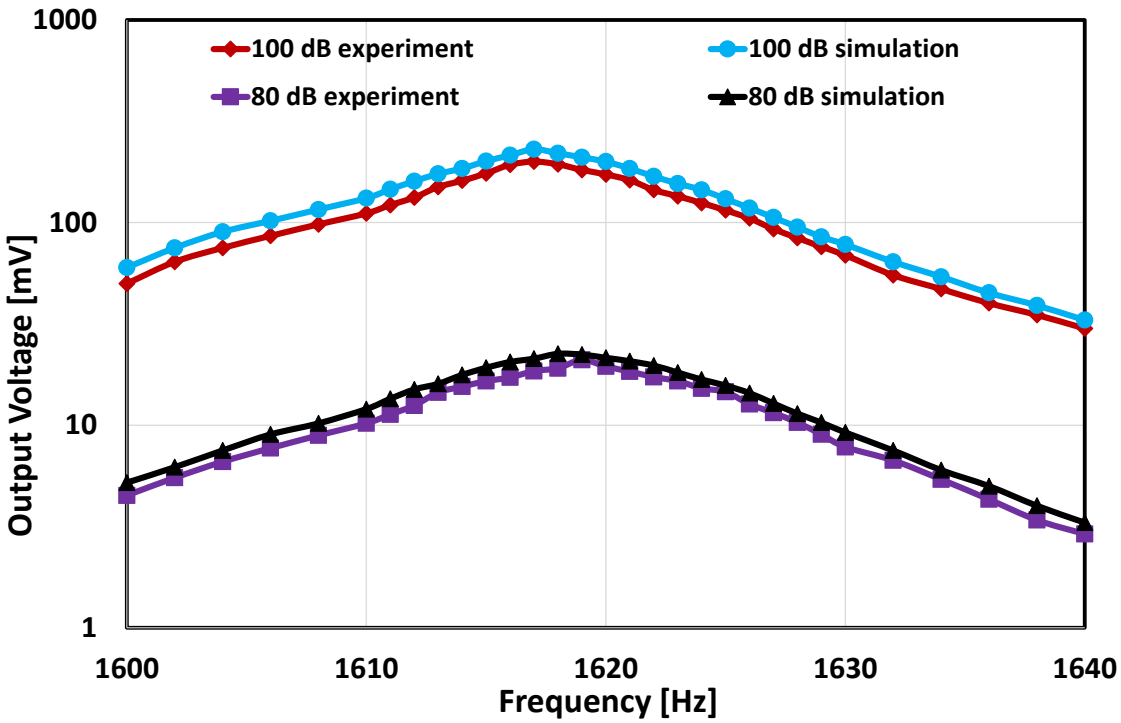

Figure 4.8 Simulation and shaker table test results of the device at two different acceleration levels corresponding to 80 and 100 dB sound pressure levels.

The transducer filters the sound mechanically by exciting only the beam with the matching resonance frequency. This system shows clear separation of frequency and provides an accurate excitation signal as an acoustic sensor mimicking the natural operation of the cochlea. The proposed design benefits from eardrum vibrations

through frequency selective piezoelectric cantilevers to generate the signals for neural stimulation. This eliminates most of the power-hungry electronics, such as microphone and active band filters, while keeping the healthy portions of the middle ear functional [59]. Hence, the proposed 8-channel thin film multi-frequency cantilever array model shows the feasibility for next-generation FICIs, which can stimulate nerves while covering the acoustic band with enough number of channels in limited volume and mass.

4.2.3. Acoustic Test Results

Figure 4.9 presents the average peak-to-peak acceleration levels of the single cantilever PLD-PZT device measured within the audible frequency spectrum under different sound levels using the acoustic setup.

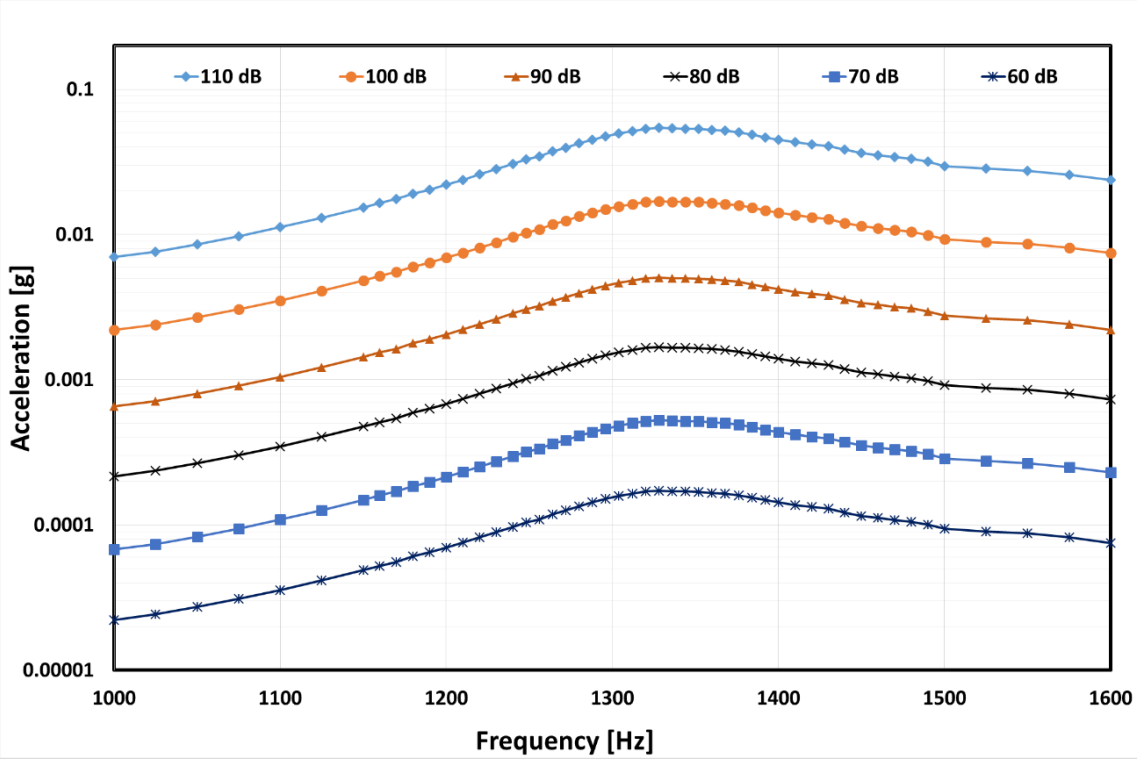

Figure 4.9 Membrane on chip acceleration characteristics for sound pressure levels from 60 to 110 dB.

As the membrane vibrates with incoming acoustic sound, the sensor starts to vibrate along with the membrane. It is critical to derive sensor acceleration characteristics along the membrane from the measured vibration behavior by taking a second-order differentiation of the displacement in the time domain. It is observed that the membrane acceleration amplitude at a given frequency interval has a 20 dB per decade slope, indicating a linear relationship between the acceleration amplitude and the input sound pressure level.

Results show that the sensor on the membrane has a maximum 0.054g at its first resonance frequency of 1325 Hz which corresponds to 110 dB input SPL. The measured acceleration demonstrates clear frequency selective characteristics, which is directly related to acoustic properties of the membrane-cantilever assembly. The acceleration and frequency characteristics of the vibrating membrane are highly dependent on the sensor attached to it due to the coupled motion. The acoustic response of the membrane changes as a result of the added mass of the sensor and the diaphragm characteristics, hence leading to deviations in the frequency and damping characteristics [62].

While the membrane transforms the incoming acoustic pressure waves into base vibrations in the ear canal, the piezoelectric sensor starts to deflect according to the acceleration level as in Figure 4.9. This deflection creates a polarization within the piezoelectric material and the sensor generates voltage by converting the mechanical motion of acoustic sound into an electrical signal and act as the eardrum itself. Figure 4.10 shows the voltage output of the thin film piezoelectric transducer that was attached to an acoustically vibrating membrane [59]. Results show that the device generates 114 mV_{pp} at 110 dB SPL. Although the membrane suppresses the voltage generation of the sensor, it is still able to generate a sufficient voltage for auditory nerve stimulation [50]. Generating higher voltage from the sensor will enable more accurate and sensitive detection by the readout circuit in the final FICI device. Also, higher voltages decrease the noise level and eliminate additional amplification which enables a reduction in stage number at readout circuitry. This decreases the power

requirements of the overall system and hence eliminate the battery requirement of cochlear implants, which is one of the main bottlenecks of conventional CIs.

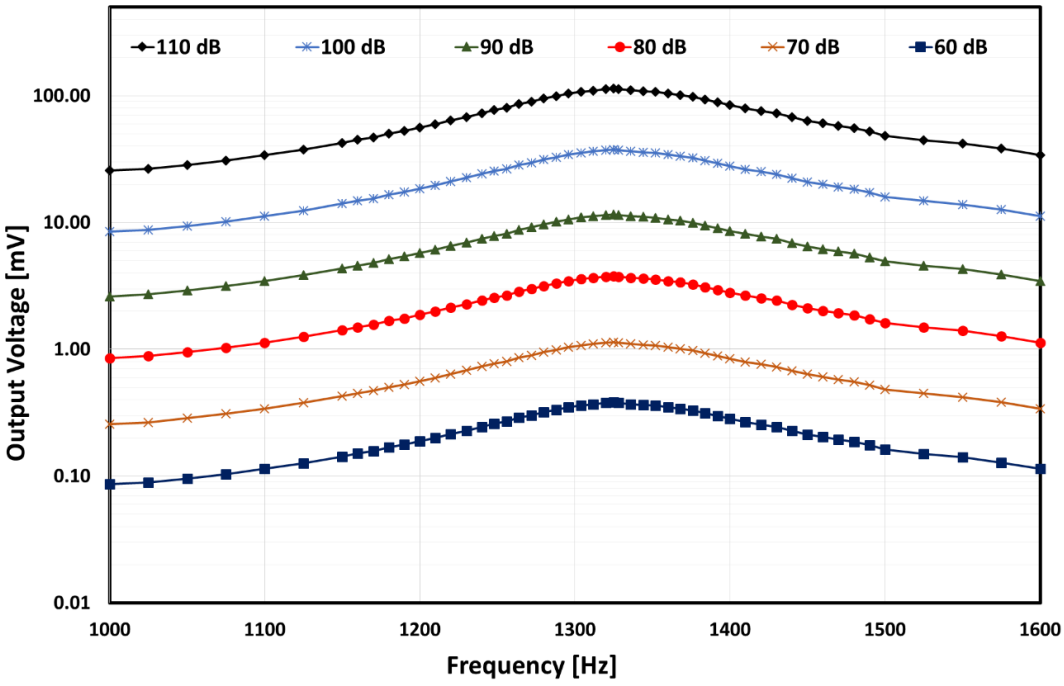

Figure 4.10 Measured acoustic results of the sensor for sound pressure levels from 60 to 110 dB SPL.

Recent studies show that critical bandwidth for speech recognition varies around 150-300 Hz in the audible frequency range [34], [63]. The study also indicates that required normalized bandwidth is slightly wider for the low-frequency channels than for the high-frequency channels. The device shows clear mechanical sensor characteristics, which has a 150 Hz bandwidth at 1325 Hz. Results indicate that bandwidth and sensitivity of the design are sufficient for detecting the hearing in audible frequency range and better than state of art thin film sensors [25]. Also, a piezo acoustic sensor with such bandpass characteristics will simplify the signal processing electronics and provide patients' continuous access to sound at every medium. This is foreseen to outplace the need for using external components and eliminating the aesthetic concerns of patients.

4.3. Multi-channel Thin Film PLD PZT Sensor Experimental Results:

4.3.1. 1st Generation Multi-channel Sensor

For demonstrating the feasibility of the proposed structure, a multi-channel cantilever thin film PLD-PZT prototype was designed and fabricated. Theory, design, and modeling of the device are explained in Chapter 2, while the detailed fabrication procedure of the chip is presented in Chapter 3. The realized device and the experimental setup for performance analysis can be seen in Figure 4.11.

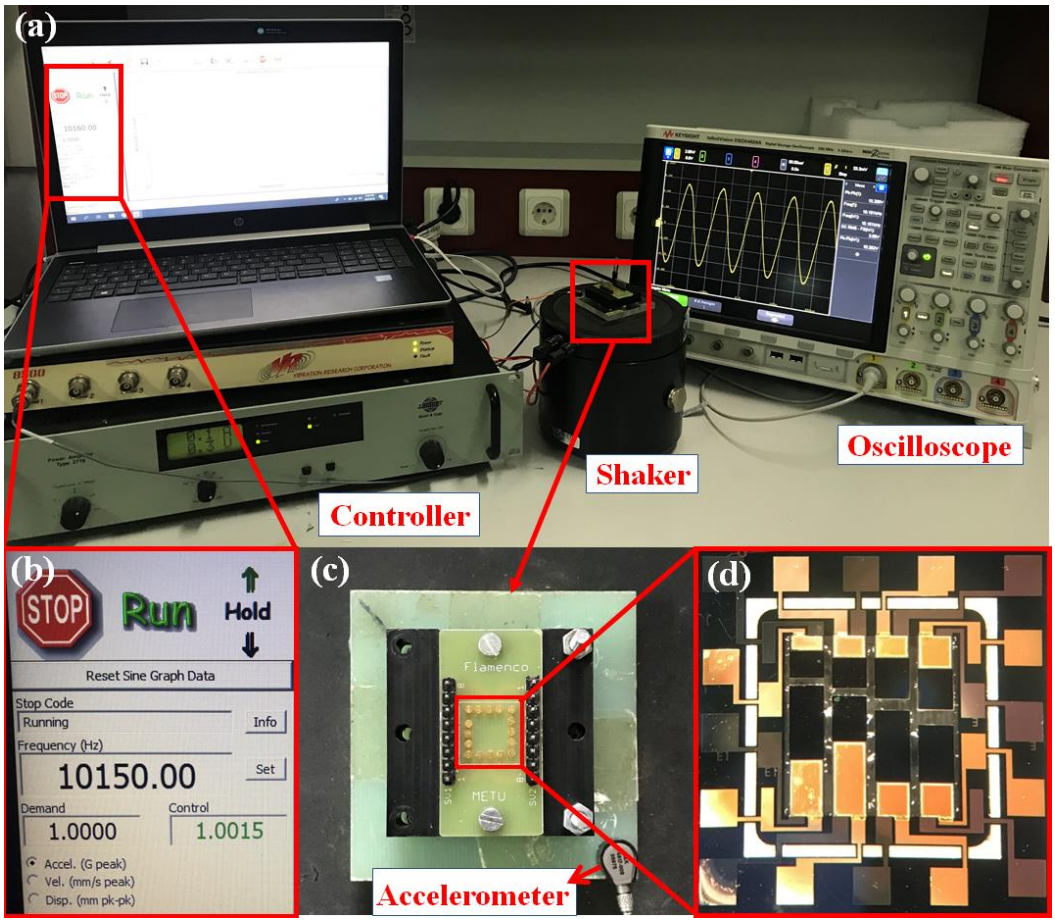

Figure 4.11 (a) The vibration characterization setup with (b) the shaker table interface showing demanded and supplied vibration (c) assembled holder attached on the shaker table (d) fabricated device with a close-up view of the transducer.

As the single channel prototype, the footprint of the microchip is optimized to fit within 5×5 mm^2 by considering the eardrum dimensions. The PLD-PZT transducer was assembled onto an 8-channel chip holder, where electrical connections between the contact lines on the PCB and the device electrodes were established using pogo pins as shown in Figure 4.1.

The PCB assembly was mounted on a shaker table, which can be vibrated at various acceleration and frequency levels set via a controller system. The voltage generated by the PLD-PZT transducer due to the vibration of the shaker table was monitored through an oscilloscope, similar shaker table setup was used as the single cantilever tests. Figure 4.12 shows the schematic view and the dimensions of the 7th channel of the fabricated device.

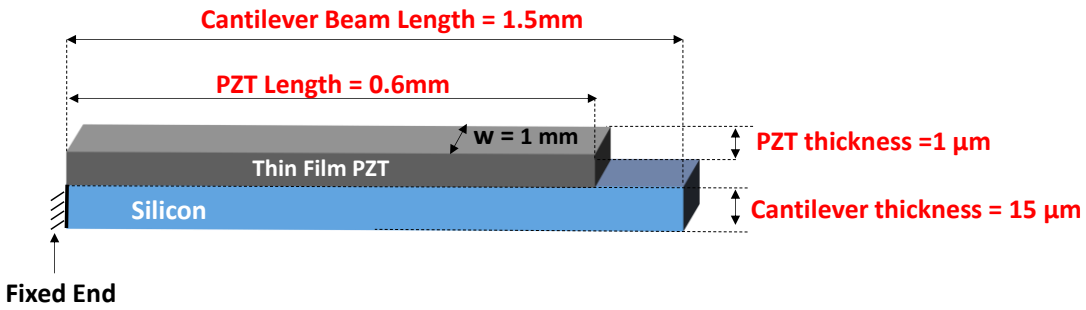

Figure 4.12 Schematic view of the 7th channel of the transducer.

The fabricated device has no tip mass due to the problems with the backside DRIE processing, which results in an increase in the resonance frequency of the device. Figure 4.13 shows the comparison of the results of the finite element analysis carried out using COMSOL Multiphysics and experimental results obtained using the shaker table setup. The resonance frequency value obtained from the simulations and experiments are 10082 Hz and 10076 Hz respectively. Experimental results are slightly lower than the simulation results due to the non-uniformity of the beam thickness. According to the finite element simulations, the device generates 11.2 mV output voltage at 1g acceleration level and at its resonance frequency, where the value is obtained to be 10 mV during the experiments performed under same conditions.

The simulation results are in a reasonable agreement with the experimental results in terms of resonance frequency and the output voltage, which can be provided by inserting each layer of device and damping ratio (0.098) into simulations. Also, fine mesh elements are inserted into the simulations to obtain more accurate result even though it increases computational time. Finally, uniformity of the beam thickness has been achieved at processes using a silicon-on-insulator (SOI) wafer for the fabrication.

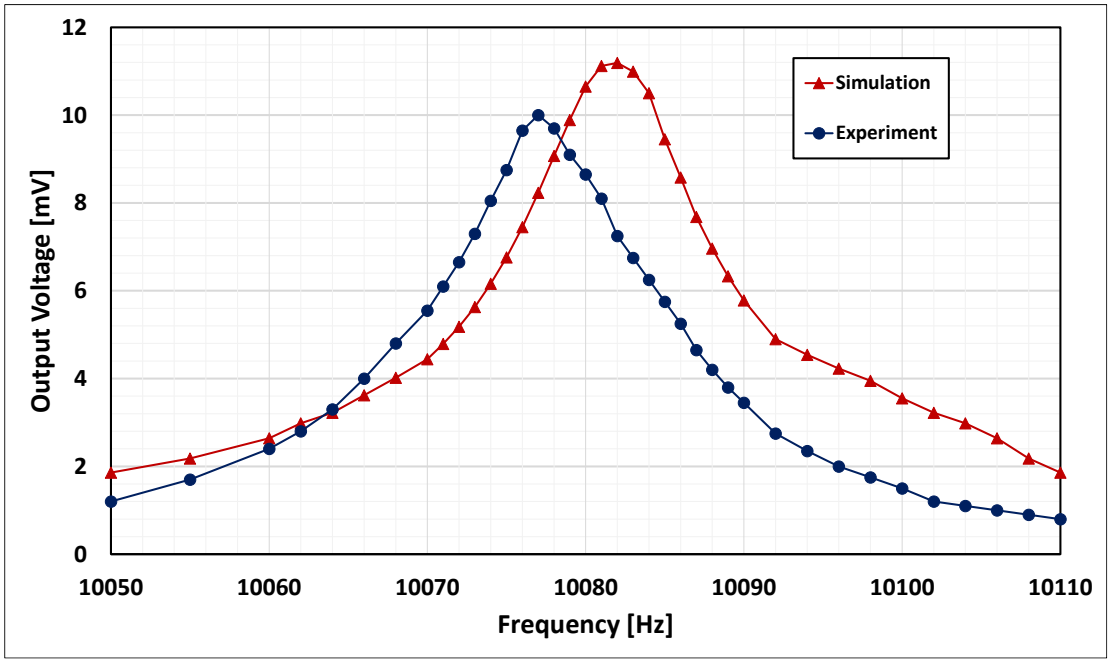

Figure 4.13 Simulation and shaker table test results of the device under consideration at 1g acceleration level.

The frequency response of the PLD-PZT transducer was obtained using the standard shaker table setup, explained in section 4.1. Figure 4.14 shows the generated voltage waveform from the device around its first resonance (10080 Hz) at 0.03g acceleration level which corresponds to a specific sound level of 100 dB. A similar decrease in the resonance frequency is observed with increased acceleration levels due to the ferroelectric properties of piezoelectric materials [60].

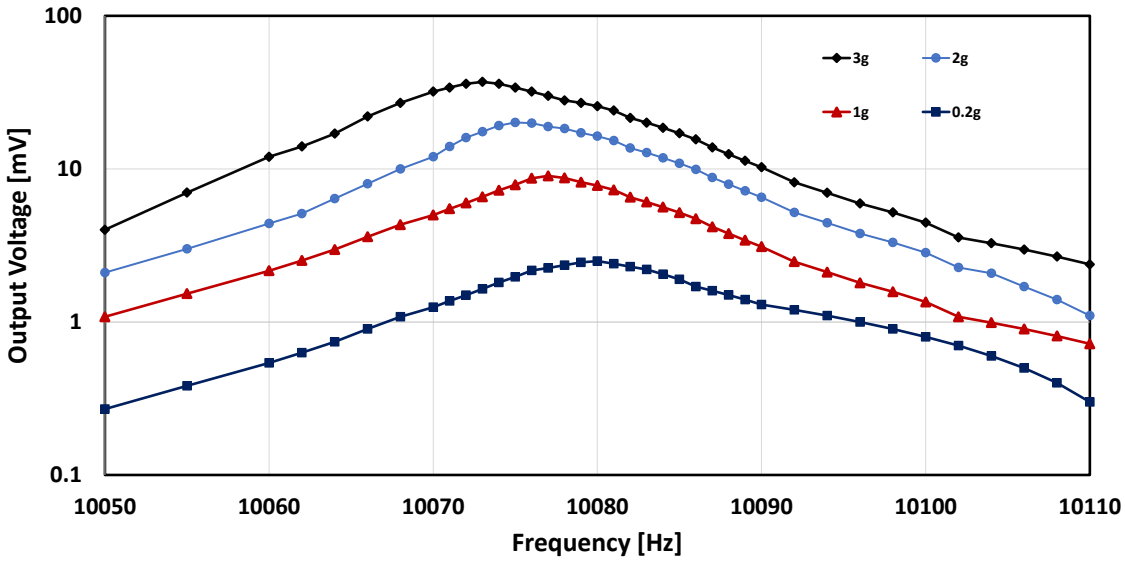

Figure 4.14 Frequency response of device under consideration at different umbo vibration levels.

Table 4.1 Comparison of the PLD PZT with alternative thin film piezoelectric materials.

Reference	Resonance Frequency (Hz)	Material	dB (SPL)	Output Voltage (mV)	Sensitivity (mV/Pa)
[25]	10200	AlN	100	2.08	0.86
[64]	10200	AlN	97	1.85	1.22
			105	3.50	0.98
This work	**10075**	**PLD**	**97**	**2.48**	**1.64**
			100	**3.50**	**1.44**
			105	**6.22**	**1.74**

Experimental results show that the prototype device generates 3.5 mV at 100 dB Sound Pressure Level (SPL), which provides high enough SNR when compared with the reported sensing voltage of state-of-the-art neural stimulation circuitry for auditory neurons [25] which is summarized in Table 4.1. The fabricated thin film piezoelectric transducer show a better performance compared with [25] in terms of the output voltage and sensitivity.

4.3.2. 2nd Generation Multi-channel Sensor

For demonstrating the feasibility of the proposed structure, a second generation multi-channel cantilever thin film PLD-PZT was fabricated. Theory, design, and modeling of the fabricated multi-channel device are explained in Chapter 2, while the detailed fabrication procedure of the 2nd generation multi-channel transducer structure is presented in Chapter 3. Figure 4.15 shows the schematic view of the fabricated device with a 600 µm tip mass structure. Tip mass usage is inevitable to tune the resonance frequency of the transducers. Also, usage of tip mass enhances the induced stress level at the fixed point, which increases the vibration level of cantilevers and provides more voltage output on the piezoelectric layer.

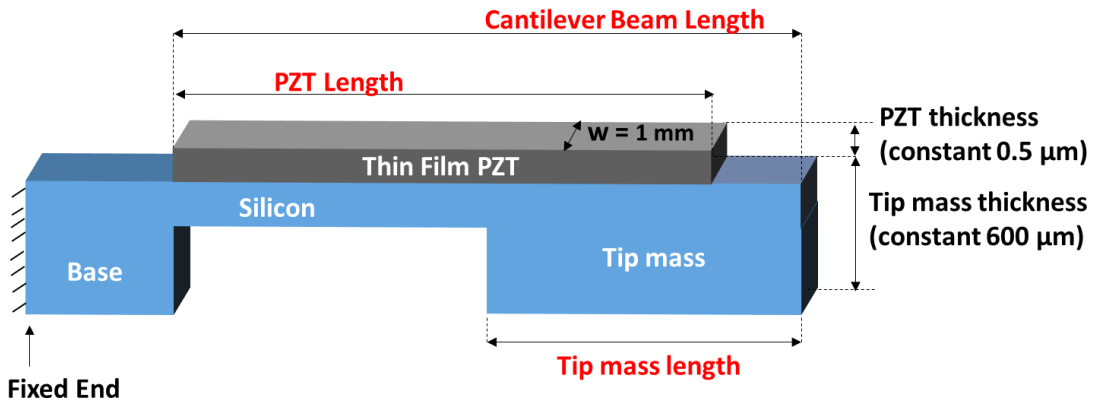

Figure 4.15 Schematic view of the transducer with tip mass structure.

Different experimental setups are constructed in order to obtain resonance and output characteristics of the fabricated devices. First, a capacitance/short test setup (Figure 4.3) has been used that enables the determination of the working channels and the fabrication yield, which is obtained to be 70 % at wafer level. Results of the test can be interpreted to understand the short circuits between the top and bottom electrodes of the channel due to a fault during the fabrication process.

The devices, which pass the capacitance/short test successfully, are tested using an LCR meter test setup for electrical characterization. This test is performed to obtain the electrical characteristics of the channels providing the resonance behavior of the devices. After obtaining electrical characteristic of the device, electromechanical characteristic of the device has been obtained through shaker table.

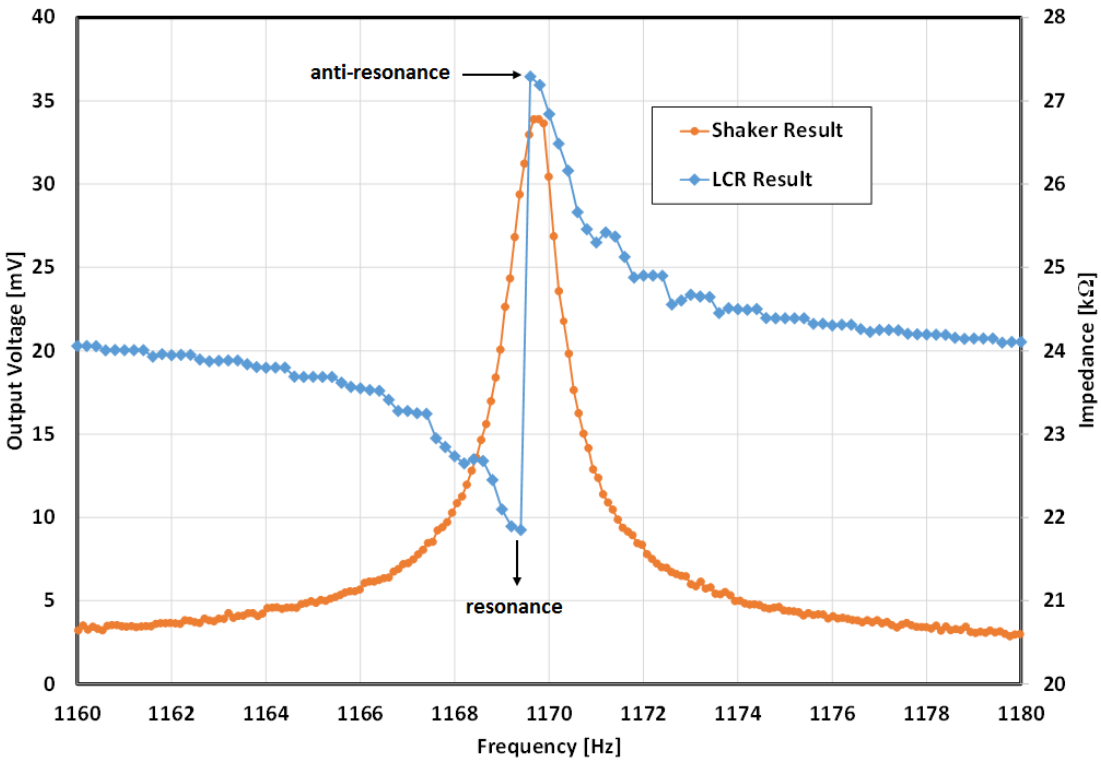

Figure 4.16 Impedance and output voltage of the 5th channel of the sensor as a function of frequency.

Figure 4.16 shows the electrical and mechanical characteristic of the device. The device has a clear resonance frequency around 1170 Hz. Piezoelectric transducer performs sensor and actuator characteristic in a sharp frequency spectrum as in the case for regular piezoelectric crystal materials. It is known that, at resonance frequency, the piezo exhibits an impedance that makes it easily driven electrically, where the device generates its maximum output voltage at its resonance frequency. As the frequency increases, the transducer's oscillations first approach the minimum impedance frequency, resonance frequency. In the resonance frequency the transducer vibrates and converts electrical energy into mechanical energy effectively. In the anti-resonance frequency, impedance increases to the maximum value.

After obtaining transducer's electrical and mechanical characteristic, it is time to test the multi-channel structure device, where the realized device and the experimental setup for performance analysis can be seen in Figure 4.11.

Figure 4.17 shows the frequency response of the multi-channel piezoelectric transducer obtained at shaker table setup, where each channel has been selected from another device in the wafer. The test results show that, fabricated multi-channel thin film device, consists of several piezoelectric cantilever beams, each of which resonates at a specific frequency within the daily acoustic band (500 Hz – 2600 Hz) and generates electricity. By this means, the transducers provide mechanical filtering.

Results show that, multi-channel transducer are able to generate sufficient sensing voltage for auditory nerve stimulation (>100 μV) for each channel at 0.1g. It is seen that, in Figure 4.17, device generates a minimum 17 mV output voltage for channel number 8, and a maximum 66 mV for channel number 3.

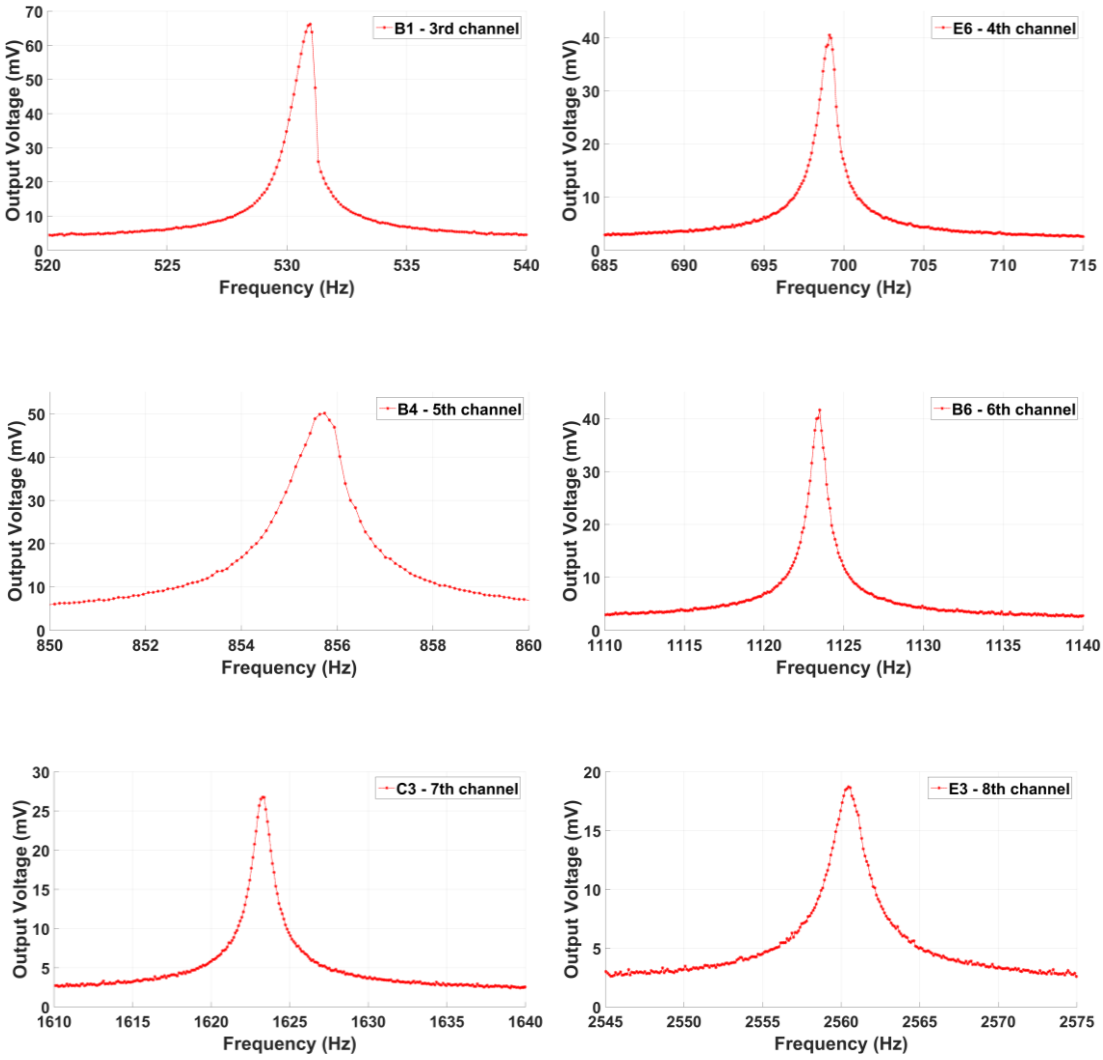

Figure 4.17 Frequency response of multi-channel PLD-PZT on the shaker table at 0.1g acceleration level (Placement of the devices in the wafer are shown in Appendix).

Figure 4.18 presents the average peak-to-peak acceleration levels of the 5th channel of the multi-channel device for different device to show the die level uniformity. The results show that, device resonates in a narrow frequency spectrum. The average resonance frequency of the three devices is around 853Hz with ± 3 Hz error margin. That shows the reliability and uniformity of the fabrication of the multi-channel thin film piezoelectric transducers.

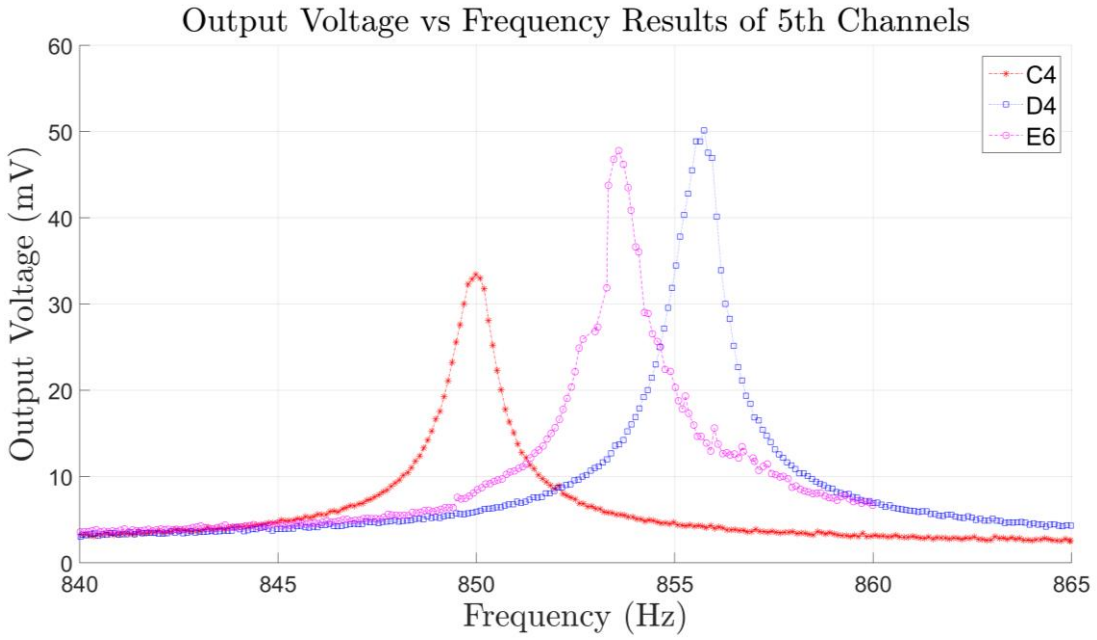

Figure 4.18 Frequency response of the 5th channel of the multi-channel structure for different device located on the wafer (Appendix). The output voltage are measured at shaker table under 0.1g acceleration.

Figure 4.19 shows the comparison of the simulation and experimental results for 6-channel multi-frequency structure at 0.1g acceleration, where each sensor resonates at a selected frequency within the daily frequency spectrum. Simulation results have been carried out using COMSOL Multiphysics, while the experimental results have been conducted at shaker table. Table 4.2 lists the resonance frequency and the output voltage results of the simulation and experimental data each frequency. Channel number, device name and corresponding cantilever length are also given for each channel.

As seen in Figure 4.19, the transducer filters the sound mechanically by exciting only the beam with the matching resonance frequency. This system shows clear separation of frequency and provides an accurate excitation signal as an acoustic sensor mimicking the natural operation of the cochlea.

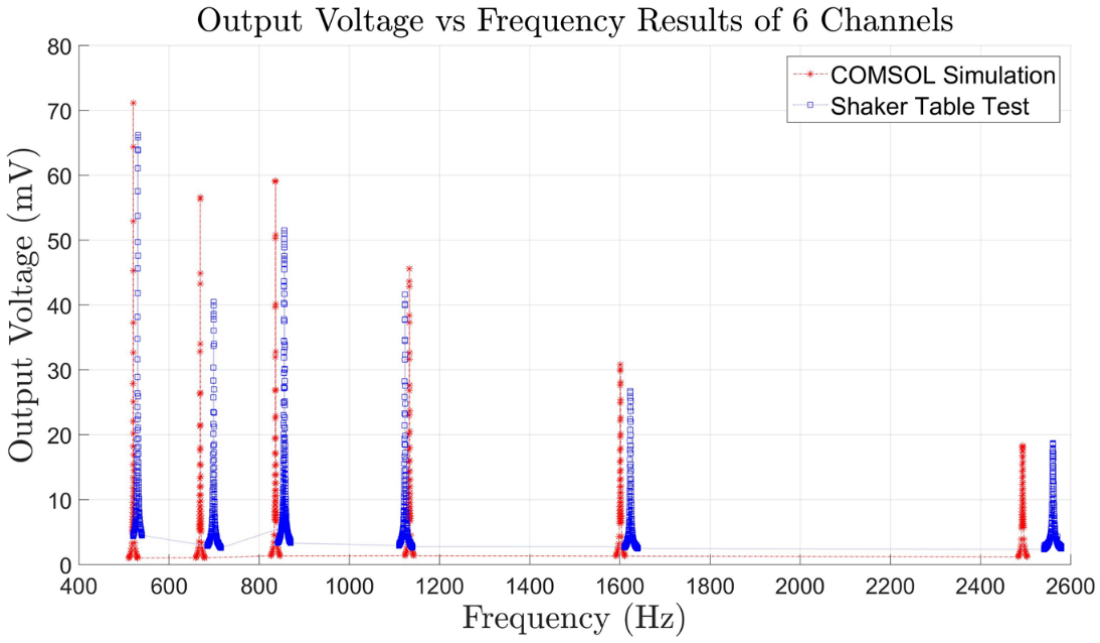

Figure 4.19 Simulation and shaker table test results of the device under consideration at 0.1g acceleration level for 6 channel device.

The simulation and experimental results are within a reasonable agreement in terms of resonance frequency and the output voltage for multi-channel transducer configuration as in the seen in Table 4.2.

Table 4.2 Specifications of the simulation and experimental results of the device under consideration at 0.1g acceleration level for 6 channel device.

Channel Number	Device Name	Beam Length (mm)	Simulation Resonance Frequency (Hz)	Experiment Resonance Frequency (Hz)	Simulation Output Voltage (mV)	Experiment Output Voltage (mV)
3	B1	2.9	520	530	71	66
4	E6	2.5	670	750	57	47
5	B4	2.1	840	855	59	52
6	B6	1.8	1135	1123	46	42
7	C3	1.5	1600	1623	31	25
8	E3	1.2	2500	2560	17	17

In the proposed multi-frequency thin film piezoelectric acoustic sensor concept, the main idea is to overcome the main bottlenecks of CIs, considering the limitations regarding footprint, volume, mass and stimulation signal. Also, the system should consist of several thin film piezoelectric cantilever beams, each of which vibrates at a resonance frequency to cover the daily acoustic band.

Results demonstrate that, fabricated multi-channel piezoelectric transducer covers the daily acoustic band (Figure 4.19) with an adequate number of channels within the small volume of the middle ear. In these acoustic band (500 Hz – 2500 Hz), the multi-channel sensor has a clear frequency distribution such that the operation band and other harmonics of each piezoelectric transducer are well separated to avoid crosstalk. In these manner, the multi-channel sensor mimics the natural operation of the cochlea.

Another important design parameter was to generate the required stimulation signal. According to Table 4.2, results show that each channel of the device generates sufficient output voltage considering the reported sensing voltage requirement of a neural stimulation circuitry for auditory neurons [50]. The power dissipation further decreases due to the higher signal-to-noise ratio of the thin film PZT transducers, which result in a lower power requirement by the interface circuitry for detecting the signal. Therefore, it can be anticipated that the battery lifetime of an implantable system increases and the frequency of battery charging decreases.

Hence, the proposed 8-channel thin film multi-frequency cantilever array model shows the feasibility for next-generation FICIs, which can stimulate nerves while covering the acoustic band with enough number of channels in limited volume and mass. The proposed design is also predicted to solve the main challenges of cochlear implants such as damage risk of external components, high cost and aesthetic concerns of patients.

4.4. Summary of the Chapter

In this chapter, the experimental results of the proposed thin film piezoelectric acoustic sensor are presented. Details of the experimental setup configurations are explained, which are used for characterization and verification of the thin film piezoelectric sensors. Later, mechanical and electrical experimental results of fabricated single-channel piezoelectric devices are presented, which are characterized by a standard probe station, LCR meter, and shaker table. Acoustical experimental results of the device are characterized by a Laser Doppler Vibrometer (LDV) setup, which demonstrate the feasibility of the proposed device. After that, a verification of the performance of the developed device is provided through a comparison of the experimental results with the simulation results. Later, experimental results of multi-channel thin film piezoelectric sensors are presented and compared with the state-of-the-art, which shows the feasibility of the next-generation FICIs. Finally, a 6-channel electrical and mechanical characterization of the multi-channel structure has been verified with the simulation results.

CHAPTER 5

CONCLUSION AND FUTURE WORK

This thesis reports the development of thin film PLD piezoelectric acoustic transducer to be placed on the eardrum for the development of next-generation, fully implantable cochlear implants. The proposed model utilizes the natural hearing mechanism and mimics the hair cells via a set of frequency-selective piezoelectric cantilevers to stimulate the auditory nerve. For this purpose, a multi-channel sensor is improved to solve the main challenges of cochlear implants by minimizing the mass, footprint, and volume of the transducers so that they can fit into the middle ear, without sacrificing the generated voltage levels. In this direction, modeling, fabrication, and characterization of a cantilever-based thin film PLD-PZT acoustic sensor are presented.

Accomplished tasks during the research are summarized as follows:

- A novel application of piezoelectric transduction from tympanic membrane vibrations for developing next-generation cochlear implants has been investigated.

- Using available implantable sensor and conventional cochlear implant data in the literature, a multi-channel thin film piezoelectric sensor is developed that satisfy all the requirements and challenges of the system: limited footprint and volume in the middle ear, number of channels, stimulation signal, and mass.

- A finite element model (FEM) study has been investigated to analyze the theory of piezoelectric transduction. COMSOL Multiphysics is chosen among other FEM applications due to its flexibility and multiphysics nature (electrical, mechanical and acoustic) of the proposed system.

- Theory of selection of Pulsed Laser Deposited (PLD) thin film piezoelectric materials among other materials has been investigated and a feasibility study has been presented.

- Anisotropic material properties of pulsed laser deposited PZT and silicon layers are explained in detail and inserted to the simulations successfully. Moreover, boundary conditions, meshed modeling, and analysis of simulations are explained in detail.

- An optimization study has been designed by a parametric sweep property of COMSOL to maximize the generated output voltage in the desired volume, footprint and mass. For this purpose, a feasibility study has been achieved to minimize the input variables. Tip mass, silicon and piezoelectric layer thicknesses and widths are optimized at constant values.

- As a proof-of-concept prototype, first a single-channel thin film PLD-PZT chip was modeled. Furthermore, the developed prototype has been fabricated using a 1 μm PLD PZT as the piezoelectric layer which is chosen due to its superior ferroelectric and piezoelectric properties.

- In this direction, a 6-mask fabrication flow has been improved using the silicon as a base layer. Fabrication procedure includes PLD-PZT and Platinum wet etch optimizations. Moreover, a parylene membrane has been fabricated to mimic the operation of the eardrum which will be coupled with the fabricated device. Finally, a flexible parylene carrier has been fabricated on glass wafer that will be used for acoustical experiments.

- The mechanical and electrical properties were characterized by a standard probe station, LCR meter, and shaker table.

- For acoustic tests, the realized device was assembled onto a flexible carrier and placed on a parylene membrane.

- Experimental results demonstrate that the generated voltage by transducers exceeds the minimum required sensing voltage for the neural stimulation circuitry and decreases the required power for readout circuitry.

- Agreement of simulation and experimental results clearly indicate that the proposed multi-frequency thin film model satisfies all the requirements of an FICI system.

- The proposed multi-channel thin film cantilever model has been fabricated similarly to the single-channel PLD-PZT fabrication procedure. This process has been optimized using 7 masks and SOI wafer is used.

- Fabricated device has been placed into a specific holder that provides electrical connections via pogo pins and characterized by a standard shaker table configuration.

- Experimental results demonstrate that the generated voltage of this device also exceeds the minimum required sensing voltage for the neural stimulation circuitry. The verification of the device performance has been proven by agreement with the simulation results. Finally, device performance has been compared with the state of the art thin film studies available in the literature and it has been shown although tip mass structure cannot be formed, proposed thin film sensor is still the best thin film sensor among other sensors in terms of generated output voltage and sensitivity. Combining the piezoelectric thin film sensor with low power CI electronics and thin-film MEMS electrodes a truly fully implantable system with no external components can be realized.

- A second generation multi-channel transducer fabrication has been conducted. The main idea of this last (3^{rd}) fabrication run is to address the issues encountered during the final masking step of the previous fabrication run.

- In the second batch, problems in the DRIE processes has been solved and multi-channel sensor with a tip mass structure has been fabricated.

- Electromechanical characterization of the fabricated multi-channel prototype has been measured by a shaker table and LCR meter.

- The test results show that, fabricated device, consists of several piezoelectric cantilever beams, each of which resonates at a specific frequency within the daily acoustic band (500 Hz – 2600 Hz).

- Consequently, the device provides mechanical filtering and shows a clear frequency selectivity mimicking the operation of the cochlea.

- Experimental results show that the voltage output of the device exceeds the minimum required sensing voltage for the neural stimulation circuitry and decreases the required power for readout circuitry

- Hence, the feasibility of the proposed next-generation FICI system, which can stimulate nerves while covering the acoustic band with enough number of channels is verified.

- The proposed design is also predicted to solve the main challenges of cochlear implants such as damage risk of external components, high cost and aesthetic concerns of patients.

While this thesis led to significant achievements contributing to the development of thin film piezoelectric acoustic transducers for FICI applications, there are still some further studies to be achieved. Future work of the presented research are summarized as follows:

- The fabricated devices should be tested with a more realistic diaphragm to analyze the vibration characteristics of the coupled structure. For this purpose, a better membrane should be developed and fabricated to imitate the eardrum.

- A 3D model of the ear itself should be obtained that models eardrum, ear canal, and ossicles. The device should be mounted and the performance of the device should be analyzed optimizing the placement of the transducer.

- In vitro and in vivo animal tests should be experimented with the piezoelectric transducers. In the beginning, transducers will be excited externally and then transducers will be implanted, and experiments should be conducted.

- Long-term mechanical, electrical and acoustical tests should be performed on transducers.

- The transducers should be tested with the integrated interface circuitry. One channel performance has been shown already, but multi-channel tests should also be conducted and the generated biphasic pulse signal should be analyzed.

- A new fabrication for multi-channel thin film piezoelectric transducers should be processed using SOI wafers at different thickness.

- A bandwidth study should be conducted depending on the performance of transducers and their compatibility with cochlear implant requirements. A balanced at bandwidth should be provided between the number of electrodes and sound perception.

REFERENCES

[1] F. G. Zeng and R. R. Fay, *Cochlear Implants: Auditory Prostheses and Electric Hearing*. New York, NY: Springer Science & Business Media, 2013.

[2] M. L. Ugalde, "Speech-brain synchronization: a possible cause for developmental dyslexia," Ph. D dissertation, Department of Linguistic and Basque Studies, University of the Basque Country, Leioa, 2017.

[3] Fred H. Bess and Larry E. Humes, *Audiology: The Fundamentals*. Richmond, TX: Lippincott Williams & Wilkins Publishers, 1990.

[4] M. F. Bear, B. W. Connors, and M. A. Paradiso, *Neuroscience: Exploring the Brain*. Philadelphia, PA: Lippincott Williams & Wilkins Publishers, 2015.

[5] D. Taft and E. Saunders, "Predicting speech information from the audiogram and vice versa," vol. 2, no. 2, 2012.

[6] M. K. Cosetti and S. B. Waltzman, "Cochlear implants: Current status and future potential," *Expert Review of Medical Devices*, vol. 8, no. 3, pp. 389-401, 2011.

[7] D. S. Haynes, J. A. Young, G. B. Wanna, and M. E. Glasscock, "Middle Ear Implantable Hearing Devices: An Overview," *Trends Amplif.*, vol. 13, no. 3, pp. 206–214, Sep. 2009.

[8] B. S. Wilson, "Cochlear implants: Current designs and future possibilities," *J. Rehabil. Res. Dev.*, vol. 45, no. 5, pp. 695–730, 2008.

[9] H. Lane, R. Hoffmeister, and B. Bahan, *A Journey into the Deaf-World*. San Diego, CA: Dawn Sign Press, 1996.

[10] "Medical gallery of Blausen Medical 2014," *WikiJournal Med.*, vol. 1, no. 2, 2014.

[11] B. S. Wilson, "Cochlear implants: Current designs and future possibilities," *J. Rehabil. Res. Dev.*, vol. 45, no. 5, pp. 695–730, 2008.

[12] F. G. Zeng, S. Rebscher, W. Harrison, X. Sun, and H. Feng, "Cochlear implants: system design, integration, and evaluation," *IEEE Annu. Rev. Biomed. Eng.*, vol. 1, no. 5, pp. 115–142, 2008.

[13] W. T. Park, K. N. O'Connor, K. L. Chen, J. R. Mallon, T. Maetani, P. Dalal, R. N. Candler, V. Ayanoor-Vitikkate, J. B. Roberson, S. Puria, and T. W. Kenny, "Ultraminiature encapsulated accelerometers as a fully implantable sensor for implantable hearing aids," *Biomed. Microdevices*, 2007.

[14] A. Vujanic, R. Pavelka, N. Adamovic, C. Kment, S. Mitic, W. Brenner, and G. Popovic, "Development of a totally implantable hearing aid," *2002 23rd Int. Conf. Microelectron. Proc. (Cat. No.02TH8595)*, vol. 1, pp. 12–15, 2002.

[15] Z. Djinović, R. Pavelka, M. Tomić, G. Sprinzl, H. Plenk, U. Losert, H. Bergmeister, and R. Plasenzotti, "In-vitro and in-vivo measurement of the animal's middle ear acoustical response by partially implantable fiber-optic sensing system," *Biosens. Bioelectron.*, vol. 103, no. November, pp. 176–181, 2018.

[16] A. J. Maniglia, G. Murray, J. E. Arnold, and W. H. Ko, "Bioelectronic microphone options for a totally implantable hearing device for partial and total hearing loss," *Otolaryngol. Clin. North Am.*, vol. 34, no. 2, pp. 469–483, 2001.

[17] W. H. Ko, R. Zhang, P. Huang, J. Guo, X. Ye, D. J. Young, and C. A. Megerian, "Studies of MEMS acoustic sensors as implantable microphones for totally implantable hearing-aid systems," *IEEE Trans. Biomed. Circuits Syst.*, vol. 3, no. 5, pp. 277–285, 2009.

[18] C. Stieger, D. Djeric, M. Kompis, L. Remonda, and R. Häusler, “Anatomical study of the human middle ear for the design of implantable hearing aids,” *Auris Nasus Larynx*, 2006.

[19] M. A.J. and A. J. Maniglia, “State of the art on the development of the implantable hearing device for partial hearing loss,” *Otolaryngol. Clin. North Am.*, 1996.

[20] M. A. Zurcher, D. J. Young, M. Semaan, C. A. Megerian and W. H. Ko, "MEMS middle ear acoustic sensor for a fully implantable cochlear prosthesis," 2007 IEEE 20th International Conference on Micro Electro Mechanical Systems (MEMS), Hyogo, 2007, pp. 11-14.

[21] P. Huang, J. Guo, C. A. Megerian, D. J. Young, and W. H. Ko, “A laboratory study on a capacitive displacement sensor as an implant microphone in totally implant cochlear hearing aid systems.,” *Conf. Proc. IEEE Eng. Med. Biol. Soc.*, vol. 2007, pp. 5692–5, 2007.

[22] X. H. Jia, N. Gao, X. Da Xu, Y. Z. Wu, H. Y. Kang, and F. L. Chi, “A new floating piezoelectric microphone for the implantable middle ear microphone in experimental studies,” *Acta Otolaryngol.*, vol. 136, no. 12, pp. 1248–1254, 2016.

[23] Y. Jung, S. Kim, J. Kwak, H. Kang, Y. H. Lee, S. Park, W. Kim, and S. Hur, “Development and characterization of piezoelectric artificial cochlear with micro actuator mimicking human cochlear,” in *Journal of Physics: Conference Series*, 2013, vol. 476, no. 1.

[24] N. Mukherjee, R. D. Roseman, and J. P. Willging, “The piezoelectric cochlear implant: Concept, feasibility, challenges, and issues,” *J. Biomed. Mater. Res.*, vol. 53, no. 2, pp. 181–187, 2000.

[25] J. Jang, J. Lee, S. Woo, D. J. Sly, L. J. Campbell, J.-H. Cho, S. J. O’Leary, M.-H. Park, S. Han, J.-W. Choi, J. Hun Jang, and H. Choi, “A

microelectromechanical system artificial basilar membrane based on a piezoelectric cantilever array and its characterization using an animal model," *Sci. Rep.*, vol. 5, 12447, 2015.

[26] W. H. Ko, J. Guo, R. Zhang, D. J. Young, and C. A. Megerian, "MEMS acoustic sensors for totally implantable hearing aid systems," *2008 IEEE Int. Symp. Circuits Syst.*, 2008.

[27] W. H. Ko, J. Guo, R. Zhang, D. J. Young, and C. A. Megerian, "MEMS acoustic sensors for totally implantable hearing aid systems," *2008 IEEE Int. Symp. Circuits Syst.*, pp. 1812–1817, 2008.

[28] D. J. Young, M. A. Zurcher, M. Semaan, C. A. Megerian, and W. H. Ko, "MEMS capacitive accelerometer-based middle ear microphone," *IEEE Trans. Biomed. Eng.*, vol. 59, no. 12, pp. 3283–3292, 2012.

[29] J. Chung, W. J. Song, J. H. Sim, W. Kim, and S. H. Oh, "Optimal ossicular site for maximal vibration transmissions to coupled transducers," *Hear. Res.*, vol. 301, pp. 137–145, 2013.

[30] K. E. Fishman, R. V Shannon, and W. H. Slattery, "Speech recognition as a function of the number of electrodes used in the SPEAK cochlear implant speech processor.," *J. Speech. Lang. Hear. Res.*, vol. 40, no. 5, pp. 1201–1215, 1997.

[31] Q. Fu, R. V. Shannon, and X. Wang, "Effects of noise and spectral resolution on vowel and consonant recognition: Acoustic and electric hearing," *J. Acoust. Soc. Am.*, vol. 104, no. 6, pp. 3586–3596, 1998.

[32] H. Uluşan, S. Chamanian, Ö. Zorlu, A. Muhtaroğlu, and H. Külah, "Neural Stimulation Interface with Ultra-Low Power Signal Conditioning Circuit for Fully-Implantable Cochlear Implants," *BioCAS 2017*, pp. 6–9, 2017.

[33] P. C. Loizou, M. Dorman, and Z. Tu, “On the number of channels needed to understand speech,” *J. Acoust. Soc. Am.*, vol. 106, no. 4, pp. 2097–2103, 1999.

[34] K. Nie, A. Barco, and F. Zeng, “Spectral and temporal cues in cochlear implant speech perception.,” *Ear Hear.*, vol. 27, no. 2, pp. 208–217, 2006.

[35] M. Haggard, “Hearing: An Introduction to Psychological and Physiological Acoustics,” *J. Neurol. Neurosurg. Psychiatry*, vol. 45, no. 12, pp. 1175–1175, 1982.

[36] D. J. Carpenter, D. L. Tucci, D. M. Kaylie, and D. O. Frank-Ito, “Disagreement in middle ear volume estimation between tympanometry and three-dimensional volume reconstruction in the context of tympanic membrane perforation,” *J. Otol.*, vol. 12, no. 2, pp. 74–79, 2017.

[37] L. Beker, O. Zorlu, N. Goksu, and H. Kulah, “Stimulating auditory nerve with MEMS harvesters for fully implantable and self-powered cochlear implants,” in *2013 Transducers and Eurosensors XXVII: The 17th International Conference on Solid-State Sensors, Actuators and Microsystems, TRANSDUCERS and EUROSENSORS 2013*, 2013, pp. 1663–1666.

[38] A. R. Moller, *Hearing : Anatomy, Physiology, and Disorders of the Auditory System*. San Diego, CA: Plural Publising, 2006.

[39] M. A. Zurcher, D. J. Young, M. Semaan, C. A. Megerian, and W. H. Ko, “Effect of incus removal on middle ear acoustic sensor for a fully implantable cochlear prosthesis,” in *Annual International Conference of the IEEE Engineering in Medicine and Biology - Proceedings*, 2006, pp. 539–542.

[40] D. J. Young, M. a. Zurcher, W. H. Ko, M. Semaan, and C. a. Megerian, “Implantable MEMS Accelerometer Microphone for Cochlear Prosthesis,” *2007 IEEE Int. Symp. Circuits Syst.*, pp. 3119–3122, 2007.

[41] D. J. Young, M. A. Zurcher, W. H. Ko, M. Semaan, and C. A. Megerian, "Implantable MEMS Accelerometer Microphone for Cochlear Prosthesis," *2007 IEEE Int. Symp. Circuits Syst.*, pp. 3119–3122, 2007.

[42] S. Guo, X. Dong, G. Wang, F. Lu, H. Kang, and Y. Wang, "Properties evaluation of piezoelectric materials in application of cochlear implant," *Ferroelectrics*, vol. 413, no. 1, pp. 272–278, 2011.

[43] T. Inaoka, H. Shintaku, T. Nakagawa, S. Kawano, H. Ogita, T. Sakamoto, S. Hamanishi, H. Wada, and J. Ito, "Piezoelectric materials mimic the function of the cochlear sensory epithelium," *Proc. Natl. Acad. Sci.*, vol. 108, no. 45, pp. 18390–18395, 2011.

[44] P. P. Mercier, A. C. Lysaght, S. Bandyopadhyay, A. P. Chandrakasan, and K. M. Stankovic, "Energy extraction from the biologic battery in the inner ear," *Nat. Biotechnol.*, vol. 30, no. 12, pp. 1240–1243, 2012.

[45] D. Accoto, M. Calvano, D. Campolo, F. Salvinelli, and E. Guglielmelli, "Energetic analysis for self-powered cochlear implants," *Proc. 31st Annu. Int. Conf. IEEE Eng. Med. Biol. Soc. Eng. Futur. Biomed. EMBC 2009*, pp. 4860–4863, 2009.

[46] D. J. Carpenter, D. L. Tucci, D. M. Kaylie, and D. O. Frank-Ito, "Disagreement in middle ear volume estimation between tympanometry and three-dimensional volume reconstruction in the context of tympanic membrane perforation," *J. Otol.*, vol. 12, no. 2, pp. 74–79, 2017.

[47] M. D. Nguyen, M. Dekkers, H. N. Vu, and G. Rijnders, "Film-thickness and composition dependence of epitaxial thin-film PZT-based mass-sensors," *Sensors Actuators, A Phys.*, vol. 199, pp. 98–105, 2013.

[48] M. Jambunathan, R. Elfrink, R. Vullers, R. Van Schaijk, M. Dekkers, and J. Broekmaat, "Pulsed laser deposited-PZT based MEMS energy harvesting devices," in *Proceedings of ISAF-ECAPD-PFM 2012, Aveiro, 2012, pp. 1-4.*

[49] K. Arora, P. Dawson, R. Dowell, and A. Vandali, “Electrical stimulation rate effects on speech perception in cochlear implants,” *Int. J. Audiol.*, vol. 48, no. 8, pp. 561–567, 2009.

[50] M. Yip, R. Jin, H. H. Nakajima, K. M. Stankovic, and A. P. Chandrakasan, “A fully-implantable cochlear implant SoC with piezoelectric middle-ear sensor and arbitrary waveform neural stimulation,” *IEEE JSSC*, vol. 50, no. 1, pp. 214–229, 2015.

[51] M. Renaud, "Piezoelectric Energy Harvesters for Wireless Sensor Networks," Ph. D dissertation, Faculteit Ingenieurswetenschappen, Katholieke Universiteit Leuven, 2009.

[52] S. Du, Y. Jia, and A. Seshia, “Maximizing Output Power in a Cantilevered Piezoelectric Vibration Energy Harvester by Electrode Design,” *J. Phys. Conf. Ser.*, vol. 660, no. 1, 2015.

[53] A. Sharma *et al.*, “Fabrication, simulation and characterisation of MEMS piezoelectric vibration energy harvester for low frequency,” in *Procedia Engineering*, 2015, vol. 120, pp. 645–650.

[54] L. Beker, “MEMS Piezoelectric Energy Harvester for Cochlear Implant Applications,” M. Sc. Thesis, The Graduate School of Natural and Applied Science, Middle East Technical University, Ankara, 2013.

[55] R. Sarpeshkar, C. Salthouse, J. J. Sit, M. W. Baker, S. M. Zhak, T. K. T. Lu, L. Turicchia, and S. Balster, “An ultra-low-power programmable analog bionic ear processor,” *IEEE Trans. Biomed. Eng.*, vol. 52, no. 4, pp. 711–727, 2005.

[56] P. A. Köllensperger, W. J. Karl, M. M. Ahmad, W. T. Pike, and M. Green, “Patterning of platinum (Pt) thin films by chemical wet etching in Aqua Regia,” *J. Micromechanics Microengineering*, vol. 22, no. 6, p. 067001, 2012.

[57] D. H. A. Blank, M. Dekkers, and G. Rijnders, “Pulsed laser deposition in Twente: From research tool towards industrial deposition,” *J. Phys. D. Appl. Phys.*, vol. 47, no. 3, 2014.

[58] A. Koyuncuoğlu, B. İlik, S. Chamanian, H. Uluşan, P. Ashrafi, D. Işık, and H. Külah, “Bulk PZT Cantilever Based MEMS Acoustic Transducer for Cochlear Implant Applications,” *Multidiscip. Digit. Publ. Inst. Proc. Proc.*, vol. 1, no. 4, p. 584, 2017.

[59] B. İlik, A. Koyuncuoğlu, Ö. Şardan-Sukas, and H. Külah, “Thin film piezoelectric acoustic transducer for fully implantable cochlear implants,” *Sensors Actuators, A Phys.*, vol. 280, pp. 38–46, 2018.

[60] F. Goldschmidtboeing, C. Eichhorn, M. Wischke, M. Kroener, and P. Woias, “The influence of ferroelastic hysteresis on mechanically excited PZT cantilever beams,” *PowerMEMS*, pp. 114–117, 2011.

[61] B. İlik, A. Koyuncuoğlu, H. Uluşan, S. Chamanian, D. Işık, Ö. Şardan-Sukas, and H. Külah, “Thin Film PZT Acoustic Sensor for Fully Implantable Cochlear Implants,” *Multidiscip. Digit. Publ. Inst. Proc.*, vol. 1, no. 4, p. 366, 2017.

[62] L. Beker, N. H. Özgüven, and H. Külah, “Optimization of an energy harvester coupled to a vibrating membrane,” in *Conference Proceedings of the Society for Experimental Mechanics Series*, 2013, vol. 6, pp. 577–583.

[63] K. W. Grant *et al.*, “Integration efficiency for speech perception within and across sensory modalities by normal-hearing and hearing-impaired individuals,” *J. Acoust. Soc. Am.*, vol. 121, no. 2, pp. 1164–1176, 2007.

[64] J. Jang, S. Kim, D. J. Sly, S. J. O’Leary, and H. Choi, “MEMS piezoelectric artificial basilar membrane with passive frequency selectivity for short pulse width signal modulation,” *Sensors Actuators, A Phys.*, vol. 203, pp. 6–10, 2013.

APPENDIX

MASK LAYOUT

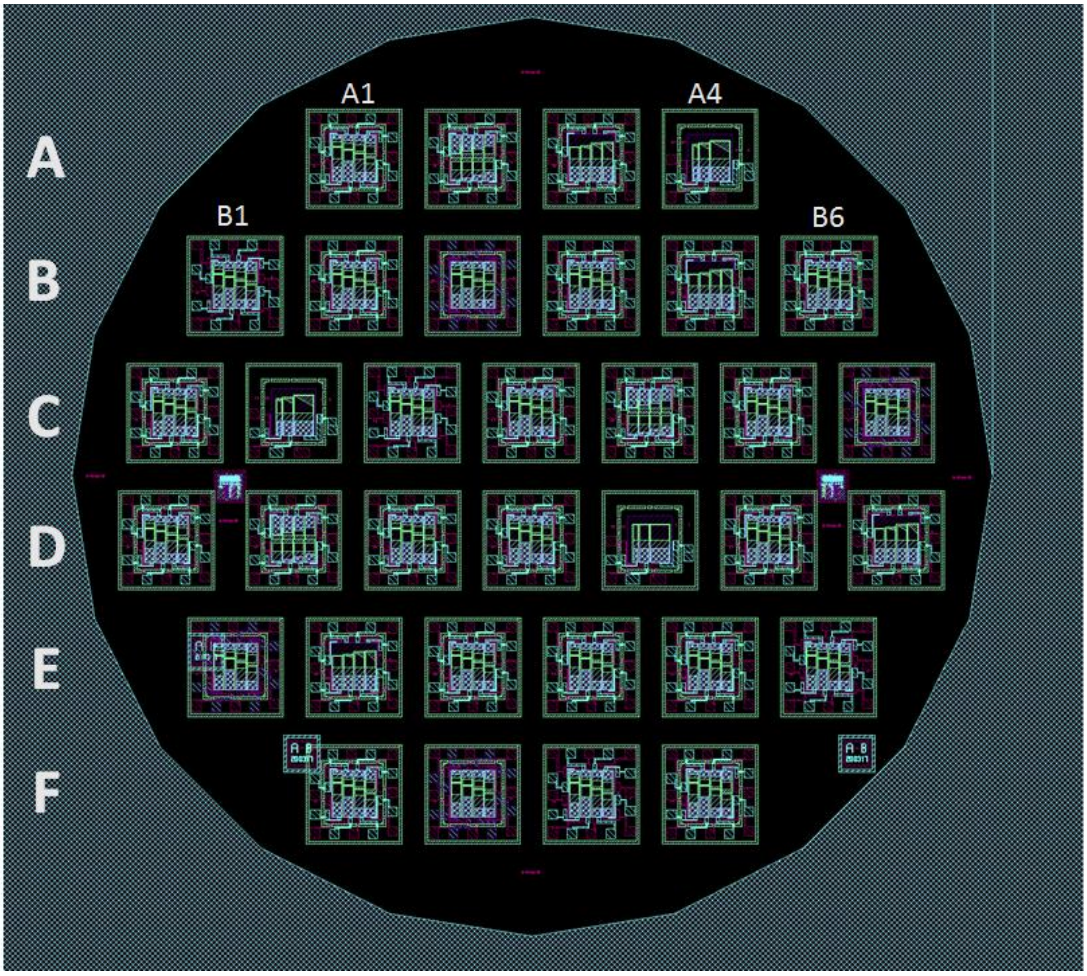

Figure 0.1Wafer-level mask layouts for the multi-channel thin film piezoelectric acoustic transducer.